ISSN 1857–9027
e-ISSN 1857–9949

МАКЕДОНСКА АКАДЕМИЈА НА НАУКИТЕ И УМЕТНОСТИТЕ
ОДДЕЛЕНИЕ ЗА ПРИРОДНО-МАТЕМАТИЧКИ И БИОТЕХНИЧКИ НАУКИ

MACEDONIAN ACADEMY OF SCIENCES AND ARTS
SECTION OF NATURAL, MATHEMATICAL AND BIOTECHNICAL SCIENCES

ПРИЛОЗИ
CONTRIBUTIONS

39
(2)

СКОПЈЕ – SKOPJE
2018

Publisher: Macedonian Academy of Sciences and Arts

*

Printed by: Vinsent Grafika, Skopje

*

Number of copies: 300

*

December 2018

Published twice a year
The Contributions, Sec. Nat. Math. Biotech. Sci. is indexed in:
Chemical Abstracts, Mathematical Reviews, Google Scholar, EBSCO and DOAJ

http://manu.edu.mk/contributions/NMBSci/

Прилози, Одд. прир. мат. биотех. науки, МАНУ	Том	Бр.	стр.	Скопје
	39	2	79–146	2018
Contributions, Sec. Nat. Math. Biotech. Sci., MASA	Vol.	No.	pp.	Skopje

TABLE OF CONTENTS

С О Д Р Ж И Н А

ПРИЛОЗИ, Одделение за природно-математички и биотехнички науки, МАНУ, том **39**, бр. 2, стр. 83–90 (2018)
CONTRIBUTIONS, Section of Natural, Mathematical and Biotechnical Sciences, MASA, Vol. **39,** No. 2, pp. 83–90 (2018)

Received: April 12, 2018
Accepted: November 13, 2018

ISSN 1857–9027
e-ISSN 1857–9949
UDC: 616-022.6:578.828]-085.281.8
DOI: 10.20903/csnmbs.masa.2018.39.2.121

Short review

ADVANCES IN TACKLING FILOVIRUSES

Života Selaković[1,*], Bogdan Šolaja[2,*]

[1]Faculty of Chemistry, University of Belgrade, Belgrade, Serbia
[2]Serbian Academy of Sciences and Arts, Belgrade, Serbia
[*]e-mail: zivota_selakovic@chem.bg.ac.rs; bogdan.solaja@sanu.ac.rs

Filoviruses are virulent pathogens that cause deadly haemorrhagic fever in humans and non-human primates. There is currently no approved drug or vaccine to tackle this disease. Two vaccine platforms that use adenovirus vectors have completed phase I studies, while a recombinant vesicular stomatitis virus-based vaccine has successfully completed a phase III trial. Intricate macromolecular therapeutics have also been developed, most notably those based on antibodies or interfering RNA or RNA-surrogates. Most small molecules active against filoviruses have not yet advanced to clinical trials, except favipiravir, which was proven to be safe, and GS-5734, which has entered trials.

Key words: ebola; Marburg; hemorrhagic fever; vaccines; small molecules

INTRODUCTION

Filoviruses (lat. *Filoviridae*) are a family of viruses belonging to the *Mononegavirales* order [1]. Most of the members of this family cause fatal hemorrhagic fever in humans and non-human primates (NHPs) [2].

The Filoviridae family is comprised of three genera – *Marburgvirus* (discovered in 1967 [3] and named after the city of Marburg in Germany), *Ebolavirus* (discovered in 1976 [4, 5] and named after the Ebola river in the Democratic Republic of the Congo) and *Cuevavirus* (discovered in 2009 [6] in Spain and named after the Spanish word for 'cave'). The former two genera have caused several outbreaks among humans in the last 50 years, resulting in at least 2.885 reported cases and 1.972 deaths [7, 8]. More recently, Ebola virus caused the first-ever filovirus epidemic of an unprecedented scale in West Africa, from 2013 to 2016, which alone accounted for at least 28.616 cases and 11.310 deaths, according to the World Health Organization [9].

There are no FDA approved drugs or vaccines to tackle this deadly virus. In this paper, we provide a review of the most promising therapeutic candidates that have been developed to date.

VACCINES

There have been several attempts to generate vaccines against filoviruses, but only three have made it into advanced phases of clinical trials. These will be described here in more detail.

Scientists from the Public Health Agency of Canada (PHAC) developed the rVSV-ZEBOV vaccine in the early 2000s [10]. As the name suggests, the *Zaire ebolavirus* (ZEBOV) glycoprotein (GP) gene was inserted into the genome of the recombinant vesicular stomatitis virus (rVSV), a replication-competent viral vector (Figure 1). The GP is the only filoviral protein expressed on the surface of the virion, and is therefore immunologically important. The vaccine was initially proven to be safe and effective in rodents, such as mice, hamsters and guinea pigs [11–13]. Afterwards, NHP trials showed that the vaccine provided full protection when administered from 31 to 7 days prior to infection, and partial protection when administered from 3 days before to 1 day after infection [14–17].

However, several phase I studies that were performed in 2014 and 2015 showed that, overall, 22% of subjects had fever after vaccination, and other adverse effects (AEs) were noted [19, 20]. Fi-

nally, a cluster-randomized phase III study was performed during the West African epidemic in the Conakry region of Guinea, and Tomkolili, and Bombali regions of Sierra Leone on a large scale [21]. A ring vaccination approach inspired by the strategy that resulted in smallpox eradication was utilized. Lists of contacts (and contacts of contacts) of infected patients were followed and archived, after which randomized 1:1 clusters were either immediately vaccinated or vaccinated with a 21 day delay. There were no cases of Ebola registered within 10 days of vaccination in the immediately vaccinated clusters (2119 people in total), while 16 cases were registered in the delayed vaccination clusters (2041 people in total). More than half (53.9%, 3149 people) of patients reported some AEs, but only 80 reported a serious AE.

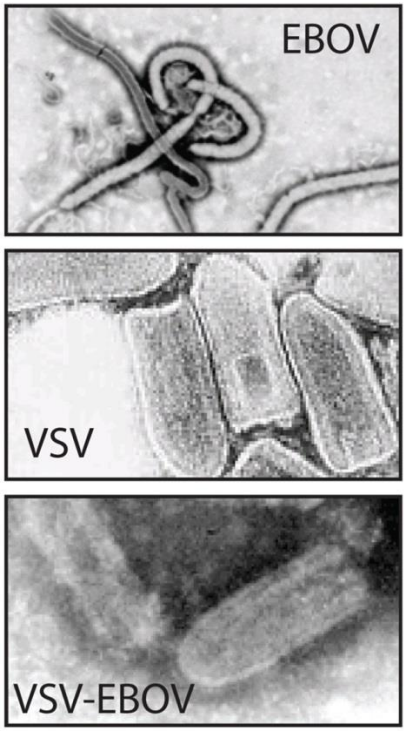

Figure 1. Transmission electron microscopy images of EBOV, VSV and rVSV-EBOV [18]

The other two advanced vaccines both utilize an adenovirus (AdV) vector. In these vaccines, the EBOV GP occupies the native adenovirus early region, furnishing a nonreplicating virus [18].

The first of the two was initially developed in the early 2000s by the National Institute of Allergy and Infectious Diseases (NIAID), beginning with a plain DNA vaccine [22]. The NIAID effort was later joined by GlaxoSmithKline. Due to safety reasons, initial experiments involved modified EBOV GP delivered by DNA vaccination, before moving on to full-length wild-type glycoprotein, which was proved to be safe in a phase I study [23]. After these results, a chimpanzee adenovirus 3 (cAd3) vector-based vaccine was evaluated [24]. The vaccine encoded both the *Zaire* and the *Sudan* species' wild-type GPs. In the NHP trials, it was, however, observed that an additional boost with an attenuated vaccine of a poxvirus (modified vaccinia Ankara, MVA) vector was needed for a longer lasting protection of 10 months after vaccination. Finally, cAd3-EBO phase I studies were initiated in 2014, with both Zaire GP, or a combination of Sudan and Zaire GPs, respectively [25, 26]. Glycoprotein-specific antibodies were induced in a dose-dependent manner in all participants, with the doses ranging from 1×10^{10} viral particle units (pu) to 2×10^{11} pu. The AEs were dose-dependent, with up to 56% of volunteers developing very mild AEs, and up to 20% developing fever, which luckily did not last more than one day. In general, there were no serious AEs. Depending on the vaccine and on the dosage used, an additional MVA boost may or may not be required for protection lasting up to 48 weeks, as evidenced from antibody titers.

Lastly, the third group of vaccine platforms utilized a human AdV vector, and specifically, that of the Ad26 serotype, which is rarer than the common Ad5, and therefore more probable to override pre-existing immunity [27–31]. Two phase I studies have been conducted, where generally Ad26-ZEBOV was used for priming, and MV-BN-Filo was used as a boosting component, or vice versa. The boosting was performed 2, 4 or 8 weeks after the prime dose. The doses used were 5×10^{10} pu for priming and 1×10^{8} pu for boosting. Volunteers were observed for up to one year (360 days), the longest of all studies, and it was concluded that the regimen is safe, providing long lasting protection with an MVA-BN-Filo prime and subsequent Ad26-EBOV boost. The reverse order was better for a more rapid immunization, *i.e.* in emergency situations.

MACROMOLECULES IN EBOV THERAPY

Four approaches stand out in the field of potential macromolecular therapeutics.

The small interfering RNA (siRNA) approach was among the first to be developed. Namely, the idea was to synthesize siRNA complementary to the messenger RNA (mRNA) that encodes viral proteins, and then deliver it to an infected cell. The siRNA will target the mRNA, and after a complex of the two is formed, the cell will recognize it as abnormal, and the mRNA will be degraded, thus preventing translation, and resulting in silencing of

the viral genes. A Canadian company developed small lipid nanoparticles that carried siRNA complementary to mRNA of EBOV L polymerase, the membrane-associated protein (VP24), and the polymerase complex protein (VP35), a complex called TKM-Ebola [32–35]. The product, which was delivered intravenously, faced difficult phase I trials during the West African epidemic, with the FDA halting the study throughout 2014 and 2015 due to safety concerns [36]. Unfortunately, in a small phase II study in Sierra Leone, the formulation was not shown to improve survival when compared to historic controls [35].

Similarly, antisense phosphorodiamidate oligomers (PMOs, Scheme 1) were invented as early as the late 1990s in order to behave as RNA surrogates, and thereby target specific RNA sequences [37]. In the early 2000s it was discovered that therapy utilizing PMOs which mimic the EBOV VP24, VP35, and RNA polymerase L sequences can protect rhesus macaques [38]. Subsequently, a private company developed formulations such as AVI 6002, AVI 6003, AVI 7537 and AVI 7228, which targeted different Ebola or Marburg genes using the PMO technology, or, more specifically, a slightly different PMO*plus* approach (Scheme 1). These reached phases I studies, where they were proven to be well tolerated and safe, with potential as post-exposure prophylaxis for filovirus infections [39, 40]. However, to the best of our knowledge, no further development has been reported [41].

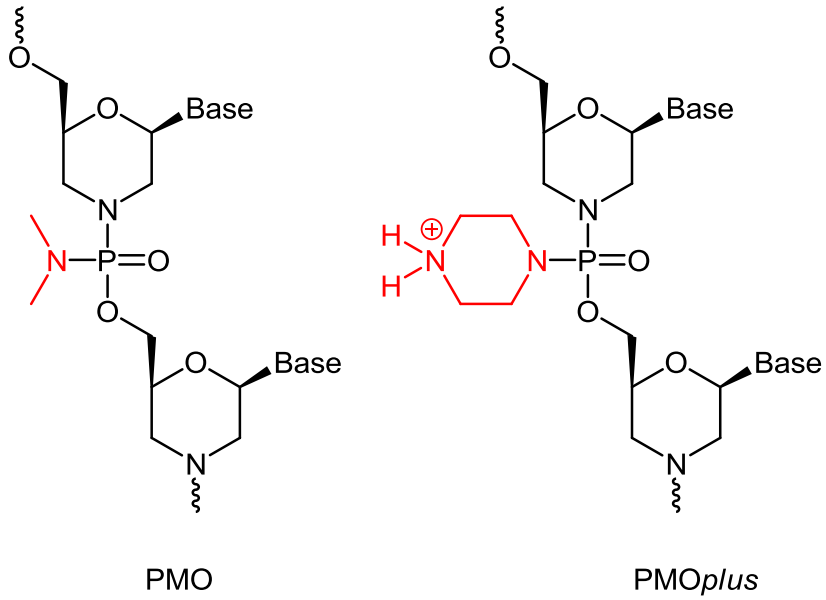

Scheme 1. Structure of PMO and PMOplus based oligomers [41]

A different approach was developed by PHAC, the United States Army Medical Research Institute for Infectious Diseases (USAMRIID), and NIAID, and was later improved upon by US-based companies [42–45]. Specifically, a cocktail of three antibodies, called ZMapp, was derived from mice infected with Ebola. More precisely, the DNA that encodes monoclonal antibodies was collected from hybridomas and produced by combining immortal myeloma cancer cell lines with splenocytes of infected mice. The DNA was modified by genetic engineering to produce antibodies suitable for humans, and the appropriate genes were delivered to tobacco plants through an *Agrobacterium* which infects the plants. Finally, a large number of antibodies was collected from the dying plant.

After the formulation was proven to be safe and effective in NHPs, clinical studies were initiated [42]. The fear of uncontrolled spread of the West African epidemic led to a clinical trial in infected humans [43]. In a group of controls that received only standard care at the time, 13 out of 35 patients (37%) died, compared to only 8 out of 36 patients (22%) who received standard care plus ZMapp. Thus, it was proven that the addition of ZMapp treatment to standard care would improve survival was 91.2%.

Finally, an approach utilizing glycodendritic structures that inhibit viral entry has been in development since the early 2000s [46]. Namely, the interaction of EBOV GP with a dendritic cell specific ICAM-3 grabbing non-integrin (DC-SIGN), which

facilitates viral entry into dendritic cells, can be inhibited by carbohydrates mimicking the glycans present in the viral GP. A multivalent presentation of carbohydrates is needed for effective interaction with lectins, therefore dendritic polymers with carbohydrate termini were developed; the most effective possess fullerene or even virus like particle (VLP) cores encompassing as many as 1620 copies of mannose at the surface [47, 48]. T-cells, which cannot otherwise be infected with EBOV, can be rendered susceptible by the addition of DC-SIGN, and these cells were used for proof-of-concept assays. Recombinant VSV expressing EBOV GP was used to mimic the virus, instead of the much harder to work with wild-type EBOV. In the assays, the dendrite polycarbohydrates showed IC_{50} values as low as ~900 pM.

SMALL MOLECULES

Since the late 1990s, a number of known and even FDA approved drugs, as well as newly synthesized small molecules, have been found to exhibit anti-EBOV activity. Above all, small molecules carry an advantage over vaccines and antibodies, in principle, being cheaper to produce. Moreover, depending on their mechanism of action, their activity may not be affected by mutations in the viral RNA. Scheme 2 outlines the most effective molecules, although many others have been, and are, being developed.

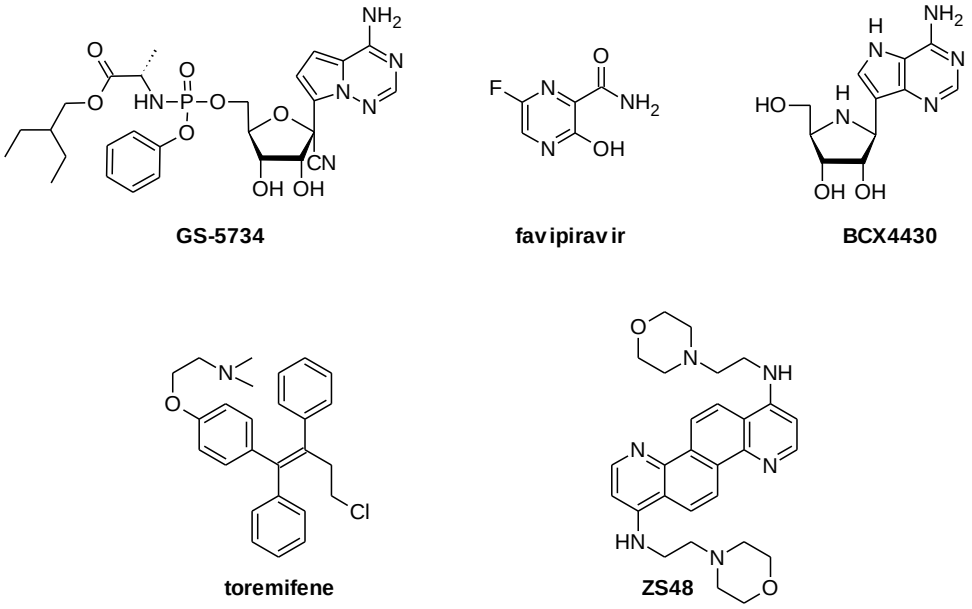

Scheme 2. Select examples of small molecules with anti-EBOV activity

Favipiravir, or T-705, is an antiviral drug developed by a Japan-based company. In essence, the compound is metabolized to a ribofuranosyl 5′-triphosphate derivative, which then enters the pathway of viral metabolism and inhibits the RNA-dependent RNA polymerase [49]. Even though it's *in vitro* activity is weak (IC_{50} = 67 μM), its toxicity is exceptionally low (CC_{50} > 1000 μM) [50]. Therefore, *in vivo* assays freely extended to doses as high as 300 mg/kg, and testing in mice proved that the compound is effective at doses as low as 30 mg/kg (under certain dosage regimes). A clinical trial was set up during the West African epidemic but performing a randomized study where one group of patients would receive standard care, while another would receive an additional experimental drug, was deemed inappropriate. Therefore, all patients received favipiravir. For the 99 patients that were treated, favipiravir was well tolerated and showed a mean decrease of viral load = 0.33 $\log_{10}$ copies/ml per day – in individuals that survived [51].

Another group of drugs, developed by USAMRIID, NIAID, and US-based private companies includes compounds such as BCX4430 and GS-5734. The drugs, which are nucleoside analogs, were reported to have a stronger affinity for viral RNA-polymerase than for that of native, host-cell (human) RNA-polymerase. These compounds, therefore, in a way similar to favipiravir, inhibit the RNA-related steps in the viral multiplication pathway. BCX4430 was discovered via a large scale high-throughput screening campaign [52]. It provided an IC_{50} value of ~3.4 μM, and it was the first small molecule to be tested in a NHP model, where

it cured 100% of monkeys with a 15 mg/kg dose, administered 2 times daily for 12 days. Under *in vitro* conditions, GS-5734, which was developed after BCX4430, proved to be superior, with an IC_{50} as low as 0.06 μM [53]. Most probably, its triphosphate metabolite is an RNA-chain terminator. The compound is not active in mice, but it did cure 100% of infected cynomolgus macaques with a 3.3 mg/kg daily dose. GS-5734 was given under compassionate use to two Ebola patients, and has entered clinical trials [54].

Lastly, an important group of EBOV inhibitors belongs to the class of compounds known as cationic amphiphilic drugs (CADs) [55, 56]. These molecules have a basic nitrogen atom separated by a flexible linker from a hydrophobic, most often aromatic, molecular core. The mode of action of these compounds is not fully elucidated, but it is clear that it is host-based, and that viral entry is being inhibited in the late endosome/lysosome stage. It is also clear these compounds increase Ca^{2+} levels within endosomes/lysosomes, while also lowering sphingosine levels and causing cholesterol accumulation [57, 58]. Toremifene, a selective estrogen receptor modulator, stands out among CADs, and its estrogen receptor related activity was proven to be irrelevant for anti-EBOV activity. Its IC_{50} value ranges from 0.97 to 1.73 μM, and it is able to cure 50% of mice with a 60 mg/kg/day dose. Our own research led to the development of diazachrysene derivatives, such as ZS48. These compounds have IC_{50} values as low as 0.34 μM, and can cure up to 90% of mice, notably with a low dose of 10 mg/kg, delivered intraperitoneally once daily for seven days [59, 60].

Acknowledgements: This research was supported by the Ministry of Science and Technological Development of Serbia, Grant 172008 (Ž. S., B. Š.) and Serbian Academy of Sciences and Arts, Grant F80 (B. Š.).

Author contributions: The manuscript was written by Ž.S. with contribution of B.Š. Both authors have given approval to the final version of the manuscript.

REFERENCES

[1] https://talk.ictvonline.org/ictv-reports/ictv_9th_report/negative-sense-rna-viruses-2011/w/negrna_viruses/197/filoviridae (accessed on 4th April, 2018).

[2] M. A. Bwaka, M-J. Bonnet, P. Calain, R. Colebunders, A. De Roo, Y. Guimard, K. R. Katwiki, K. Kibadi, M. A. Kipasa, K. J. Kuvula, B. B. Mapanda, M. Massamba, K. D. Mupapa, J-J. Muyembe-Tamfum, E. Ndaberey, C. J. Peters, P. E. Rollin, E. Van den Ende, Ebola hemorrhagic fever in Kikwit, Democratic Republic of the Congo: clinical observations in 103 patients. *J. Infect. Dis.*, **179** (1999), S1 – S7.

[3] R. Siegert, H. L. Shu, W. Slenczka, D. Peters, G. Müller. Zur Ätiologie einer unbekannten, von Affen ausgegangenen menschlichen Infektionskrankheit, *Deutsche Medizinische Wochenschrift*, **92** (1967), pp. 2341–2343.

[4] K. M. Johnson, P. A. Webb, J. V. Lange, F. A. Murphy, Isolation and partial characterisation of a new virus causing haemorrhagic fever in Zaire. *Lancet*, **309** (1977), pp. 569–571.

[5] E. T. W. Bowen, G. Lloyd, W. J. Harris, G. S. Platt, A. Baskerville, E. E Vella. Viral haemorrhagic fever in southern Sudan and northern Zaire. Preliminary studies on the aetiological agent, *Lancet*, **309** (1977), 571–573.

[6] A. Negredo, G. Palacios, S. Vázquez-Morón, F. L. González, H. N. Dopazo, F. Molero, J. Juste, J. Quetglas, N. Savji, M. de la Cruz Martínez, J. E. Herrera, M. Pizarro, S. K. Hutchison, J. E. Echevarría, W. I. Lipkin, A. Tenorio, Discovery of an Ebolavirus-Like Filovirus in Europe, *PLoS Pathogens*, **7** (2011), e1002304.

[7] https://www.cdc.gov/vhf/ebola/outbreaks/history/chronology.html (accessed on 4th April, 2018)

[8] https://www.cdc.gov/vhf/marburg/outbreaks/chronology.html (accessed on 4th April, 2018)

[9] http://apps.who.int/ebola/ebola-situation-reports (accessed on 4th April, 2018)

[10] S. M. Jones, U. Stroher, L. Fernando, X. Qiu, J. Alimonti, P. Melito, M. Bray, H. D. Klenk, Feldmann, H. Assessment of a vesicular stomatitis virus-based vaccine by use of the mouse model of Ebola virus hemorrhagic fever. *J. Infect Dis*, **196** (2007), S404–12.

[11] T. Lambe, G. Bowyer, K. J. Ewer, A review of Phase I trials of Ebola virus vaccines: what can we learn from the race to develop novel vaccines? *Phil. Trans. R. Soc. B*, **372** (2017), 20160295.

[12] G. Wong, J. Audet, L. Fernando, H. Fausther-Bovendo, J. B. Alimonti, G. P. Kobinger, X. Qiu, Immunization with vesicular stomatitis virus vaccine expressing the Ebola glycoprotein provides sustained long-term protection in rodents. *Vaccine*, **32** (2014), pp. 5722–5729.

[13] E. de Wit, A. Marzi, T. Bushmaker, D. Brining, D. Scott, J. A. Richt, T. W. Geisbert, H. Feldmann, Safety of recombinant VSV–Ebola virus vaccine vector in pigs. *Emerg Infect Dis.*, **21** (2015), pp. 702–704.

[14] S. M. Jones, H. Feldmann, U. Ströher, J. B. Geisbert, L. Fernando, A. Grolla, H. D. Klenk, N. J. Sullivan, V. E. Volchkov, E. A. Fritz, K. M. Daddario, L. E. Hensley, P. B. Jahrling, T. W. Geisbert, Live attenuated recombinant vaccine protects nonhuman primates against Ebola and Marburg viruses. *Nat Med.*, **11** (2005), pp. 786–790.

[15] H. Feldmann, S. M. Jones, K. M. Daddario-DiCaprio, J. B. Geisbert, U. Ströher, A. Grolla, M. Bray, E. A. Fritz, L. Fernando, F. Feldmann, L. E. Hensley, T. W. Geisbert, Effective post-exposure treatment of Ebola infection. *PLoS Pathog.,* **3** (2007), e2.

[16] T. W. Geisbert, K. M. Daddario-DiCaprio, M. G. Lewis, J. B. Geisbert, A. Grolla, A. Leung, J. Paragas, L. Matthias, M. A. Smith, S. M. Jones, L. E. Hensley, H. Feldmann, P. B. Jahrling, Vesicular stomatitis virus-based Ebola vaccine is well-tolerated and protects immunocompromised non-human primates, *PLOS Pathog.,* **4** (2008), e1000225.

[17] A. Marzi, S. J. Robertson, E. Haddock, F. Feldmann, P. W. Hanley, D. P. Scott, J. E. Strong, G. Kobinger, S. M. Best, H. Feldmann, VSV-EBOV rapidly protects macaques against infection with the 2014/15 Ebola virus outbreak strain, *Science,* **349** (2015), pp. 739–742.

[18] K. J. Chappell, D. Watterson, Fighting Ebola: A window for vaccine re-evaluation? *PLoS Pathog.*, **13** (2017), e1006037.

[19] J. A. Regules *et al.,* A recombinant vesicular stomatitis virus Ebola vaccine — preliminary report. *N. Engl. J. Med.,* **376** (2015), pp. 330–341.

[20] S. T. Agnandji *et al.,* Phase 1 trials of rVSV Ebola vaccine in Africa and Europe, *N. Engl. J. Med.,* **374** (2016), pp. 1647–1660.

[21] A. M. Henao-Restrepo *et al,* Efficacy and effectiveness of an rVSV-vectored vaccine in preventing Ebola virus disease: final results from the Guinea ring vaccination, open-label, cluster-randomised trial (Ebola Ça Suffit!), *The Lancet,* **389** (2017) pp., 505–518.

[22] J. E. Martin, N. J. Sullivan, M. E. Enama, I. J. Gordon, M. Roederer, R. A. Koup, R. T. Bailer, B. K. Chakrabarti, M. A. Bailey, P. L. Gomez, C. A. Andrews, Z. Moodie, L. Gu, J. A. Stein, G. J. Nabel, B. S. Graham, A DNA vaccine for Ebola virus is safe and immunogenic in a phase I clinical trial. *Clin Vaccine Immunol*., **13** (2006), pp. 1267–1277.

[23] H. Kibuuka *et al,* Safety and immunogenicity of Ebola virus and Marburg virus glycoprotein DNA vaccines assessed separately and concomitantly in healthy Ugandan adults: a phase 1b, randomised, double-blind, placebo-controlled clinical trial. *Lancet,* **385** (2015), pp. 1545–1554.

[24] D. A. Stanley *et al.,* Chimpanzee adenovirus vaccine generates acute and durable protective immunity against ebolavirus challenge, *Nat Med.,* **20** (2014) pp. 1126–1129.

[25] M. D. Tapia *et al.,* Use of ChAd3-EBO-Z Ebola virus vaccine in Malian and US adults, and boosting of Malian adults with MVA-BN-Filo: a phase 1, single-blind, randomised trial, a phase 1b, open-label and double-blind, dose-escalation trial, and a nested, randomised, double-blind, placebo-controlled trial. *Lancet Infect Dis*, **16** (2016), pp. 31–42.

[26] J. E. Ledgerwood *et al,* Chimpanzee Adenovirus vector Ebola vaccine. *N. Engl. J. Med*., **376** (2017), pp. 928–938.

[27] J. E. Ledgerwood, P. Costner, N. Desai, L. Holman, M. E. Enama, G. Yamshchikov, S. Mulangu, Z. Hu, C. A. Andrews, R. A. Sheets, R. A. Koup, M. Roederer, R. Bailer, J. R. Mascola, M. G. Pau, N. J. Sullivan, J. Goudsmit, G. J. Nabel, B. S. Graham, VRC 205 Study Team. A replication defective recombinant Ad5 vaccine expressing Ebola virus GP is safe and immunogenic in healthy adults, *Vaccine*, **29** (2010), pp. 304–313.

[28] F. C. Zhu *et al.,* Safety and immunogenicity of a novel recombinant adenovirus type-5 vector-based Ebola vaccine in healthy adults in China: preliminary report of a randomised, double-blind, placebo controlled, phase 1 trial, *Lancet*, **385** (2015), pp. 2272–2279.

[29] T. W. Geisbert, M. Bailey, L. Hensley, C. Asiedu, J. Geisbert, D. Stanley, A. Honko, J. Johnson, S. Mulangu, M. G. Pau, J. Custers, J. Vellinga, J. Hendriks, P. Jahrling, M. Roederer, J. Goudsmit, R. Koup, N. J. Sullivan, Recombinant adenovirus serotype 26 (Ad26) and Ad35 vaccine vectors bypass immunity to Ad5 and protect nonhuman primates against ebolavirus challenge, *J. Virol.,* **85** (2011), pp. 4222–4233.

[30] G. Shukarev, B. Callendret, K. Luhn, M. Douoguih, EBOVAC1 consortium. A two-dose heterologous prime-boost vaccine regimen eliciting sustained immune responses to Ebola Zaire could support a preventive strategy for future outbreaks. *Hum Vaccin Immunother*, **13** (2017), pp. 266–270.

[31] R. L. Winslow, I. D. Milligan, M. Voysey, K. Luhn, G. Shukarev, M. Douoguih, M. D. Snape, Immune responses to novel Adenovirus type 26 and modified vaccinia virus Ankara-vectored Ebola vaccines at 1 year, *JAMA*, **317** (2017), pp. 1075–1077.

[32] T. W. Geisbert *et al.*, Postexposure protection of non-human primates against a lethal Ebola virus challenge with RNA interference: a proof-of-concept study, *Lancet*, **375** (2010) pp. 1896–1905.

[33] https://www.forbes.com/sites/davidkroll/2014/08/07/fda-moves-on-tekmiras-ebola-drug-while-sarepta-sits-unused/#4ef9d3e44373 (accessed on 4th April, 2018).

[34] E. P. Thi, C. E. Mire, A. C. H. Lee, J. B. Geisbert, J. Z. Zhou, K. N. Agans, N. M. Snead, D. J. Deer, T. R. Barnard, K. A. Fenton, I. MacLachlan, T. W. Geisbert, Lipid nanoparticle siRNA treatment of Ebola virus Makona infected nonhuman primates. *Nature*, **521** (2015), pp. 362–365.

[35] J. Dunning *et al.,* Experimental Treatment of Ebola Virus Disease with TKM-130803: A Single-arm phase 2 clinical trial, *PLoS Med*, **13** (2016), e1001997.

[36] https://www.reuters.com/article/us-health-ebola-tekmira/fda-modifies-partial-clinical-hold-on-tekmira-ebola-study-idUSKBN0N11AF20150410 (accessed on 4th April, 2018)

[37] J. E. Summerton, *Morpholino Oligomers: Methods and Protocols, Springer*, 2017.

[38] K. L. Warfield, D. L. Swenson, G. G. Olinger, D. K. Nichols, W. D. Pratt, R. Blouch, D. A. Stein, M. J. Aman, P. L. Iversen, S. Bavari, Gene-specific countermeasures against Ebola virus based on antisense phosphorodiamidate morpholino oligomers, *PLoS Pathog.*, **2** (2006), e1.

[39] A. E. Heald, P. L. Iversen, J. B. Saoud, P. Sazani, J. S. Charleston, T. Axtelle, M. Wong, W. B. Smith, A. Vutikullird, E. Kaye, Safety and pharmacokinetic profiles of phosphorodiamidate morpholino oligomers with activity against Ebola virus and Marburg virus: Results of two single-ascending-dose studies, *Antimicrob. Agents Chemother.*, **58** (2014), pp. 6639–6647.

[40] A. E. Heald *et al.*, AVI-7288 for Marburg virus in nonhuman primates and humans, *N. Engl. J. Med.*, **373** (2015), pp. 339–348.

[41] https://www.sarepta.com/our-product (accessed on 4th April, 2018)

[42] X. Qiu *et al.*, Reversion of advanced Ebola virus disease in nonhuman primates with ZMapp, *Nature*, **514** (2014), pp. 47–53.

[43] PREVAIL II Writing Group; Multi-National PREVAIL II Study Team; R. T. J. Davey, L. Dodd, M. A. Proschan, J. Neaton, J. Neuhaus Nordwall, J. S. Koopmeiners, J. Beigel, J. Tierney, H. C. Lane, A. S. Fauci, M. B. F. Massaquoi, F. Sahr, D. A. Malvy, Randomized, Controlled trial of ZMapp for Ebola virus infection, *N. Engl. J. Med.*, **375** (2016), 1448–1456.

[44] G. G. J. Olinger, J. Pettitt, D. Kim, C. Working, O. Bohorov, B. Bratcher, E. Hiatt, S. D. Hume, A. K. Johnson, J. Morton, M. Pauly, K. J. Whaley, C. M. Lear, J. E. Biggins, C. Scully, L. Hensley, L. Zeitlin, Delayed treatment of Ebola virus infection with plant-derived monoclonal antibodies provides protection in rhesus macaques, *PNAS*, **109** (2012), pp. 18030–18035.

[45] J. A. Wilson, M. Hevey, R. Bakken, S. Guest, M. Bray, A. L. Schmaljohn, M. K Hart, Epitopes involved in antibody-mediated protection from Ebola virus, *Science*, **287** (2000), pp. 1664–1666.

[46] F. Lasala, E. Arce, J. R. Otero, J. Rojo, R. Delgado, Mannosyl glycodendritic structure inhibits DC-SIGN-Mediated Ebola virus infection in cis and in trans, *Antimicrob. Agents Chemother*., **47** (2003), pp. 3970–3972.

[47] R. Ribeiro-Viana, M. Sánchez-Navarro, J. Luczkowiak, J. R. Koeppe, R. Delgado, J. Rojo, B. G. Davis, Virus-like glycodendrinanoparticles displaying quasi-equivalent nested polyvalency upon glycoprotein platforms potently block viral infection. *Nat. Commun.*, **3** (2012), p.1303.

[48] B. M. Illescas, J. Rojo, R. Delgado, N. Martín, Multivalent glycosylated nanostructures to inhibit Ebola virus infection, *J. Am. Chem. Soc.*, **139** (2017), pp. 6018−6025.

[49] Z. Jin, L. K. Smith, V. K. Rajwanshi, B. Kim; J. Deval, The Ambiguous base-pairing and high substrate efficiency of T-705 (favipiravir) ribofuranosyl 5′-triphosphate towards influenza A virus polymerase, *PLoS One*, **8** (2013), e68347.

[50] L. Oestereich, A. Lüdtke, S. Wurr, T. Rieger, C. Muñoz-Fontela, S. Günthera, Successful treatment of advanced Ebola virus infection with T-705 (favipiravir) in a small animal model, *Antiviral Research*, **105** (2014), pp. 17–21.

[51] D. Sissoko *et al.*, Experimental treatment with favipiravir for Ebola virus disease (the JIKI trial): A historically controlled, single-arm proof-of-concept trial in Guinea, *PLoS Med.*, **13** (2016), e1001967.

[52] T. K. Warren, J. Wells, R. G. Panchal, K. S. Stuthman, N. L. Garza, S. A. Van Tongeren, L. Dong, C. J. Retterer, B. E. Eaton, G. Pegoraro, S. Honnold, S. Bantia, P. Kotian, X. Chen, B. R. Taubenheim, L. W. Welch, D. M. Minning, Y. S. Babu, W. P. Sheridan, S. Bavari, Protection against filovirus diseases by a novel broad-spectrum nucleoside analogue BCX4430, *Nature*, **508** (2014), pp. 402−405.

[53] T. K. Warren, R. Jordan, M. K. Lo, A. S. Ray, R. L. Mackman, V. Soloveva, D. Siegel, M. Perron, R. Bannister, H. C. Hui, N. Larson, R. Strickley, J. Wells, K. S. Stuthman, S. A. Van Tongeren, N. L. Garza, G. Donnelly, A. C. Shurtleff, C. J. Retterer, D. Gharaibeh, R. Zamani, T. Kenny, B. P. Eaton, E. Grimes, L. S. Welch, L. Gomba, C. L. Wilhelmsen, D. K. Nichols, J. E. Nuss, E. R. Nagle, J. R. Kugelman, G. Palacios, E. Doerffler, S. Neville, E. Carra, M. O. Clarke, L. Zhang, W. Lew, B. Ross, Q. Wang, K. Chun, L. Wolfe, D. Babusis, Y. Park, K. M. Stray, I. Trancheva, J. Y. Feng, O. Barauskas, Y. Xu, P. Wong, M. R. Braun, M. Flint, L. K. McMullan, S.-S. Chen, R. Fearns, S. Swaminathan, D. L. Mayers, C. F. Spiropoulou, W. A. Lee, S. T. Nichol, T. Cihlar, S. Bavari, Therapeutic efficacy of the small molecule GS-5734 against Ebola virus in rhesus monkeys, *Nature*, **531** (2016), pp. 381–385.

[54] M. K. Lo, R. Jordan, A. Arvey, J. Sudhamsu, P. Shrivastava-Ranjan, A. L. Hotard, M. Flint, L. K. McMullan, D. Siegel, M. O. Clarke, R. L. Mackman, H. C. Hui, M. Perron, A. S. Ray, T. Cihlar, S. T. Nichol, C. F. Spiropoulou, GS-5734 and its parent nucleoside analog inhibit filo-, pneumo-, and paramyxoviruses, *Sci. Rep.*, **7** (**2017**), 43395.

[55] C. J. Shoemaker, K. L. Schornberg, S. E. Delos, C. Scully, H. Pajouhesh, G. G. Olinger, L. M. Johansen, J. M. White, Multiple cationic amphiphiles induce a Niemann-Pick C phenotype and inhibit Ebo-

la virus entry and infection, *PloS One*, **8**, (2013), e56265.

[56] L. M. Johansen, J. M. Brannan, S. E. Delos, C. J. Shoemaker, A. Stossel, C. Lear, B. G. Hoffstrom, L. Evans DeWald, K. L. Schornberg, C. Scully, J. Lehár, L. E. Hensley, J. M. White, G. G. Olinger, FDA-approved selective estrogen receptor modulators inhibit Ebola virus infection, *Sci. Transl. Med.*, **5** (2013), 190ra79.

[57] H. Fan, X. Du, J. Zhang, H. Zheng, X. Lu, Q. Wu, H. Li, H. Wang, Y. Shi, G. Gao, Z. Zhou, D.-X. Tan, X. Li, Selective inhibition of Ebola entry with selective estrogen receptor modulators by disrupting the endolysosomal calcium, *Sci. Rep.*, **7** (2017), 41226.

[58] Y. Zhao, J. Ren, K. Harlos, D. M. Jones, A. Zeltina, T. A. Bowden, S. Padilla-Parra, E. E. Fry, D. I. Stuart, Toremifene interacts with and destabilizes the Ebola virus glycoprotein, *Nature*, **535** (2016), pp. 169–172.

[59] Ž. Selaković, D. Opsenica, B. Eaton, C. Retterer, S. Bavari, J. C. Burnett, B. A. Šolaja, R. G. Panchal, A limited structural modification results in a significantly more efficacious diazachrysene-based filovirus inhibitor, *Viruses*, **4** (2012), pp. 1279–1288.

[60] Ž. Selaković, V. Soloveva, D. Gharaibeh, J. Wells, S. Šegan, R. G. Panchal, B. A. Šolaja, Anti-Ebola activity of diazachrysene small molecules, *ACS Inf. Dis.*, **1** (2015), pp. 264–271.

НАПРЕДОК ВО БОРБАТА ПРОТИВ ФИЛОВИРУСИ

Života Selaković[1,*], Bogdan Šolaja[2,*]

[1]Faculty of Chemistry, University of Belgrade, Belgrade, Serbia
[2]Serbian Academy of Sciences and Arts, Belgrade, Serbia
[*]e-mail: zivota_selakovic@chem.bg.ac.rs; bogdan.solaja@sanu.ac.rs

Филовирусите се вирулентни патогени кои предизвикуваат смртоносна хеморагична треска кај луѓето и нехумани примати. Засега не постои одобрен лек или вакцина за борба против оваа болест. Две платформи на вакцини што користат аденовируси ги имаат поминато испитувањата од фазата I, додека вакцината заснована на везикуларен стоматитен вирус успешно ја има поминто фазата III од испитувањата. Развиени се и сложени макромолекулски терапевтски средства, најпознатото од нив е засновано на антитела или на интерферентна RNA или на сурогати RNA. Најголем дел од малите молекули активни против филовирусите сè уште не се дојдени до фаза на клинички истражувања, освен фавипиравир, за кој е докажано дека е безбеден, и GS-5734, кој е влезен во фазата на истражувања.

Клучни зборови: ебола; Марбург; хеморагична треска; вакцини; мали молекули

ПРИЛОЗИ, Одделение за природно-математички и биотехнички науки, МАНУ, том **39**, бр. 2, стр. 91–101 (2018)
CONTRIBUTIONS, Section of Natural, Mathematical and Biotechnical Sciences, MASA, Vol. **39,** No. 2, pp. 91–101 (2018)

Received: November 3, 2018
Accepted: December 11, 2018

ISSN 1857–9027
e-ISSN 1857–9949
UDC: 544.22-386
DOI: 10.20903/csnmbs.masa.2018.39.2.122

Original scientific paper

DINUCLEAR COPPER(II) ACETATE COMPLEX WITH CAFFEINE, A FAST MECHANOCHEMICAL SYNTHESIS

Marina Tašner, **Draginja Mrvoš-Sermek***, **Emina Hajdarpašić**, **Dubravka Matković-Čalogović**

Department of Chemistry, Faculty of Science, University of Zagreb, Croatia
*e-mail: mrvos@chem.pmf.hr

A new dinuclear paddle-wheel copper(II) complex with caffeine was synthesized by the solvent-based and mechanochemical methods from copper(II) acetate and caffeine in a 1:1 molar ratio. Mechanochemical synthesis was found to be the fastest and easiest way to prepare the complex. The reaction proceeds with addition of small amounts of methanol or ethanol. The complex was characterized by FT-IR spectroscopy, elemental and thermoanalytical methods (TG and DSC) and X-ray diffraction methods. The molecular and crystal structure was determined by the single crystal X-ray diffraction method. The complex molecule consists of a centrosymmetric dinuclear unit, $[Cu_2(\mu\text{-}Ac)_4(caf)_2]$, with two copper(II) atoms bridged by four acetato groups, and *N*-coordinated caffeine (caf) molecules in the apical positions.

Key words: copper(II); paddle-wheel structure; caffeine; crystal structure; mechanochemical synthesis

INTRODUCTION

Caffeine (3,7-dihydro-1,3,7-trimethyl-1*H*-purine-2,6-dione) is a purine alkaloid with very interesting pharmacological properties as a therapeutic agent with analeptic activity. The coordination chemistry of the purine type ligands has been subjected to intensive studies because of the importance of the interaction between these ligands and metal ions in many biological systems [1, 2].

A few crystal structures of copper(II) compounds with caffeine (caf) in which the copper(II) atoms are five coordinated have been described. Two monomeric examples are triaqua(caf)nitratocopper(II) nitrite [3] and aqua(caf)dichlorocopper(II) [4]. Caffeine usually prefers the nitrogen atom as the donor atom, especially in the copper(II) carboxylate complexes [5–14] (see Table 1). In $[Cu_2(flufenamato)_4(caf)(H_2O)]$ [15] two copper(II) atoms are bridged by four carboxylato groups, but one apical ligand is a caffeine molecule and the other one is a water molecule. The only example in the series of dimeric copper(II) carboxylates where both apical position are occupied by *O*-coordinated caffeine molecules is $[Cu_2(3,5\text{-dinitrobenzoato})_4(caf)_2]$ [16]. The authors comment that the possible reason why this caffeine complex does not contain metal−N bonding is a steric effect caused by the size of the 3,5-dinitrobenzoato ligand.

In general, copper(II) carboxylates can contain a mononuclear, dinuclear or polynuclear structural unit. Scheme 1 shows some of the most frequently encountered coordination modes of carboxylate ligands in metal complexes.

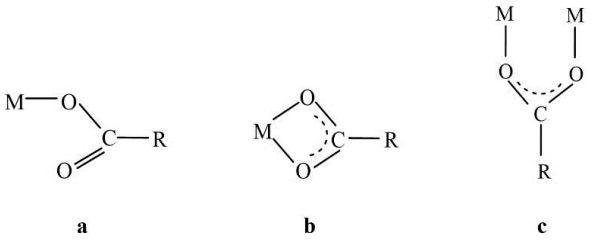

Scheme 1. Carboxylate coordination modes:
(a) monodentate; (b) chelate; (c) bidentate bridging

All of the dinuclear $[Cu_2(RCOO)_4XY]$ complexes, ($RCOO^-$ = carboxylate; X, Y = usually *N*- or *O*-donor ligands), have the paddle-wheel cage structure, as shown in Figure 1, in which each of the four carboxylate ligands is bound to both copper(II) ions in a bridging bidentate fashion. Each copper atom is coordinated by four oxygen atoms from the carboxylate ligands in the equatorial plane and can further accommodate a monodentate ligand, such as caffeine, in the apical position.

Some geometric parameters in the dinuclear complexes of the $[Cu_2(RCOO)_4(caf)_2]$ type, with caffeine as a *N*- or *O*-donor are presented in Table 1. In the Cambridge Structural Database (CSD) [17], Version 1.2.1 (2018), there are 12 such crystal structures. There is a relationship between the Cu···Cu distances and the distance of the copper(II) atom from the 4O equatorial basal plane towards the apical caffeine ligand, as the former is elongated the latter also increases. However, there is no relationship with the Cu-N bond length. The observed differences in the geometry of the paddle-wheel unit can be attributed to the influence of different $RCOO^-$ ligands.

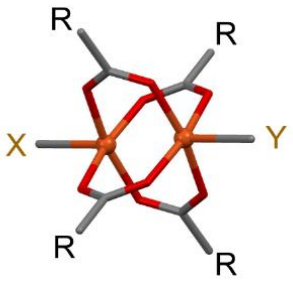

Figure 1. Drawing of a paddle-wheel unit. $RCOO^-$ = carboxylate, X and Y are usually *N*- or *O*-donor ligands. Copper atoms are shown as spheres.

Table 1. Summary data of the $[Cu_2(RCOO)_4(caf)_2]$ complexes

Refcode* /Formula or name of $RCOO^-$	*d*(Cu···Cu) / Å	*d*(Cu-O_{eq}) (av)** / Å	*d*(Cu-N_{ap}) / Å	Cu-4O_{eq} plane / Å	Ref.
KUBJUM $C_6H_5COO^-$	2.647(1)	1.967(2, 11)	2.222(3)	0.204	[5]
XIRCOQ (2*S*)-2-(6-methoxy-naphthalen-2-yl)propionato	2.649(1)	1.963(5, 16)	2.226(4)	0.216	[6]
QOPHOT $CH_3CH(Br)COO^-$ (monoclinic form)	2.6735(8)	1.943(4, 2)	2.183(5)	0.222	[7]
KIGMOD 2-[(2-Hydroxy-benzoyl)oxy]benzoato	2.680(1)	1.968(4, 15)	2.168(5)	0.219	[8]
REPVEO / $CH_3CH(Br)COO^-$ (triclinic form)	2.694(1)	1.966(5, 13)	2.231(7)	0.221	[9]
QOXLAQ 2-Iodobenzoato	2.7041(6)	1.966(2, 8)	2.238(2)	0.236	[10]
DAJVAL/ CH_2ClCOO^-	2.711(3)	1.98(4, 1)	2.23(4)	0.236	[11]
RERVAL $C_6H_5C(O)COO^-$	2.745(1)	1.975(4, 5)	2.161(5)	0.259	[12]
FOZKOM / CCl_3COO^- (benzene solvate)	2.852(2)	1.973(4, 17)	2.121(5)	0.315	[13]
KUHFUO / CCl_3COO^-	3.062(2)	2.011(2, 16)	2.0458(2)	0.415	[14]
			d(Cu-O_{ap}) / Å		
KELXEF 3,5-dinitrobenzoato	2.661(3)	1.958(2, 25)	2.180(3)	0.200	[16]
			d(Cu-O_{ap}) / Å *d*(Cu-N_{ap}) / Å		
KUHGUP*** / CCl_3COO^-	2.7364(9)	1.956(7, 12)	2.112(4) 2.115(4)	0.241	[14]

* in CSD

** the first number in parentheses is the e.s.d. and the second is the maximum deviation from the mean value

*** polymeric

Mechanochemical synthesis by neat grinding (NG) or liquid-assisted grinding (LAG), either done by using agate mortar and pestle or by ball-milling, is now a widely used method for synthesis without solvent or with just a small amount of a solvent. This is especially important in "green chemistry" by avoiding large amounts of organic solvents. In a review by Friščić and co-workers [18] syntheses by the NG or LAG methods resulting in different coordination polymers, metal-organic frameworks (MOFs) and metallodrugs have been discussed. They have shown that the reaction of copper(II) oxide with acetic acid by the LAG (water) method proceeded *via* an intermediate solvate of acetic acid with copper(II) acetate hydrate, which subsequently transformed into the final product copper(II) acetate hydrate [19]. Copper(II) acetate hydrate was also used in the first solvent-free synthesis of a porous MOF in a ball-milling reaction with isonicotinic acid. Technologically important porous framework HKUST-1, [$Cu_3(btc)_2$, btc = 1,3,5-benzenetricarboxylate], was obtained by grinding copper(II) acetate with 1,3,5-benzenetricarboxylic acid. In $Cu_3(btc)_2$ a pair of Cu^{2+} ions is chelated by four carboxylate bridges forming a paddle-wheel moiety. 1,3,5-benzenetricarboxylate is a linker molecule to three neighboring pairs of copper ions forming thus a 3D network [20, 21].

As a part of our interest in copper(II) complexes with molecules of biological importance [22, 23] we describe the synthesis and crystal structure of a new dinuclear copper complex tetrakis(μ-acetato-*O*:*O'*)-bis(1,3,7-trimethylpurine-2,6-dione) dicopper(II), [$Cu_2(\mu\text{-Ac})_4(caf)_2$], Ac = CH_3COO^- .

EXPERIMENTAL

General considerations

Chemicals were obtained from Sigma-Aldrich and used without previous purification. Elemental C, H, N analysis: Perkin-Elmer 2400 Series II CHNS analyzer in the Analytical Services Laboratories of the Ruđer Bošković Institute, Zagreb, Croatia. FT-IR spectra (KBr pellets): PerkinElmer Spectrum Two. TG and DTA curves were obtained by using Mettler-Toledo TGA/SDTA 851e module. The samples of about 2 to 5 mg were placed in aluminium pans (40 μl). The TGA and DTA curves were obtained with a heating rate of 10 °C min^{-1} under a oxygen flow of 200 ml min^{-1}. The samples were heated from room temperature up to 600 °C. DSC measurements were performed on a Mettler-Toledo DSC823^e module in aluminium pans (40 μl), heated in oxygen (200 ml min^{-1}) at a rate of 10 °C min^{-1}. The samples were heated from room temperature up to 500 °C. The data collection and analysis was performed using the program package STARe Software 9.01 [24]. A Retch MM200 grinder operating at 25 Hz frequency and teflon jars (14 ml in volume; using stainless steel grinding ball of 8 mm in diameter) were used for the grinding experiment.

Single-crystal X-ray diffraction

The single crystal X-ray diffraction data were collected at 293 K on an Oxford Diffraction Xcalibur 3 CCD diffractometer with graphite-monochromated MoK_α radiation (λ = 0.71073 Å). The data were reduced using CrysAlisPRO software package [25]. The solution, refinement, and analysis of the structure was done using the software integrated in the WinGX system [26]. The structure was solved by the Patterson method using SHELXS [27] and refined by the full-matrix least-squares method based on F^2 against all data (SHELXL) [28]. All non-hydrogen atoms were refined anisotropically. The hydrogen atoms were introduced in calculated positions and refined using the appropriate riding model. Geometrical calculations were made using PLATON [29] and molecular graphics were prepared using Mercury [30], ORTEP-3 [31] and POV-Ray [32]. The main crystallographic data with refinement details are summarized in Table 2.

Powder X-ray diffraction

Powder X-ray diffraction (PXRD) data were collected on a PANalytical Aeris diffractometer in the Bragg-Brentano geometry using CuK_α radiation. The sample was contained on a zero background Si plate. Patterns were collected in the scan range of 2θ = 5–50° with the step size of 0.0027° and at 9 s per step. The data were visualized using the HighScore Plus program [33].

Table 2. Crystal data and details of crystal structure refinement

Compound	**$[Cu_2(\mu\text{-}Ac)_4(caf)_2]$**
Formula	$C_{24}H_{32}Cu_2N_8O_{12}$
M_r	751.66
Habit and colour	prism, dark blue-green
Crystal dimension / mm^3	0.18 × 0.21× 0.39
Crystal system, space group	triclinic, P −1
a / Å	7.9252(2)
b / Å	9.1257(3)
c / Å	11.2138(3)
α / °	103.931(3)
β / °	100.629(2)
γ / °	99.372(3)
V / Å^3	755.17(4)
Z	1
D_c / g cm^{-3}	1.653
μ / mm^{-1}	1.483
F (000)	386
Θ range for data collection / °	4.147 − 29.497
h, k, l range	−10:10; −12:12; −15:15
No. of measured reflections	21467
No. independent reflections (R_{int})	4187
No. observed reflections, $I \geq 2\sigma(I)$	3889
R^a, wR^b [$I \geq 2\sigma(I)$]	0.0228
R, wR [all data]	0.0253
Goodness of fit on F^2, S^c	1.033
Max., min. electron density / e Å^{-3}	0.312, −0.208
Maximum Δ/σ	0.001
CCDC no.[d]	1873412

(a) $R = \Sigma||F_o| - |F_c| / \Sigma|F_o|$
(b) $wR = [\Sigma(F_o^2 - F_c^2)^2 / \Sigma w(F_o^2)^2]^{1/2}$
(c) $S = \Sigma[w(F_o^2 - F_c^2)^2 / (N_{obs} - N_{param})]^{1/2}$
(d) CCDC number contains the supplementary crystallographic data for this paper.
These data are provided free of charge by the Cambridge Crystallographic Data Centre.

Synthesis of $[Cu_2(\mu\text{-}Ac)_4(caf)_2]$

Mechanochemical synthesis: the liquid-assisted grinding method was used. Copper(II) acetate monohydrate (0.199 g, 1 mmol) and caffeine (0.194 g, 1 mmol) were weighed into a teflon jar, and 2 drops of methanol or ethanol were added. Milling was performed at room temperature for 1 hour.

Slurry method: neat grinding was performed by grinding copper(II) acetate (0.199 g, 1 mmol) and caffeine (0.194 g, 1 mmol) with a mortar and pestle for 15 min. A homogenized mixture of copper(II) acetate monohydrate and caffeine is obtained in this way (Fig. 2a, left). If two drops of methanol are added while grinding (LAG/MeOH) the powder is still only the mixture of reactants. The powder was then mixed with a few drops of methanol or ethanol in an Eppendorf tube to form a slurry. A change in color from cyan to dark blue-green occurs very fast. The reaction is completed in minutes (Figure 2a, right).

Solution–based synthesis: a solution of caffeine (0.194 g, 1 mmol) in 15 ml methanol (or ethanol) was added to a solution of copper(II) acetate monohydrate (0.199 g, 1 mmol) in 12 ml methanol. The mixture was heated to 60° and refluxed for 1 hour and then left to cool at room temperature.

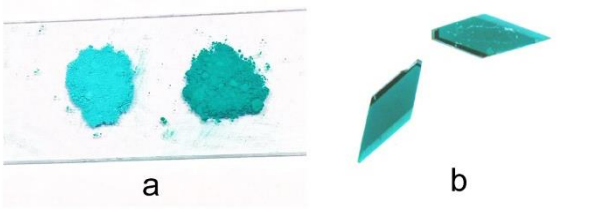

Figure 2. a) Powder on the left (light blue-green; cyan) was obtained after NG or LAG (mortar and pestle) for 15 min. It is a mixture of copper(II) acetate monohydrate and caffeine. Powder on the right is that of $[Cu_2(\mu\text{-}Ac)_4(caf)_2]$, obtained after addition of methanol or ethanol to the NG/LAG powder to form a slurry. It is of dark blue-green color.
b) Single crystals of $[Cu_2(\mu\text{-}Ac)_4(caf)_2]$ obtained by the solution–based synthesis.

Dark blue-green crystals were isolated by filtration, washed several times with cold ethanol and dried in air (Figure 2b). Anal. $C_{24}H_{32}N_8O_{12}Cu_2$ (751.66). Calc′d: C 38.34; H 4.26; N 14.91 %. Found: C 38.20; H 4.22; N 14.85 %.

RESULTS AND DISCUSSION

Synthesis

The complex was obtained by the reaction of copper(II) acetate monohydrate, $Cu(Ac)_2{\cdot}H_2O$, and caffeine ($C_8H_{10}N_4O_2$) in a 1:1 molar ratio both by the solution–based method in methanol and mechanochemically by the LAG method with methanol or ethanol in a ball mill (Scheme 2). Taking into account the proper formula of the dimeric complex of copper(II) acetate monohydrate, $[Cu_2(\mu\text{-}Ac)_4(H_2O)_2]$, the ratio to caffeine is 1:2. It was found that the exchange of the two coordinated H_2O molecules with caffeine molecules occurs only by the assistance of methanol or ethanol.

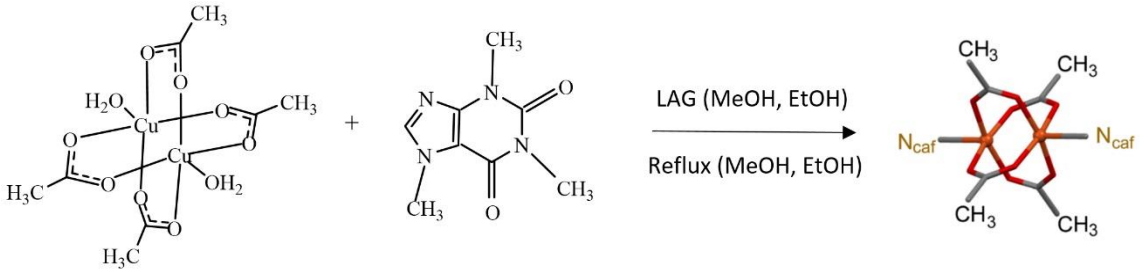

Scheme 2. Synthesis of $[Cu_2(\mu\text{-}Ac)_4(caf)_2]$

Several other mechanochemical procedures were tried and the reaction products were monitored by PXRD. Neat grinding (NG) and LAG of copper(II) acetate monohydrate (Figure 3a) and caffeine (Figure 3b) in the 1:1 ratio with added water ground with a mortar and pestle were performed for 15 min. Such short grinding with or without addition of water resulted only in the mixture of copper(II) acetate and caffeine (Figure 3c). The same procedure was tried with LAG (methanol) but such short grinding with no compensation done for evaporation of methanol resulted in the same mixture. To obtain the complex with caffeine this mixture had to be soaked with methanol or ethanol to form a slurry (Figure 3g). PXRD pattern of the product of LAG for 1 hour in a ball mill with added water showed presence of copper(II) acetate monohydrate, however the highest caffeine peak almost disappeared and two new low angle peaks formed that could not be assigned, but there were no peaks of the caffeine complex (Figure 3d). On contrary, LAG with methanol or ethanol in a ball mill for 1 hour resulted in the caffeine complex $[Cu_2(\mu\text{-}Ac)_4(caf)_2]$ (Figure 3h). The same complex was obtained by the solution-based method which gave single-crystals suitable for the crystal structure determination (Figure 3i).

Tella *et al*. [34] have recently published a synthesis of $[Cu(caf)_2(H_2O)(Ac)]Ac$ by both mechanochemical and solution–based methods, however the molar ratio of $Cu(Ac)_2{\cdot}H_2O$ and caffeine was 1:2 ($[Cu_2(\mu\text{-}Ac)_4(H_2O)_2]$:caffeine = 1:4). Therefore, during this synthesis the dinuclear paddle-wheel unit would be broken and a mononuclear complex obtained. The authors have characterized this complex by elemental analysis, FT-IR, UV–Vis and 1H NMR spectra but not by the single-crystal X-ray diffraction. The proposed structure consists of copper atom coordinated with two bidentately donating caffeine ligands through the nitrogen atom of the imidazole group and the oxygen atom of the pyrimidine group, a water molecule and an acetate ligand. One acetate is proposed to be a free anion. A caf-

feine molecule to be bidentately coordinating one copper atom we consider highly unlikely. In our opinion only a polymeric structure would be possible. We followed their synthetic procedure (1 mmol of copper(II) acetate and 2 mmol of caffeine were ground together with a mortar and pestle for 15 min; a bluish-green powder was washed with methanol) and collected the PXRD pattern of the product before washing with methanol and obtained only a mixture of copper(II) acetate monohydrate and caffeine, with more caffeine than in our 1:1 synthesis (Figure 3e). Upon washing with a small amount of methanol the same caffeine complex is formed as in our synthesis but there is an excess of unreacted caffeine (Figure 3f). There are no peaks that correspond to their powder pattern. It has to be noted that they have made an error and instead of a powder pattern of copper(II) acetate monohydrate they gave a pattern of copper(II) chloride dihydrate.

Contrary to Tella *et al*., the same complex as ours was obtained by a solution-based method in ethanol (reflux for 4 hours) by Hamdani *et al.* [35]. The ratio of copper(II) acetate monohydrate and caffeine was 1:2, and not 1:1 as in our synthesis.

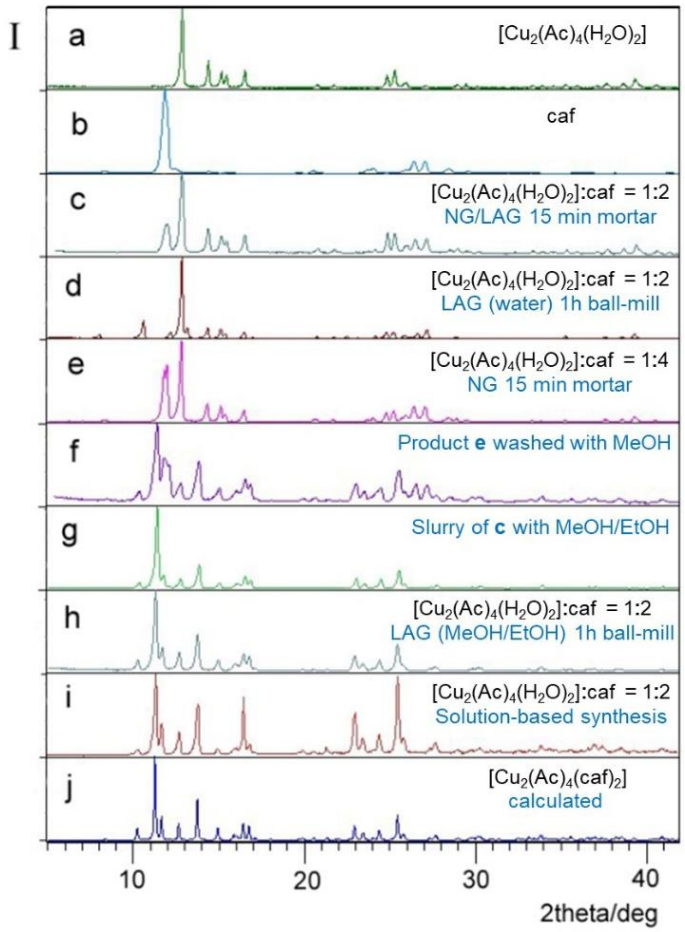

Figure 3. Powder diffractograms of: (a) copper(II) acetate monohydrate ($Cu(Ac)_2 \cdot H_2O = [Cu_2(\mu\text{-}Ac)_4(H_2O)_2]$); (b) caffeine; (c) product of NG or LAG (water) for 15 min by hand; (d) product of LAG (water) for 1 hour in a ball-mill; (e) product of NG for 15 min by hand (procedure by Tella *et al*.); (f) product (e) washed with MeOH; (g) product (c) with added MeOH or EtOH to form a slurry; (h) product of LAG (MeOH or EtOH) for 1 hour in a ball mill; (i) solution-based synthesis; (j) calculated powder pattern from the crystal structure of $[Cu_2(\mu\text{-}Ac)_4(caf)_2]$.

FT-IR spectroscopy

Table 3 presents the most important IR spectral bands for caffeine, copper(II) acetate monohydrate and $[Cu_2(\mu\text{-}Ac)_4(caf)_2]$ obtained *via* the solution–based and mechanochemical methods. The carboxylate stretching frequencies $\nu(-COO^-)_{asym}$ at 1620 cm^{-1} and $\nu(-COO^-)_{sym}$ at 1426 cm^{-1} are characteristic for copper(II) carboxylate compounds [15, 36, 37] (Figure 4). The two strong band at 1700 cm^{-1} and 1660 cm^{-1} were attributed to $\nu(CO)_{asym}$ and $\nu(CO)_{sym}$ / $\nu(-C=N)$ in free caffeine, the latter

shifted to 1650 cm^{-1} in the copper complex. The δ(HCN) + ν_{ring}(imid) + ν_{ring}(pyrim) stretching and deformation of the heterocyclic imidazol and pyrimidine fragments was found at 1550 cm^{-1} [38, 39]. This band shifted to 1541 cm^{-1} in the complex indicating that the (C=N) imidazole fragment of caffeine is involved in coordination with the metal ion through the N9 nitrogen atom. Hamdani *et al*. obtained the same IR spectrum as ours indicating that they also prepared $[Cu_2(\mu\text{-}Ac)_4(caf)_2]$.

Table 3. Characteristic IR bands (cm^{-1}) in caffeine, copper(II) acetate monohydrate and $[Cu_2(\mu\text{-}Ac)_4(caf)_2]$

Caffeine	Copper(II)acetate monohydrate	$[Cu_2(\mu\text{-}Ac)_4(caf)_2]$	Attribution
1700		1700	$\nu(-C=O)_{asym}$
1660		1650	$\nu(-C=O)_{sym}/\nu(-C=N)$
1550		1541	δ(HCN) + ν_{ring}(imid) + ν_{ring}(pyrim)
	1610 1590	1620	$\nu(-COO^-)_{asym}$
	1435 1415	1426	$\nu(-COO^-)_{sym}$

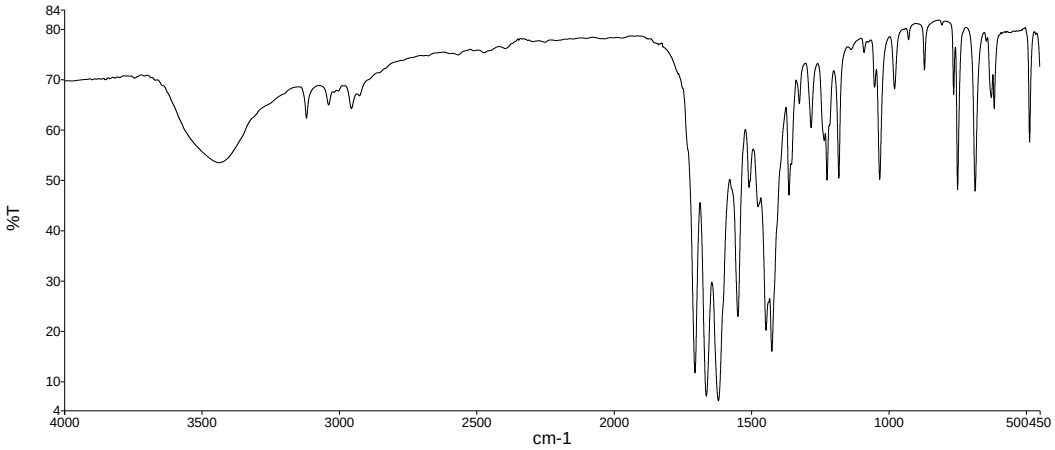

Figure 4. Infrared spectra of $[Cu_2(\mu\text{-}Ac)_4(caf)_2]$ obtained *via* the solution–based or mechanochemical method (LAG, MeOH)

Thermal analysis

Complex $[Cu_2(\mu\text{-}Ac)_4(caf)_2]$ was heated from room temperature to 600 °C (TG) and from room temperature to 500 °C (DSC) in an oxygen atmosphere. The TG curve of the complex shows two degradation steps. The first step between 234 and 272 °C is accompanied by a 32.3 % weight loss (calculated 31.4 %) corresponding to the elimination of the acetato ligands. This step is represented by two exothermic peaks at 255 and 287 °C on the DSC curve. Three exothermic peaks with maxima at 363, 368 and 375 °C are associated with the elimination of two caffeine molecules (observed weight loss 45.1 %, calculated 51.6 %). The remaining residue of 21.5 % at 600 °C is CuO.

X-ray crystal structure

The X-ray structure of $[Cu_2(\mu\text{-}Ac)_4(caf)_2]$ is depicted in Figure 5. The complex molecule contains the dinuclear paddle-wheel unit with two copper atoms and four bridging acetate ligands. It is centrosymmetric with the center of inversion located between the two copper atoms so there is a half of the molecule in the asymmetric unit. Each of the copper(II) atoms is coordinated by four acetato groups as equatorial ligands and one nitrogen atom from the caffeine ligand, localised at the apex of a distorted square pyramid.

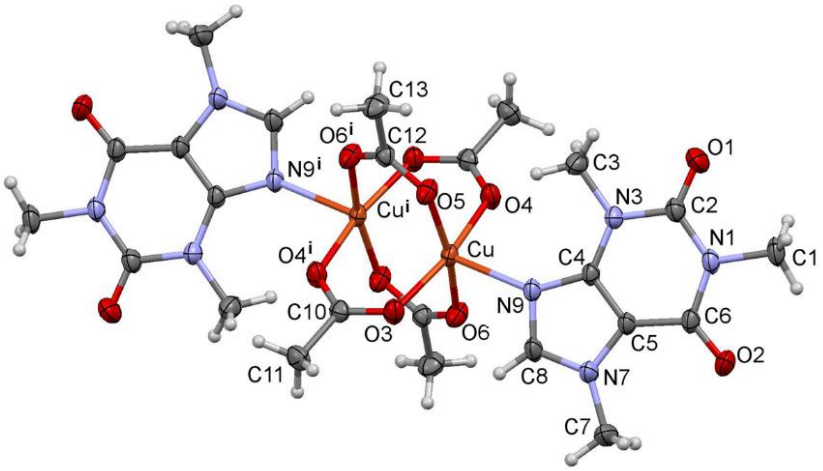

Fig. 5. Molecular structure of $[Cu_2(\mu\text{-}Ac)_4(caf)_2]$ with the atom labeling scheme. Symmetry code: *i* = 1-*x*, 1-*y*, -*z*. The ellipsoids are at the 40 % probability level. Hydrogen atoms are depicted as spheres of arbitrary radii.

The Cu···Cu distance of 2.6350(3) Å is the shortest one among the known dinuclear $[Cu_2(RCOO)_4(caf)_2]$ complexes (Table 1). The displacement of the Cu atom from the equatorial plane (atoms O3−O6) toward the apical atom of N(9) amounts to 0.202(1) Å. The apical Cu−N(caf) bond length is 2.2585(10) Å being the longest one in comparison to other complexes (Table 1). Each Cu(II) ion has four oxygen atoms from different carboxylate groups in the equatorial positions, with Cu−O distances in the range from 1.9689(10) to 1.9716(10) Å, Table 4. These values are comparable to those found in other Cu(II) carboxylates.

The geometry of the caffeine ligand linked to the metal center indicates delocalization of π- electrons within the pyrimidine and imidazole ring of caffeine. Both rings are planar with a maximum deviation of N9 amounting to 0.025(1) Å from the least-squares plane through the ring atoms. Maximum ring substituent deviation from this plane is that of C(3) being 0.066(2) Å.

The complex structure is stabilized by weak C3-H···O5 intramolecular hydrogen bond. There are also only weak intermolecular hydrogen bonds of the C-H···O type interconnecting the complex molecules in a 3D structure since C-H groups are the only available hydrogen bond donors. The relevant characteristics of H-bonds are given in Table 5 and the packing is shown in Figure 6.

Table 4. Selected bond distances (Å) and valence angles (°) for $[Cu_2(\mu\text{-}Ac)_4(caf)_2]$

Bond distances	
Cu−O3	1.9716(10)
Cu−O4	1.9554(10)
Cu−O5	1.9624(10)
Cu−O6	1.9689(10)
Cu−N9	2.2585(10)
Bond angles	
O3−Cu−O4	168.02(4)
O3−Cu−O5	90.96(5)
O3−Cu−O6	87.43(5)
O5−Cu−O6	168.31(4)
O3−Cu−N9	95.24(4)
O4−Cu−N9	96.51(4)
O5−Cu−N9	99.38(4)
O6−Cu−N9	92.30(4)

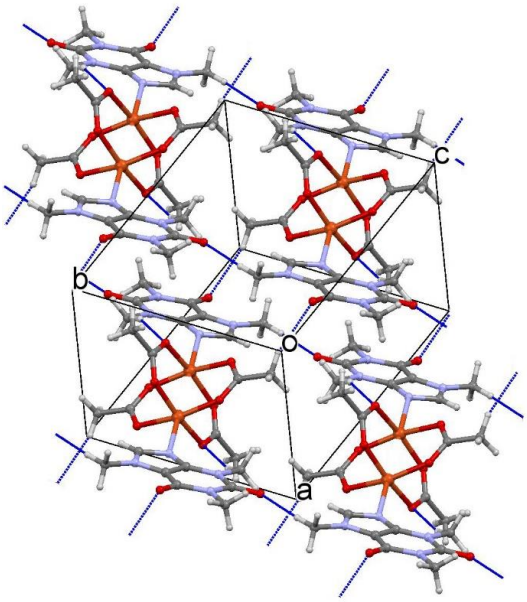

Figure 6. Packing diagram of $[Cu_2(\mu\text{-}Ac)_4(caf)_2]$ in the unit cell. Hydrogen bonds are shown by blue dotted lines.

Table 5. Hydrogen bonding parameters

	Distance /Å			Angle /°	
D−H···A	D−H	H···A	D···A	D−H···A	Symmetry code
C3−H···O5	0.96	2.49	3.4028(19)	159	
C7−H···O1	0.96	2.28	3.232(2)	172	$x, -1+y, z$
C11−H···O2	0.96	2.53	3.451(2)	161	$1-x, 1-y, 1-z$

CONCLUSION

By direct reaction of copper(II) acetate monohydrate with caffeine in the 1:1 molar ratio, either by the solution-based method or mechanochemically (LAG with methanol or ethanol) the dinuclear complex, $[Cu_2(\mu\text{-}Ac)_4(caf)_2]$, was prepared. It was found that the addition of methanol or ethanol is necessary for the formation of the complex since NG or LAG with water did not result in the complex formation. We have found that the replacement of water molecules by caffeine molecules in the paddle-wheel copper(II) acetate complex proceeds also in a slurry at room temperature only by the addition of a few drops of methanol or ethanol to the homogenized mixture of the reactants (with a mortar and pestle for 15 min). This is the fastest and easiest way to prepare the complex. The obtained complex consists of the paddle-wheel dimeric $Cu_2(O_2CCH_3)_4$ unit with *N*-coordinated caffeine molecules in both apical positions. Each copper(II) atom is five coordinated (distorted square-pyramidal) with four oxygen atoms from four acetato anions in the equatorial positions and the caffeine N atom in the apical position (Cu-N 2.2585(10) Å). The Cu···Cu distance is 2.6350(3) Å. The copper(II) atoms are displaced from the O4 equatorial plane by 0.202(1) Å toward the apical N-atom of caffeine.

Acknowledgment. We thank the Croatian Science Foundation for funding the project IP-2014-09-4274.

REFERENCES

[1] M. Melnik, O. Sprusansky, P. Musil, Bio-medical aspects of purine alkaloids, *Adv. Biol. Chem.*, **4** (2014), pp. 274–280.

[2] S. V. Paston, A. M. Polyanichko, O. V. Shulenina, Study of DNA interactions with Cu^{2+} and Mg^{2+} ions in the presence of caffeine, *J. Struct. Chem.*, **58** (2017), pp. 399–405.

[3] M. B. Cingi, A. Ch. Villa, A. G. Manfredotti, C. Guastini, Crystal structure of triaquanitratocaffeinecopper(II) nitrite monohydrate, *Cryst. Struct. Commun.*, **1** (1972), pp. 363–365.

[4] G. Bandoli, M. B. Cingi, D. A. Rizzardi, Preparation, crystal and molecular structure of aquadichlorocaffeinecopper(II), *Inorg. Chim. Acta*, **20** (1976), pp.71–76.

[5] T. Kawata, H. Uekusa, S. Ohba, T. Furukawa, T. Tokii, Y. Muto, M. Kato, Magneto-structural correlation in dimeric copper(II) benzoates, *Acta Cryst.*, B**48** (1992), pp. 253–261.

[6] M. Koman, M. Melnik, J. Moncol′, T. Glowiak, Caffeine in copper(II) complexes: crystal and molecular structure of di(caffeine)tetrakis(naproxenato)dicopper(II), *Inorg. Chem. Commun.*, **3** (2000), pp. 489–492.

[7] F. Valach, M. Tokarčik, M. Melnik, Distortion isomerism and plasticity of the coordination sphere of binuclear Cu(II) complexes: Crystal structure of the monoclinic isomer of $[Cu_2(2\text{-bromopropionato})_4(caffeine)_2]$, *Journal of Coord. Chem.* **62** (2009), pp. 225–233.

[8] Z. Ma, B. Moulton, Supramolecular medicinal chemistry: mixed-ligand coordination complexes, *Mol. Pharmaceutics*, **4** (2007), pp. 373–385.

[9] F. Valach, M. Melnik, G. Bernardinelli, K. K. Fromm, A structural study of copper(II) carboxylates: crystal structure and physical characterization of $[Cu_2(2\text{-bromo-propionato})_4(caffeine)_2]$, *J. Chem. Crystallogr.*, **36** (2006), pp. 571–579.

[10] F. Valach, M. Tokarčik, T. Maris, D. J. Watkin, C. K. Prout, Bond-valence approach to the copper-copper and copper-nitrogen bonding in binuclear copper(II) complexes: Structure of tetrakis(2-iodobenzoato)bis(caffeine)dicopper(II) at 210 K, *J. Organomet. Chem.*, **622** (2001), pp. 166–171.

[11] B. Koreň, F. Valach, P. Sivý, M. Melnik, Structures of binuclear copper(II) chloroacetate complexes: tetrakis(μ-monochloroacetato-*O,O′*)-bis[3,7-dihydro-1,3,7-trimethyl-1*H*-purine-2,6-dione)copper(II)], $[Cu_2(C_2H_2ClO_2)4(C_8H_{10}N_4O_2)_2]$, *Acta Cryst.*, C**41** (1985), pp. 1160–1162.

[12] A. Harada, M. Tsuchimoto, S. Ohba, K. Iwasawa, T. Tokii, Structures and magnetic properties of dimeric copper(II) benzoylformates, *Acta Cryst.*, B**53** (1997), pp. 654–661.

[13] H. Horie, S. Husebye, M. Kato, E. A. Meyers, Y. Muto, I. Suzuki, T. Tokii, R. A. Zingaro, The magnetic properties of three copper(II) trichloroacetate; Adducts with caffeine and the crystal structure of dicaffeinetetrakis(μ-trichloroacetato)dicopper(II)dibenzene solvate, $[Cu(CCl_3COO)_2(C_8H_{10}N_4O_2)_2]_2 \cdot 2C_6H_6$, *Acta. Chem. Scand. A*, **40** (1986), pp. 579–589.

[14] H. Uekusa, S. Ohba, T. Tokii, Y. Muto, M. Kato, S. Husebye, O.W. Steward, S.-C. Chang, J. P. Rose, F. Pletcher, I. Suzuki, Magneto-structural correlations of dimeric copper(II) trichloroacetates, *Acta Cryst.*, B**48** (1992**),** pp. 650–667.

[15] M. Melnik, M. Koman, T Glowiak, Structure, spectral and magnetic behaviours of tetrakis(flufenamato)(caffeine)(aqua)dicopper(II). The firs example of two nonequivalent ligands at the apex, *Polyhedron*, **17** (1998), pp.1767–1771.

[16] P. Stachová, J. Moncol, D. Valigura, T. Lis, Unusual *O*-coordination of caffeine in tetrakis(μ-3,5-dinitrobenzoato-κ^2O:O')bis[(caffeine-κO)copper(II)], *Acta Cryst.*, C**62** (2006), pp. m375–m377.

[17] C. R. Groom, I. J. Bruno, M. P. Lightfoot and S. C. Ward, *Acta Cryst.*, B**72** (2016), pp. 171–179.

[18] T. Friščić, I. Halasz, V.Štrukil, M. Eckert-Maksić, R. E. Dinnebier, Clean and efficient synthesis using mechanochemistry: coordination polymers, metal-organic frameworks and metallodrugs, *Croat. Chem. Acta*, **85**(3) (2012), pp. 367–378.

[19] F. C. Strobridge, N. Judaš, T. Friščić, A stepwise mechanism and the role of water in the liquid-assisted grinding synthesis of metal–organic materials, *CrystEngComm* **12** (2010), pp. 2409−2418.

[20] A. Pichon, S. L. James, An array-based study of reactivity under solvent-free mechanochemical conditions — insights and trends, *CrystEngComm*, **10** (2008) pp. 1839–1847.

[21] W. Yuan, A. L. Garay, A. Pichon, R. Clowes, C. D. Wood, A. I. Cooper, S. L. James, Study of mechanochemical formation and resulting properties of an archetypal MOF: $Cu_3(BTC)_2$ (BTC = 1,3,5-benzenetricarboxylate), *CrystEngComm*, **12** (2010) pp. 4063–4065.

[22] J. Pejić, D. Vušak, G. Szalontai, B. Prugovečki, D. Mrvoš-Sermek, D. Matković-Čalogović, J. Sabolović, Disorder at the chiral Cα center and room-temperature solid-state cis–trans isomerization; synthesis and structural characterization of copper(II) complexes with D-allo, L-isoleucine, *Cryst. Growth Des*., **18** (2018), pp. 5138–5154.

[23] D. Vušak, B. Prugovečki, D. Milić, M. Marković, I. Petković, M. Kralj, D. Matković-Čalogović, Synthesis and crystal structure of solvated complexes of copper(II) with serine and phenanthroline and their solid-state-to-solid-state transformation into one stable solvate. *Cryst. Growth Des.* **17** (2017), pp. 6049–6061.

[24] STARe Software V.9.01., MettlerToledo GmbH, (2006).

[25] CrysAlisPro Software System, Version 1.171.39.19; Rigaku Oxford Diffraction (2017).

[26] L. J. Farrugia, *J. Appl. Crystallogr*., **45** (2012), pp. 849-854.

[27] G. M. Sheldrick, A short history of SHELX, *Acta Cryst.*, A**64** (2008), pp. 112-122.

[28] G. M. Sheldrick, Crystal structure refinement with SHELXL, *Acta Cryst.*, C**71** (2015), pp. 148-155.

[29] A. Spek, Structure validation in chemical crystallography, *Acta Cryst.*, D**65** (2009), pp. 148−155.

[30] C. F. Macrae, I. J. Bruno, J. A. Chisholm, P. R. Edgington, P. McCabe, E. Pidcock, L. Rodriguez-Monge, R. Taylor, J. van de Streek, P. A. Wood, Mercury CSD 2.0 – new features for the visualization and investigation of crystal structures, *J. Appl. Crystallogr*., **41** (2008), pp. 466−470.

[31] L. J. Farrugia, ORTEP-3 for Windows – a version of ORTEP-III with a Graphical User Interface (GUI), *J. Appl. Crystallogr*., **30** (1997) pp. 565−566.

[32] POV-Ray, version 3.6; Persistence of Vision Pty. Ltd., Persistence of Vision Raytracer, (2004), available at http://www.povray.org/.

[33] T. Degen, M. Sadki, E. Bron, U. König, G. Nénert, *Powder Diffraction*, Supplement S2, **29** (2014), pp. S13-S18.

[34] A. C. Tella, J. A. Obaleye, U. B. Eke, A. Y. Isaac, O. M. Ameen, Solvent-free synthesis, X-ray studies and in vitro inhibitory activities of copper(II) complexes of non-steroidal anti-inflammatory drugs, *Res. Chem. Intermed*, **40** (2014), pp. 1441–1457.

[35] H. EL Hamdani, M. EL. Amane, Y. Kennouche, M. Bouhdada, A. Ahmami, M. Hadad, Synthesis and characterization of the mixed ligand complexes $[M(Ac)_2(caf)_2]$ M=Ni(II), Co(II), Zn(II), $[Cu_2(\mu\text{-}Ac)_4(caf)_2]$, Ac=$CH_3COO^-$, caf=caffeine, *J. Mar. Chim. Heterocycl*., **15** (2016), pp. 41–49.

[36] M. Melnik, Binuclear caffeine adducts of Cu(II) acetate and Cu(II) chloroacetates with unusually high antiferromagnetic interaction, *Inorg. Nucl. Chem*., **43** (1981), pp. 3035–3038.

[37] S. J. Jenniefer, P. T. Muthiah, Synthesis, characterization and X-ray structural studies of four copper(II) complexes containing dinuclear paddle wheel structures, *Chem. Cent. J.*, **7** (2013), pp. 1–15.

[38] K. Nakamoto, *Infrared Spectra of Inorganic and Coordination Compounds*, J. Wiley & Sons., Inc. New York, 2009.

[39] F. Ucun, A. Sağlam, V. Güçlü, Molecular structures and vibrational frequencies of xanthine and methyl derivatives (caffeine and theobromine) by abinitio Hartree-Fock and density functional theory calculations, *Spectrochim. Acta* Part A, **67** (2007), pp. 342–349.

БИНУКЛЕАРЕН БАКАРЕН(II) АЦЕТАТЕН КОМПЛЕКС СО КОФЕИН, БРЗА МЕХАНОХЕМИСКА СИНТЕЗА

Marina Tašner, **Draginja Mrvoš-Sermek***, **Emina Hajdarpašić**, **Dubravka Matković-Čalogović**

Department of Chemistry, Faculty of Science, University of Zagreb,
Horvatovac 102a, 10 000 Zagreb, Croatia

e-mail: mrvos@chem.pmf.hr;

Синтетизиран е нов бинуклеарен пропелерски тип (paddle-wheel) на бакарен(II) комплекс со кофеин со помош на механохемиски метод заснован на растворувач, а поаѓајќи од бакар(II) ацетат и кофеин во моларен сооднос 1:1. Најдено е дека механохемиската синтеза е најбрз и најлесен начин за подготовка на комплексот. Реакцијата се одвива со додавање на мало количество метанол или етанол. Комплексот е карактеризиран со помош на FT-IR спектроскопија, анализа на хемиските елементи, термоаналитички методи (TG and DSC) и метод на рендгенска дифракција. Молекулската и кристалнта структура се определени со помош на рендгенска дифракција од монокристал. Комплексната молекула се состои од центросиметрична бинуклеарна единка од типот $[Cu_2(\mu\text{-}Ac)_4(caf)_2]$, што ја чинат два бакарни(II) атома премостени преку четири ацетатни групи, како и *N*-координирани кофеински (caf) молекули во апикални положби.

Клучни зборови: бакар(II); пропелерска (paddle-wheel) структура; кофеин; кристална структура; механохемиска синтеза

ПРИЛОЗИ, Одделение за природно-математички и биотехнички науки, МАНУ, том **39**, бр. 2, стр. 103–121 (2018)
CONTRIBUTIONS, Section of Natural, Mathematical and Biotechnical Sciences, MASA, Vol. **39,** No. 2, pp. 103–121 (2018)

Received: September 30, 2018
Accepted: November 13, 2018

ISSN 1857–9027
e-ISSN 1857–9949
UDC: 543.552
DOI: 10.20903/csnmbs.masa.2018.39.2.123

Review

RECENT ADVANCES AND PROSPECTS OF SQUARE-WAVE VOLTAMMETRY

Valentin Mirčeski[1,2,*] , Leon Stojanov[1], Sławomira Skrzypek[2]

[1]Institute of Chemistry, Faculty of Natural Sciences and Mathematics
Ss. Cyril and Methodius University, Skopje, Republic of Macedonia
[2] Department of Inorganic and Analytical Chemistry, Faculty of Chemistry,
University of Lódż, Poland
[*]e-mail: valentin@pmf.ukim.mk

This review concerns recent methodological advances of square-wave voltammetry as one of the most sophisticated members of the pulse voltammetric techniques. Besides addressing recent theoretical works and representatives of advanced analytical studies, an emphasis is given to a few novel methodological concepts such as kinetic analysis at constant scan rate, cyclic square-wave voltammetry, multisampling square-wave voltammetry, and electrochemical faradaic spectroscopy. For the purpose of improving analytical performances of the technique two new methods are proposed for the first time.

Key words: square-wave voltammetry; electrode mechanisms; electrode kinetics

INTRODUCTION

Square-wave voltammetry (SWV) is a well-known and versatile voltammetric technique for analytical application, mechanistic studies and kinetic measurements of electrode processes [1–3]. It is a member of the large family of pulse voltammetric techniques, and it can be considered as a special form of the popular differential pulse voltammetry [4]. In a historical perspective the technique originates from the Kalousek commutator [5] and Barker square-wave polarography [6–8]. The popularity of the technique has been permanently increasing since the seminal work of Osteryoungs [9, 10], remarkable theoretical work of Lovrić [11] and contributions of others [12–24]. Methodological development and application of the technique have been reviewed over the years [25–36] and two specialized monographs are exclusively dedicated to SWV [1, 37].

Basic features of the potential modulation, together with the simulated response in the course of experiment, are depicted in Figure 1. In the contemporary SWV, the potential modulation comprises of a staircase potential combined with square-shaped potential pulses (Figure 1A), which was first introduced by Ramaley and Krause [38, 39]. The main parameters of the potential cycle, composed of two neighbouring pulses (Figure 1B), are the height of the pulses (referred to as SW amplitude, E_{sw}) and the duration of the single potential cycle τ (Figure 1B). Commonly, the duration of a potential cycle is expressed in terms of SW frequency (f), defined as $f = 1/\tau$. In terms of the duration of a potential pulse t_p ($\tau = 2t_p$), the frequency could be defined as $f = 1/(2t_p)$. The physical meaning of the frequency, as critical time parameter, can be understood as a number of potential cycles in a unit of time. Besides, the scan rate of the overall experiment can be defined as $v = f\Delta E$, where ΔE is the step of the staircase potential (cf. Figure 1B).

Relative to the direction of the staircase modulation, forward and reverse (backward) potential pulses can be distinguished. In the course of each potential cycle the electrode reaction is driven in both anodic and cathodic directions by the two opposite pulses, thus providing an insight into the electrode mechanism. In the course of the experiment, the current varies with time as theoretically predicted in Figure 1C. However, it is not the real outcome

of the experiment as the current sampling is done at the end of each potential pulse only, aiming to discriminate against the charging current [1, 10]. The forward (I_f) and backward (reverse) (I_r) component of the SW voltammogram (Figure 1D) correspond to the currents associated to the forward and backward potential pulses, respectively (cf. Figure 1C). An important feature of the SW voltammetric response is that both forward and backward components are plotted versus the potential of the staircase modulation, i.e. the mid potential of the two adjoining pulses (cf. Figure 1B). For these reasons two current values are assigned to each potential value of the staircase modulation. The net SW component (I_{net}) (cf. Figure 1D) is calculated by subtracting the backward from the forward currents, which most frequently is a bell-shaped curve, enabling precise determination of the position (E_p – net peak potential) and the height (net peak current ΔI_p) (Figure 1D).

Besides addressing recent representative examples from the field of theory and analytical application of the technique, the current review focuses mainly on the methodological development achieved in the last several years. A few promising methods in the direction of expanding and facilitating the application of the technique for mechanistic and kinetic analysis of electrode processes are addressed. In the end, for the purpose of improving analytical performances of the technique two new methodological concepts are elaborate briefly for the first time.

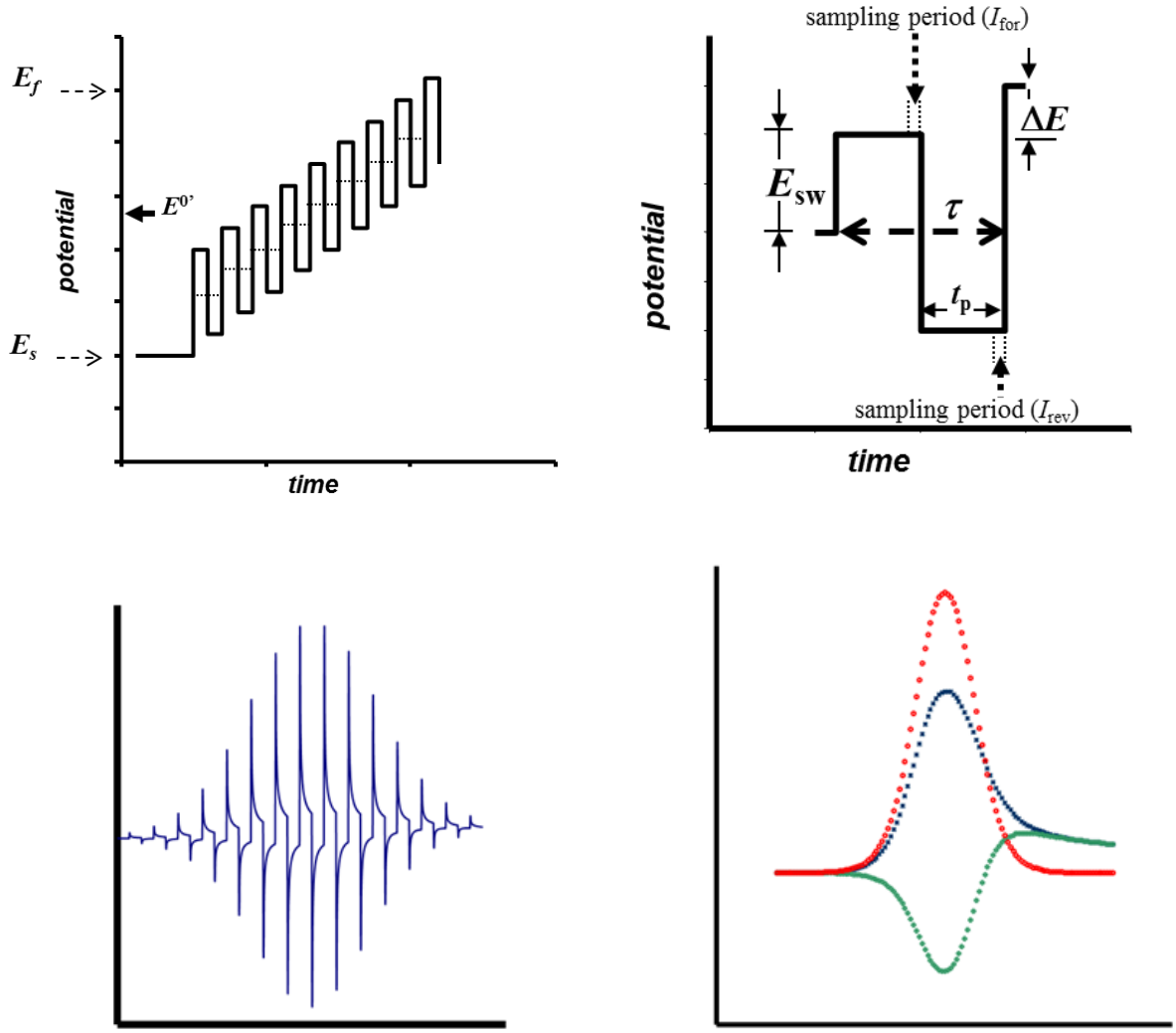

Figure 1. (A) Potential modulation in square-wave voltammetry; **(B)** Single potential cycle in square-wave voltammetry; **(C)** Variation of the current in the course of the square-wave voltammetry; **(D)** Typical square-wave voltammogram consisting of forward (Ψ_f), reverse (Ψ_r) and net component (Ψ_{net}).

ELECTRODE MECHANISMS AND ANALYTICAL APPLICATIONS

A variety of electrode mechanisms have been analyzed applying SWV in the past several years. In general, the advances in the theory of pulse voltammetric techniques, including SWV, can be found in the mini review of Molina *et al*. [40]. Electrode mechanism including three electrode reactions coupled with two chemical reactions (ECECE mechanism) was developed by Lovrić [41], building up on the previous theoretical study of three-step electrode reaction [42]. In [41] three reversible electrode reactions that are connected by two reversible chemical reactions have been considered, with emphasize on the influence of the basic thermodynamic parameters. Lovrić also developed theoretical model of an electrode process of amalgam forming ions at spherical electrodes [43], as well as the theory of an electrode reaction followed by the dimerization of the product [44].

Fatouros and Krulic analyzed specific conditions when the responses under conditions of pulse voltammetry and linear scan voltammetry match [45]. It has been shown that the forward component of the SW voltammetric response of a reversible electrode reaction of a solution resident redox couple at a macroscopic electrode under certain experimental conditions can match with the response of simple linear sweep voltammetry.

Molina *et al*. discussed the effects of unequal diffusion coefficients and coupled chemical equilibria on the SWV response at disc and hemispherical microelectrodes [46]. It has been pointed out that under non-steady-state conditions the case of unequal diffusion coefficients gives rise to a complex behaviour of the SW voltammetric response, being significantly different from the theoretical predictions established under the assumption of equal diffusion coefficients.

Vettorelo and Garay developed a theory of complex and important electrode system coupled with adsorption and regenerative catalytic reaction [47], proposing diagnostic criteria for characterisation of the experimental system, while Garcia-Araez *et al*. proposed simple and efficient procedure for measuring the rate of transport of redox species through membranes by using SWV [48]. SWV has been applied by Rama Kant to analyze theoretically the response at rough electrodes [49]. An explicit mathematical expression is proposed relating the staircase, cyclic staircase, differential pulse, and square-wave voltammetric response of finite fractal electrode to the statistical morphological characteristics.

There exist numerous analytically oriented studies including SWV and their full citation is virtually impossible, thus only a few representative examples will be briefly mentioned. A useful collection of references on the analytical application of SWV can be found in the recent reviews on electrochemical sensors for forensic drug analysis [50], application of bismuth electrodes in contemporary electroanalysis [51], electrochemical biosensors [52], and electrochemical methods for determination of the antioxidant capacity of food [53]. Cao *et al.* presented an advanced state-of-the-art strategy for multi-antibiotics detection using SWV [54]. The same authors presented dual-signalling electrochemical aptasensor using ferrocene and $[Ru(NH_3)_6]^{3+}$ as two signal indicators, quantified with SWV, reaching subpicomolar limit of detection [55]. Sedova *et al*. studied complex kinetic and thermodynamic behaviour of strand displacement at the electrode surface in detection of single base mismatches [56]. In the mechanistically oriented study, where SWV was used as an electroanalytical tool for detection of a redox label, they have found a complex interplay between the position of the redox label, variations in strand displacement kinetics, and alterations in the melting temperature of DNA duplexes tethered on the gold surface. D'Eramo *et al.* reported on the application of SWV for simultaneous determination of eugenol, thymol and carvacrol (CA) in honey samples at a glassy carbon electrode [57]. Taleb *et al.* [58] reported on the preparation of electrochemical sensor using self-organized gold nanoparticle modified highly oriented pyrolytic graphite electrode, which was applied for the analysis of copper and silver ions with SWV. The sensor exhibited remarkable performances in terms of preparation, simplicity, and detection limit. Finally, Domenech-Carbó *et al*. [59] reported on an important application of SWV in the solid-state electrochemistry of organosulfur compounds existing in petroleum and its derived matrices according to the methodology of the voltammetry of immobilized microparticles.

RECENT METHODOLOGICAL ADVANCES OF SWV

Kinetic analysis at a constant scan rate

Commonly, kinetic analysis in voltammetry is performed by changing the scan rate, which affects the critical time of the voltammetric experiment. As previously mentioned, the frequency (f) is the critical time parameter in SWV (cf. Figure 1B). Adjusting the frequency one defines the available time to drive the electrode reaction in both cathodic and anodic directions at a given potential. Hence, all intrinsic kinetic parameters controlling the response are frequency related; e.g. for a quasireversible electrode reaction of a solution resident redox couple

Ox/Red the electrode kinetic parameter is $\kappa = \frac{k_s}{\sqrt{Df}}$ [1], where k_s is the formal rate constant and D is the common diffusion coefficient of both Ox and Red. For an electrode mechanisms coupled with chemical reactions (e.g. EC, CE, EC' etc.) addition chemical kinetic parameter appears, defined as $\lambda = \frac{k_c}{f}$, where k_c is the first order rate constant of the coupled chemical reaction [1]. Thus, variation of the frequency affects particular kinetic parameter, which is the basic of the methodology for estimation of kinetic rate constants. However, the system is frequently affected by several parameters and the frequency exhibits a complex influence, making the estimation of the rate constants tedious.

To circumvent the latter complexity, a simple methodology has been developed for kinetic analysis at a constant scan rate, i.e. at constant frequency, taking advantage of the pulse height (amplitude (E_{sw})) [60]. Let us first note that during a single potential pulse (cf. Figure 1B) the actual sampling of the forward (I_f) and reverse (I_r) currents is done at the potentials of the forward and reverse pulse, respectively, which differ between each other for the absolute potential value of $2E_{sw}$. Thus, the actual driving force is the sum of the potential of the step and the amplitude. This implies the electrode kinetics can be significantly affected by the amplitude only, while keeping the frequency constant. The latter provides significant advantage in the kinetic analysis, as the comparison of the experimental and theoretical voltammograms is simplified to a large extend when all frequency related kinetic parameters are kept constant.

This is the basis of the simple methodology for electrode kinetic measurement by analyzing the peak potential separation of the forward and reverse SW voltammetric components as a function of the amplitude [61]. Indeed, the methodology was introduced for the first time almost two decades ago [62], by considering only fast surface confined electrode reactions, which are attributed with net peak splitting. The method was recently generalized by considering electrode processes of a solution resident redox couple [61], as well as stripping electrode mechanisms. Experimental conformation was done for both surface confined electrode processes [63] and a dissolved redox couple [61]. It is further expected to challenge this simple approach for mechanisms coupled with chemical reactions.

Figure 2 illustrates the evolution of the forward and backward SW components of a surface confined electrode reaction by increasing the amplitude. The electrode reaction is attributed with the electrode kinetic parameter, $\omega = \frac{k_{sur}}{f}$ where k_{sur} is the formal rate constant of the electrode reaction expressed in units of s^{-1}. The increasing amplitude causes an enhancement of both the intensity and peak potential separation of the response. The inset of the Figure 2A displays the peak potential separation (ΔE_p) as a function of the electron-normalized amplitude (nE_{sw}) for different electrode kinetic parameters. The data clearly imply that the studied feature is sensitive to the electrode kinetics enabling estimation of the formal rate constant. The original method was further developed by the recent contribution of Bonazzola and Gordillo for the electrode kinetics of surface confined processes [64].

At this point, it is however useful to note that besides the electrode kinetics, the peak potential separation is partly consequence of the conventional way of presenting the data in SWV, where the forward and reverse voltammetric components are plotted vs. the potential of the staircase modulation, though they are measured at respective potentials of potential pulses. To avoid this artefact in the kinetic analysis we have recently introduced the so called *"potential corrected SW voltammograms"* [61]. Indeed, in the latter variant of SWV only the forward and reverse components are considered, avoiding the net SW components, which are plotted vs. the real potentials of the pulses, instead of being plotted versus the potentials of the staircase potential modulation. Such simple correction can be easily done to any SW voltammograms by appropriate shift of the forward and reverse components for the value of the SW amplitude along the potential axis, as shown in Figure 2B. In potential corrected SW voltammograms, the peak potential separation bares information on the electrode kinetics only [61].

Besides the peak potential separation, the SW amplitude can be related to the peak currents of all three components of the response [65]. As shown in Figure 3, the morphology of the response depends dramatically on the SW amplitude, in terms of the peak current ratio of the forward and backward components, exemplified with the quasireversible electrode reaction of a solution resident redox couple. Whether electrode reaction appears as an irreversible process (Figure 3A-(*1*)), or as a relatively fast quasireversible process (Figure 3A-*(3)*), depends markedly on the amplitude. This phenomenon was studied in detail revealing that the kinetic regions of the electrode reaction depend strongly on the amplitude. Figure 3B displays typical variation of the dimensionless net-peak current with the electrode kinetic parameter of the electrode reaction of a dissolved redox couple. Note the linearly increasing part of the curves is associated to the typical quasi-

revesible behaviour of the reaction [1]. Obviously, the quasireversible kinetic interval depends strongly on the amplitude, being shifted toward lower values at higher amplitudes (cf. Figure 3B). In other words, large amplitude provides sufficient driving force to make intrinsically slow electrode processes relatively fast. Thus, increasing the amplitude enables kinetic estimation of slow electrode processes [65].

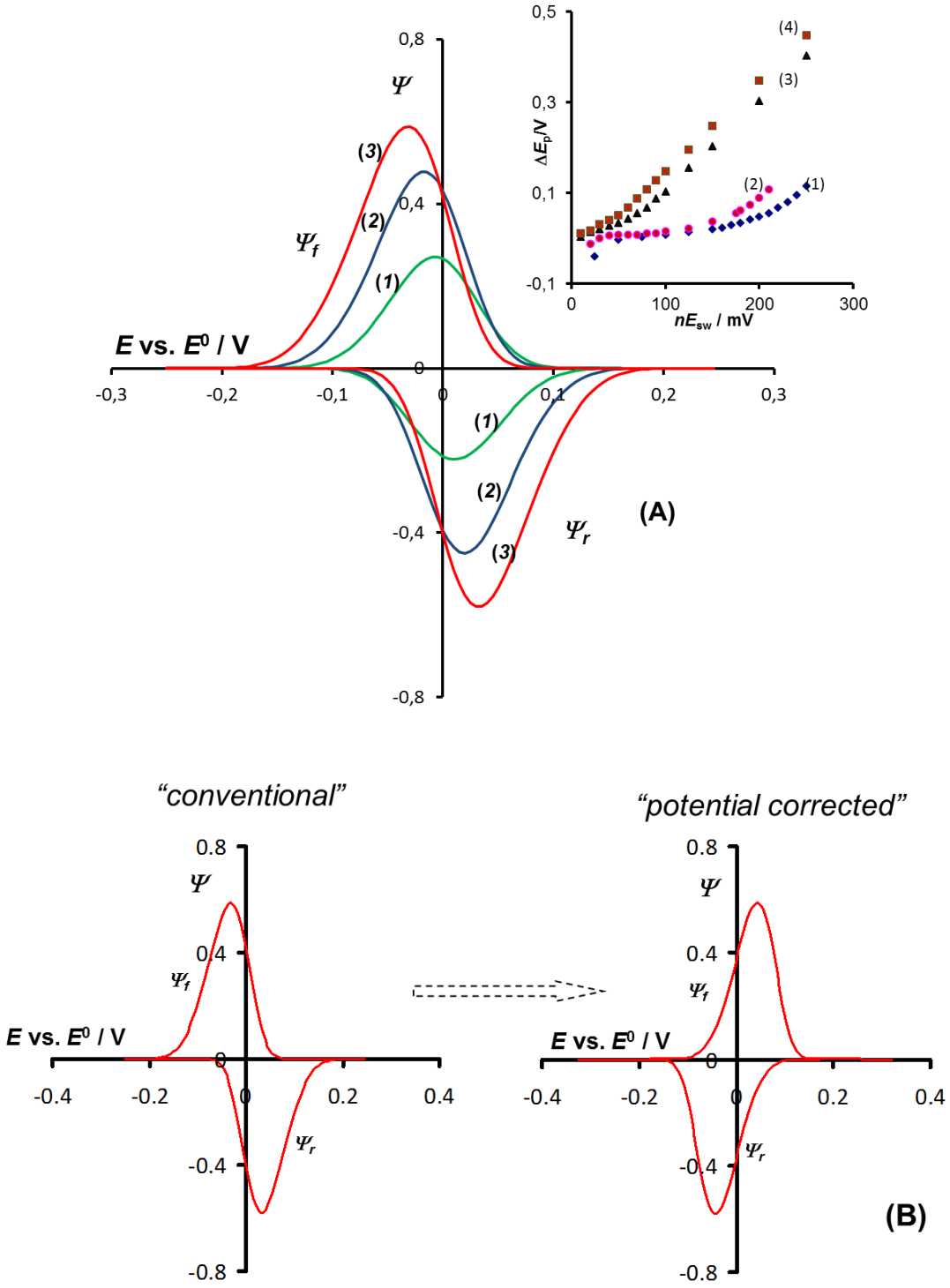

Fig. 2. Quasireversible electrode reaction of a surface confined redox couple. **(A)** Evolution of the simulated forward and reverse SW components with increasing amplitude of the potential modulation of nE_{sw} = 25 (***1***); 50 (***2***) and 75 mV (***3***). The other conditions of simulations are: electrode kinetic parameter $\omega = 1$, electron transfer coefficient $\alpha = 0.5$, and scan increment ΔE = 5 mV. The inset shows the dependence of the peak potentials separation on the SW amplitude for electrode kinetic parameter of ω = 0.05 (***1***); 0.1 (***2***); 1 (***3***) and 2 (***4***). **(B)** Conventional and potential corrected SW voltammogram showing the forward and reverse components for conditions corresponding to curve (***3***) in panel (**A**).

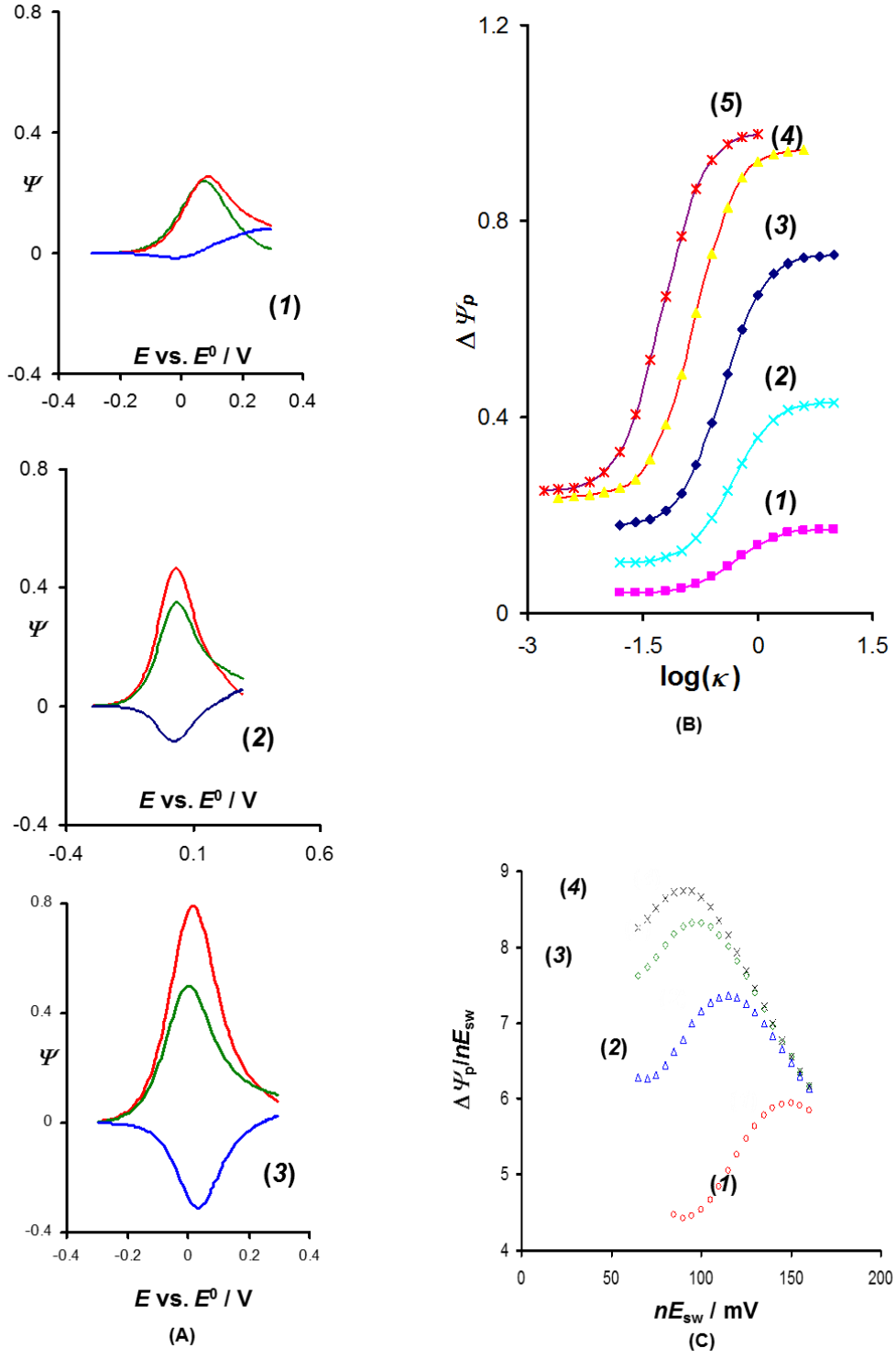

Figure 3. Quasireversible electrode reaction of a dissolved redox couple at a planar electrode. **(A)** The evolution of the simulated SW voltammograms at different amplitudes of E_{sw} = 60 (***1***), 120 (***2***) and 180 mV (***3***). Conditions of the simulations are: electrode kinetic parameter $\kappa = 0.06$, electron transfer coefficient $\alpha = 0.5$, stoichiometric number of electrons $n = 1$, and scan increment ΔE = 5 mV. **(B)** The dependence of the dimensionless net peak current on the logarithm of the electrode kinetic parameter for different amplitudes. The conditions of the simulations are: E_{sw} = 10 (***1***); 25 (***2***); 50 (***3***); 100 (***4***) and 150 mV (***5***). **(C)** The dependence of the amplitude-based quasireversible maximum on the electrode kinetic parameter. Simulations are conducted for $n = 2$ and $\kappa =$ 0.01 (***1***); 0.03 (***2***); 0.05 (***3***) and 0.06 (***4***).

Foregoing theoretical considerations provides a basis for development of a new kinetic method by means of the analysis of the net-peak current-amplitude relation. Interestingly, Figure 3C shows that the ratio of the net peak current and the electron-normalized amplitude ($\Delta\Psi_p/nE_{sw}$) is a parabolic function of the amplitude, for a single electrode reaction. This feature was termed as *amplitude-based quasireversible maximum*, by analogy to the well-known *quasireversible maximum* of surface confined or adsorption complicated electrode processes [1, 11]. The position of the amplitude-based quasireversible maximum is sensitive to the electrode kinetics enabling estimation of the formal rate constant in a simple, fast and efficient procedure. Unlike the conventional quasireversible maximum, the amplitude-based quasireversible maximum is not limited to adsorption complicated electrode processes, rather than it is a general feature of a broad class of electrode mechanisms. The methodology was experimentally supported with a variety of electrode mechanisms including 2-methyl-2-nitropropane [65], alizarine, vitamin B12 and vitamin K2 [63].

Finally, it is worth mentioning that a possible drawback of both amplitude-based methodologies is related to the fact that by using large amplitude values, i.e. E_{sw} > 150 mV) distortions of the experimental curves are possible due to significant contribution of the charging current, which has to be considered in the course of the real experimental analysis.

Approaching slow electrode processes – the role of the step potential increment in SWV

As previously mentioned, the main time parameter in SWV is the frequency, with the typical interval values provided by the modern instrumentation from 5 to 2000 Hz. For the minimal frequency of 5 Hz one gets the maximal duration of a single potential cycle, τ = 200 ms ($\tau = 1/f$), revealing that one deals with intrinsically fast technique. The latter could be considered as a drawback when slow electrode processes are considered (unfortunately the majority of electrode reactions are relatively sluggish). In the previous section, (Kinetic analysis at a constant scan rate), it was revealed that kinetics of the electrode reaction, i.e., the electrochemical reversibility, can be significantly affected by increasing the amplitude, transforming intrinsically slow processes in electrochemically quasireversible reactions (cf. Figure 3). However, besides the amplitude, in a quest to analyze slow electrode processes there could be another tool in hand; it is the step potential increment ΔE of the staircase potential modulation (cf. Figures 1A and B). The latter assumption stem from the expectation that along the frequency the electrochemical reversibility depends on the overall scan rate defined as $v = \Delta E f$. Unfortunately, there is a gap in the theory of SWV regarding the role of the step potential increment and the overall scan rate in the electrochemical reversibility. Jadresko *et al.* [66] studied the effect of the scan rate in SWV and staircase voltammetry for the case of reversible electrode processes of a solution resident redox couple, however the analysis of quasireversible electrode mechanisms is still missing. For these reasons, we illustrate briefly the effect of the step potential increment, in order to emphasize the potential usage in studying electrode kinetics.

Figure 4A illustrates how the step potential increment affects profoundly the morphology of the response for the case of a quasireversible electrode reaction of a dissolved redox couple. The electrode reaction attributed with the electrode kinetic parameter κ = 0.1 appears quasireversible for ΔE = 0.5 mV (Figure 4A, panel (*1*)), whereas it is almost completely irreversible for ΔE = 20 mV (Figure 4A, panel (*2*)). On the other hand, the intensity of the response enhances significantly by increasing the step increment (compare panels 1 and 2 in Figure 4A). Obviously, the scan increment has a complex and profound effect to the voltammetric response of a quasireversible electrode reaction. Figure 4B summarizes in more detail the effect of the step potential increment to the typical kinetic regions of the electrode reaction considering the variation of the net peak current with the logarithm of the electrode kinetic parameter. The scan increment has a significant influence in the lower parts of the curves, which is associated to relatively slow and irreversible electrode processes, in agreement with the study of Jadresko *et al*. [66]. More specifically, the typical quasireversible kinetic region is expanded toward slower processes by decreasing the step increment (Figure 4B), implying that kinetic analysis of sluggish electrode reactions can be assessed by decreasing the step increment for a given frequency of the potential modulation. For $\log(\kappa) \geq 0$, the linearly increasing part of all curves merges into a single line, regardless of the step potential, indicating that in this kinetic region the electrochemical reversibility mainly depends on the frequency (cf. Figure 4B). Figure 4C also illustrates that the peak potential separation ΔE_p between the forward and backward components depends on both amplitude and the step potential increment. Obviously, lowering the step potential increment (curve 1 in Figure 4C) enables application of lower amplitude values (curve 3 in Figure 4C), which is highly advantageous in terms of precision and sensitivity of the method based on the amplitude variation [61].

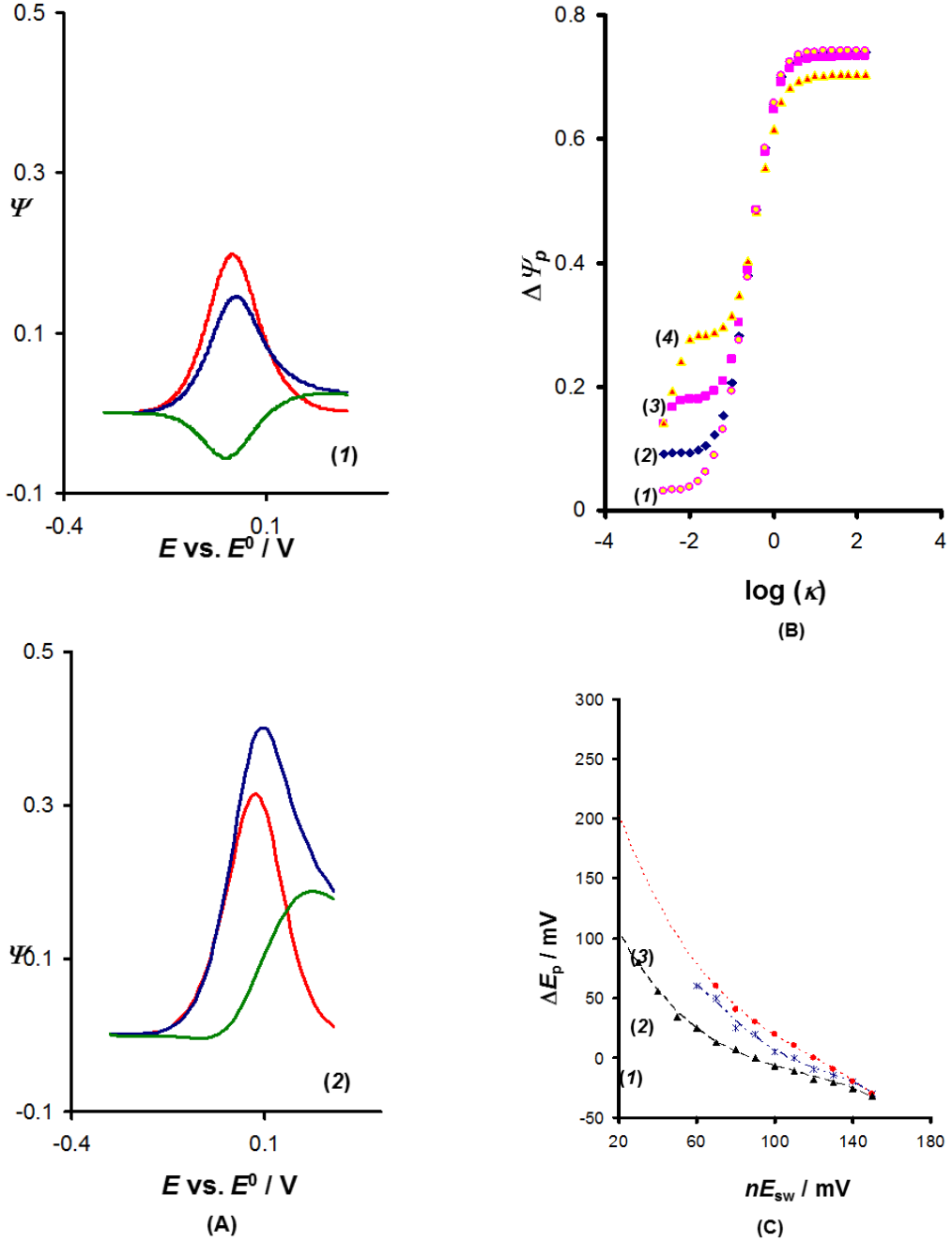

Figure 4. Quasireversible electrode reaction of a dissolved redox couple at a planar electrode. **(A)** The effect of the step potential increment on the morphology of the SW voltammograms for electrode kinetic parameter of $\kappa = 0.1$, electron transfer coefficient $\alpha = 0.5$ and stoichiometric number of electrons $n = 1$. The amplitude of the modulation is $E_{sw} = 50$ mV and the step increment is $\Delta E = 0.5$ (*1*) and 20 mV (*2*). **(B)** The effect of the step potential increment on the quasireversible kinetic region for $\Delta E = 0.1$ (*1*); 1 (*2*); 5 (*3*) and 20 mV (*4*). **(C)** Peak potential separation as a function of the SW amplitude for the step potential increment of $\Delta E = 1$ (*1*); 5 (*2*) and 10 mV (*3*).

To rationalize the effect of the scan increment let us note that the scan rate of the overall potential modulation can be significantly changed by altering the step potential increment for a given frequency ($v = \Delta E f$). In turn, the scan rate determines the overall time of the voltammetric experiment, affecting the thickness of the diffusion layer and the rate of the diffusional mass transport for processes of a dissolved redox couple. For instance, at $f = 5$ Hz, the scan rate changes from $v = 0.5$ mV/s to 100 mV/s for $\Delta E = 0.1$ and 20 mV, respectively. It is three order of magnitude variation of the overall scan rate which has marked influence to the electrochemical reversibility of a given electrode reaction. Though

the interplay of the frequency and scan rate is very complex, it is highly advised to inspect in detail the effect of the step increment and to develop methodology for kinetic estimation of slow electrode processes. A general recommendation would be to apply as small as possible step potential increment when sluggish electrode mechanisms are subject of the study.

In-depth analysis of chronoamperometric features of electrode processes – multisampling procedure in SWV

Understanding SWV as a repetitive double-step chronoamperometric technique, a novel methodology has been recently proposed for advanced analysis based on the multisampling current procedure [67]. The basic idea is graphically illustrated in Figure 5, showing a single potential cycle in SWV (Figure 5A) where the current is sampled at several time intervals at the last portion of the pulse. Instead of single current measurement, the multisampling current procedure enables construction of a series of so called *multi-sampled SW voltammograms*, which reflect the chronoamperometric behaviour of the electrode reaction. Proposed procedure is useful when the experiment is conducted at a low frequency, i.e. long duration of the potential pulses, allowing to sample the current at the last portion of each pulse without sacrificing the large ratio of the faradaic to the charging current [1, 11].

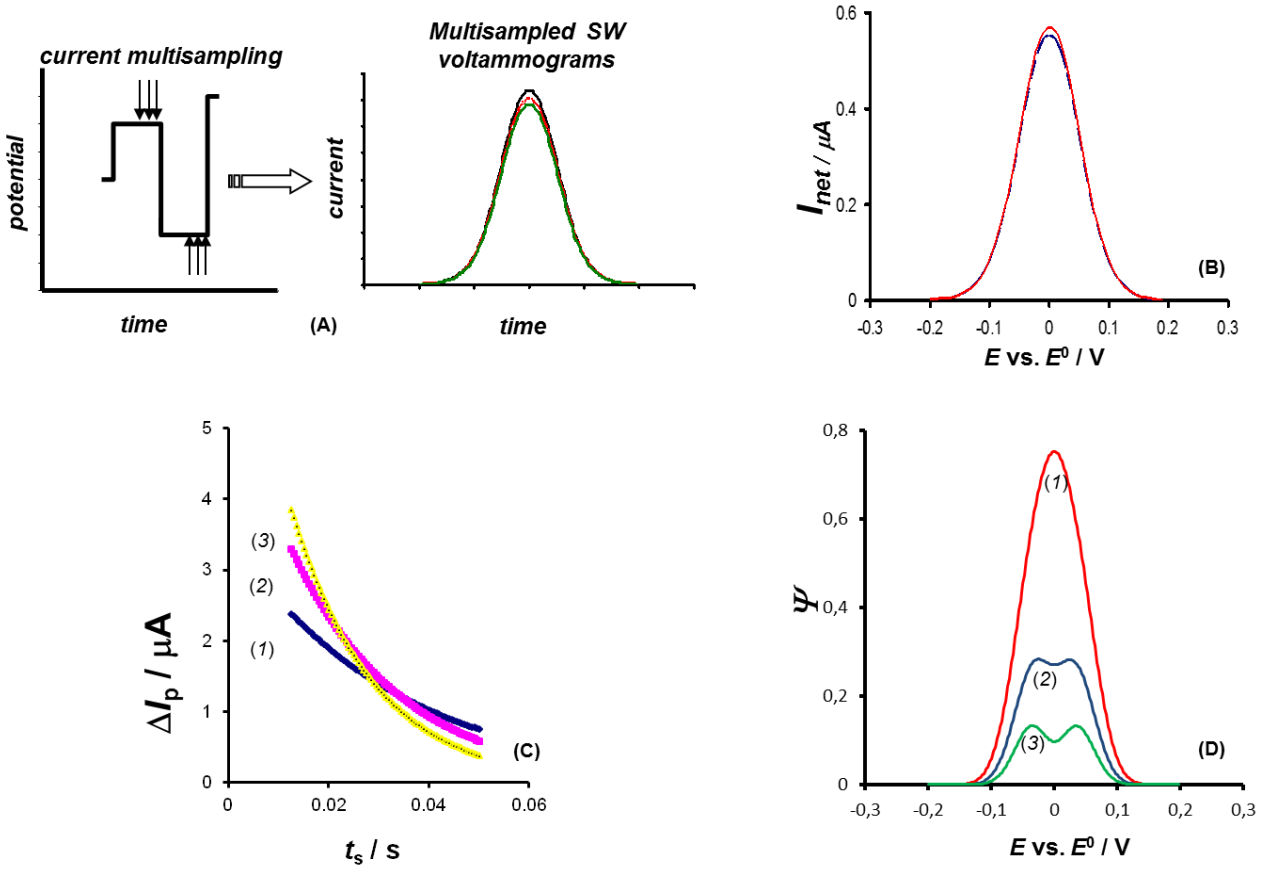

Figure 5. (A) Multisampling current procedure in the course of a single potential cycle in SWV and corresponding multisampled net SW voltammograms. **(B)** Comparison of net voltammetric components of a reversible electrode reaction of a dissolved redox couple simulated at f = 10 Hz (t_p = 50 ms) by sampling the current at t_s = 40 ms (red line) with the conventional voltammogram (blue dashed line) simulated for f = 12.5 Hz (t_p = t_s = 40 ms). **(C)** Quasireversible electrode reaction of a surface confined redox couple. The dependence of the real net peak current of multisampled SW voltammograms on the sampling time for the formal rate constant of k_{sur}/s^{-1} = 10 (***1***); 15 (***2***), and 25 (***3***). Electron transfer coefficient is α = 0.5, stoichiometric number of electrons n = 1, frequency f = 10 Hz, amplitude E_{sw} = 50 mV, and scan increment is ΔE = 2 mV. **(D)** Evolution of the multisampled theoretical net voltammograms of surface confined electrode reaction for a sampling time of t_s = 30 (***1***);40 (***2***) and 50 ms (***3***). The formal rate constant is k_{sur} = 35 s^{-1}. The other conditions are identical as for the panel (**C**).

Figure 5B illustrates the difference between multisampled and conventional SW voltammograms for a reversible electrode reaction of a solution resident redox couple. The red line corresponds to the net voltammogram simulated at f = 10 Hz (duration of a single pulse t_p = 50 ms) but sampling the current at t_s = 40 ms, whereas the blue dashed line refers to the conventional voltammogram simulated at f = 12.5 Hz ($t_p = t_s$ = 40 ms). Even though in the two cases the current is sampled at equal time (40 ms), the outcome of the two assumed experiments is not identical, revealing the difference in the multisampling and conventional SWV.

The main advantage of multisampling SWV originates from the fact that in a single experiment one can construct a series of SW voltammograms, the analysis of which might enable full characterisation of the reaction [67]. A theoretical example of such analysis is presented in Figure 5C showing the variation of the net peak current of the multisampled net voltammograms as a function of the sampling time for a surface confined electrode reaction. The net peak current variation with sampling time is sensitive to the electrode kinetics enabling estimation of the formal rate constant. Moreover, the evolution of the net voltammogram from a single peak to the split net peak, typical for a surface confined electrode reaction, can be observed by analyzing multisampled voltammograms (Figure 5D). Let us recall that the peak splitting in conventional SWV is achievable either by increasing the SW amplitude or decreasing the frequency of the potential modulation [62]. Obviously, in multisampling SWV, the phenomenon can be observed conducting a single votammetric experiment only, which seems to be a unique feature of the proposed methodology. The proposed method is promising for an advanced analysis of electrode processes, as initially experimentally verified with the reactions of Eu^{3+} and azobenzene [67]. It is however worth mentioning that the full implementation of the method depends yet on the modification of current sampling protocol in the modern digital instrumentation.

Square-wave voltammetry in a cyclic fashion mode

It is commonly claimed that SWV unifies the advantages of pulse voltammetric techniques (with respect to the high ratio of the faradaic to the charging current, i.e., high analytical sensitivity), and cyclic voltammetry (with respect to the ability to study electrode mechanism). Nevertheless, in conventional SWV mechanistic features are accessible only for relatively fast electrode processes attributed with high electrochemical reversibility under given experimental conditions. For slow processes, as discussed in the previous section, a series of obstacles need to be overcome. A possible solution could be found in coupling the conventional SWV with cyclic voltammetry to yield the potential modulation presented in Figure 6A. The theoretical basis of this highly promising technique are found in the works of Chen [68], Bottomley [69–71], Molina [72], as well as in a series of studies in which SWV was applied in a reverse mode [73–76].

Figure 6B shows a typical theoretical response of the *cyclic square-wave voltammetry* of a slow, quasireversible electrode reaction of a dissolved redox couple. The response is rich with electrochemical data, consisting of six voltammetric curves, attributed to the direct and reversal SW potential scan. For the sake of simplicity, the cyclic square-wave voltammogram might feature the net components of the direct and reversal scan only. Analyzing the same electrode reaction shown in Fig. 6B with conventional SWV yields an irreversible voltammetric response with barely developed backward component. On the contrary, under conditions of cyclic square-wave voltammetry the processes appears as quasireversible one considering the net components of the response, providing an insight into the mechanistic and kinetic aspects of the electrode reaction.

Figure 6C shows a typical response of a $\mathbf{EC_{rev}}$ electrode mechanism, where the quasireversible electrode reaction of a dissolved redox couple (**E**) is coupled with a follow-up reversible homogeneous chemical reaction ($\mathbf{C_{rev}}$), attributed with a equilibrium rate constant log(K) = 10 and different kinetics of the chemical step [1]. As the kinetics of the chemical reaction increases, the net component of the reversal SW voltammetric scan diminishes, in analogy to the cyclic voltammetric features. Recall that the dimensionless chemical kinetic parameter is defined as $\varepsilon = \frac{k}{f}$; $k = k_f + k_b$ is cumulative rate constant where k_f and k_b are rate constants of the direct and reverse chemical reaction of the chemical step [1]. The evolution of the response presented on Figure 6C is similar to the conventional cyclic voltammetry, the difference being in the advanced sensitivity and high quality of the electrochemical data under conditions of cyclic square-wave voltammetry.

In conclusion, it has to be stressed that there is a necessity for the analysis of a variety of electrode mechanisms under conditions of cyclic square-wave voltammetry in order to establish qualitative diagnostic criteria as well as to develop methods for determination of thermodynamic and kinetic parameters of electrode reactions.

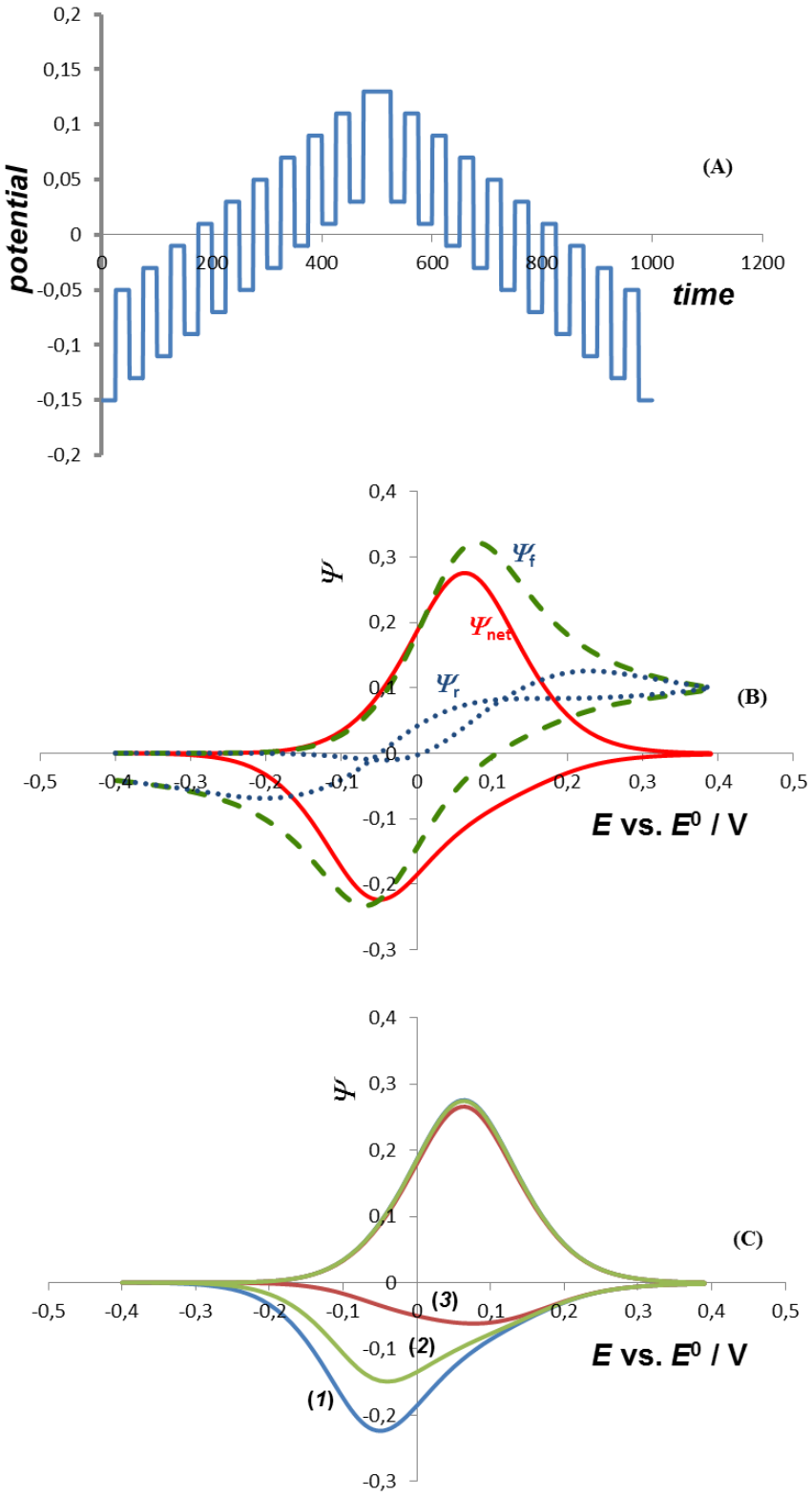

Figure 6. (A) Potential modulation in cyclic square-wave voltammetry. **(B)** Typical voltammetric response of a quasireversible electrode reaction of a solution resident redox couple showing, forward, reverse and net component. Simulations are conducted for electrode kinetic parameter $\kappa = 1$, electron transfer coefficient $\alpha = 0.5$, stoichiometric number of electrons $n = 1$, amplitude $E_{sw} = 50$ mV, and scan increment $\Delta E = 10$ mV. **(C)** Typical response of an **EC**$_{rev}$ mechanism for the chemical kinetic parameter of: $\log(\varepsilon) = -5$ (***1***); –2 (***2***) and –1 (***3***). The equilibrium constant of the chemical step is $\log(K) = 10$ and the electrode kinetic parameter is 0.1. The other conditions are identical as for panel (**B**).

Simplified form of square-wave voltammetry – square-wave chronoamperometry

Square-wave chronoamperometry is a simplified form of conventional square-wave voltammetry developed for the purpose of simplification and broadening the scope of the technique [77]. The theoretical base of this renewed idea is found in the early works of Smit and Wijnen [78–80], in the methodology known as cyclic potential-step method. Square-wave chronoamperometry is a pulse-form chronoamperometric experiment, the excitation signal being obtained by combining a constant potential (mid-potential, E_{mid}) with a short-duration, small potential pulses, as depicted in Figure 7A. Indeed, the proposed experiment is a repetitive double-step chronoamperometric experiment conducted with small potential pulses. The main tool in hand for electrokinetic purposes is again the frequency (f), the height of potential pulses (E_{sw}, i.e. SW amplitude), as well as the mid potential (E_{mid}). Current sampling and presentation of chronoamperometric data is analogous to SWV, consisting of forward, reverse, and net (differential) chronoamperometric curve (Figure 7B). Additionally, for electrokinetic purposes, the typical way of presenting the data is in the form of a "spectrum" of net currents as a function of the frequency (Figure 7C), which is the reason to coin an alternative name of the technique – *electrochemical faradaic spectroscopy*.

The first, and the most striking feature of the response is that the net chronoamperometric component does not depend on time of the experiment, as illustrated in Figure 7D, referring to the reversible electrode reaction of a solution resident redox couple. Such chronoamperometric behaviour is opposite to the conventional chronoamperometry (cf. Figure 7D), where the current decays with time ($\sim \frac{1}{\sqrt{t}}$), as typical for diffusion controlled processes at macroscopic electrodes. Thus, the response under conditions of electrochemical faradaic spectroscopy at a macroscopic electrode resembles the steady state response in conventional chronoamperometry at microelectrodes governed by a spherical diffusion mass transport.

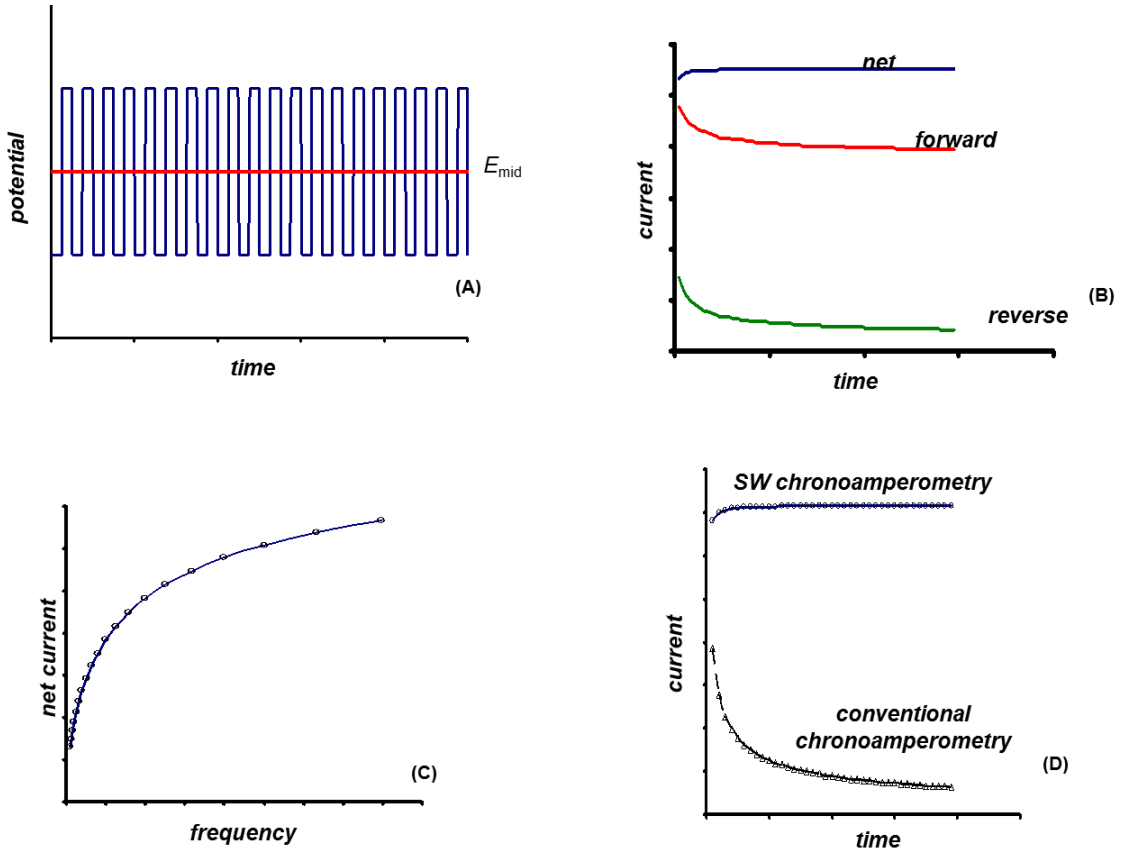

Figure 7. Electrochemical faradaic spectroscopy (EFS): **(A)** A scheme of the excitation signal; **(B)** typical response of EFS in a form of square-wave chronoamperogram; **(C)** typical response of EFS in a form of a spectrum of net currents of different frequencies. **(D)** Comparison of the net response in EFS and conventional chronoamperometry.

Figure 8 illustrates that the frequency spectrum is sensitive to both electrode kinetics and mechanism, exemplified with the quasireversible electrode reaction of a solution resident redox couple (curve ***1***), surface confined electrode reaction (curve ***2***), and $\mathbf{E_{rev}C'}$ regenerative catalytic mechanism of a reversible electrode reaction of a dissolved redox couple (curve ***3***) [1]. The theoretical analysis is conducted at the mid potential identical to the corresponding formal potentials of each electrode mechanism, with 20 potential cycles (i.e., in total 40 potential pulses at amplitude of E_{sw} = 20 mV). The parabolic spectrum of the surface confined electrode reaction is a consequence of the specific chronoamperometric features related to the phenomenon known as *quasireversible maximum* [1, 11].

Generally, the proposed simple technique unifies the advantages of both conventional square-wave voltammetry and chronoamperometry. With respect to the kinetics of the electrode reaction of a dissolved redox couple the technique appears to be even more sensitive than SWV and conventional chronoamperometry [77]. Moreover, in comparison to SWV even faster electrode reactions can be studied by adjusting the mid-potential (E_{mid}) at values $E_{mid} < E^{0'}$. Finally, it has to be mentioned, similar to the case of multisampling current procedure (section In-depth analysis of chronoamperometric features…), the application of the new methodology depends on the implementation of the technique in the modern instrumentation. Moreover, the complete theoretical development considering a variety of electrode processes should follow.

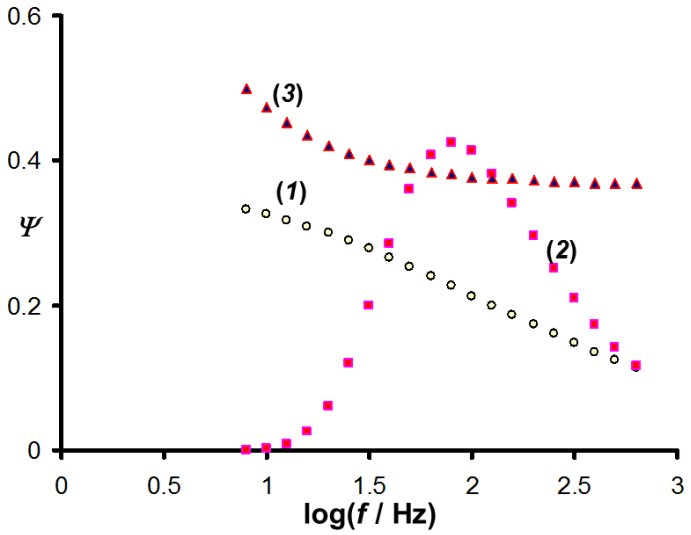

Figure 8. Typical frequency spectrum in electrochemical faradaic spectroscopy for (***1***) a quasireversible electrode reaction of a solution resident redox couple with a formal rate constant k_s = 0.01 cm s^{-1}; (***2***) quasireversible surface confined electrode reaction with a formal rate constant k_{sur} = 100 s^{-1}; and (***3***) reversible catalytic electrode mechanism with the catalytic rate constant k_c = 10 s^{-1}. The other conditions of the simulations are: stoichiometric number of electrons n = 1, electron transfer coefficient α = 0.5, amplitude E_{sw} = 20 mV, and number of potential cycles p = 20. The dimensionless currents correspond to the 19th potential cycle measured for different frequencies.

TOWARDS ENHANCED SENSITIVITY OF SQUARE-WAVE VOLTAMMETRY

Finally, in a quest for improved analytical performances of SWV two new ideas are presented here for the first time. The full elaboration will be given in subsequent separate publications. The first one is an attempt to increase the sensitivity of SWV by simple processing of conventional net voltammograms, leading to the methodology provisionally termed as *cumulative square-wave voltammetry*. In cumulative voltammetry the current at a given potential (Ψ_{cum}) is calculated as a sum of all previous current values of the conventional SWV (Ψ), i.e., $\Psi_{cum} = \sum_j \Psi_j$. The result of such operation, which could be regarded as primitive integration, is presented in Figure 9, comparing conventional (left ordinate) with the new, cumulative net voltammogram (right ordinate). The cumulative voltammogram is a sigmoid curve with a limiting current (Ψ_{lim}) that is an order of magnitude higher than the net peak-current of the conventional SW voltammogram ($\Delta\Psi_p$) (compare the range of values of the two ordinates). For the conditions of Figure 9, the ratio is $\Psi_{lim}/\Delta\Psi_p$ = 26.5. In order to illustrate the prom-

ising potential of the proposed methodology toward an increased analytical sensitivity, the inset of Figure 9 compares theoretically constructed calibration lines of conventional and cumulative SWV. While the improvement in the sensitivity of the technique is obvious, it should be noted that the limit of detection of two techniques is expected to be identical, as they rely on the same set of electrochemical data.

The first, preliminary experimental verification of the proposed methodology has been done with the experiments with H_2O_2 measurement at macroscopic Pt electrode, where the slope of the calibration line increased from 21.26 to 693.07 A mmol^{-1} l for conventional and cumulative SWV, respectively (data not shown).

From the mechanistic point of view it can be mentioned that the half-wave of the cumulative voltammogram is identical to the net peak potential. It can be also shown that the rising part of the cumulative voltammogram is a linear function of the potential. The slope of the linear part of the cumulative voltammogram and the half-wave potential are sensitive to the electrochemical reversibility, thus enabling further processing and estimation of the kinetic parameters.

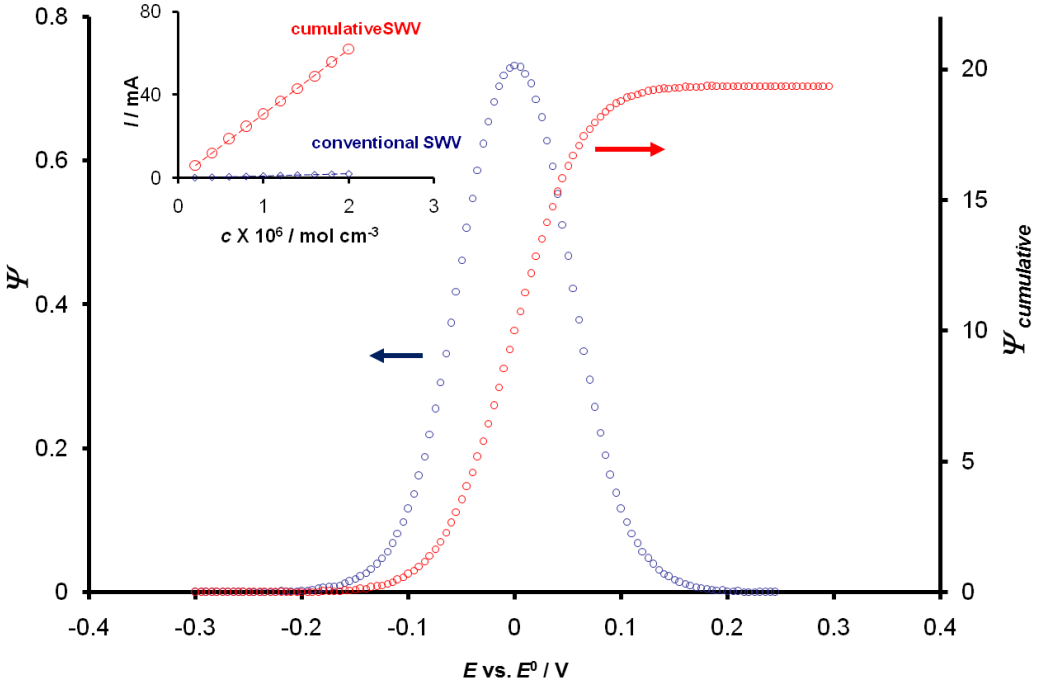

Figure 9. Cumulative square-wave voltammetry of a quasireversible electrode reaction at a planar electrode of a solution resident redox couple. Comparison of the cumulative (right ordinate) with the conventional SW voltammogram (left ordinate). Conditions of the simulations are: electrode kinetic parameter $\log(\kappa) = 1.8$, electron transfer coefficient $\alpha = 0.5$, stoichiometric number of electrons $n = 1$, amplitude $E_{sw} = 50$ mV, and scan increment $\Delta E = 5$ mV. The inset shows the theoretical calibration curves for the cumulative and conventional SWV. Conditions of the simulations are: formal rate constant $k_s = 10^{-3}$ cm s^{-1}, electrode surface area $A = 0.01$ cm^2; common diffusion coefficient $D = 1 \times 10^{-6}$ cm^2 s^{-1} and frequency $f = 10$ Hz. The other conditions are identical as for the main graph.

Besides sensitivity, the improvement of the limit of detection of SWV is a highly challenging issue in the overall methodological development of the technique. In the family of pulse voltammetric techniques SWV and differential pulse voltammetry (DPV) [4] compete for dominance in electroanalytical chemistry in general. While SWV seems to be superior when electrode mechanisms and kinetics are the subject of the study, analytical performances of the two techniques are quite comparable. In SWV, the frequency is the main time parameter ($f = 1/\tau = 1/2t_p$) (Figure 10A), while in DPV both duration of the step (t_s) and the pulse (t_p) can be deliberately altered (Figure 10B). In many cases, the right choice of the ratio t_s/t_p provides superior analytical performances of DPV. In order to unify the advantages of the two techniques a hybrid potential modulation is proposed, as depicted in Figure 10C. The later can be understood as a modified form of DPV, where the single pulse is replaced with two, equal, oppositely oriented pulses. Clearly, the underlying idea is to keep the ability of the hybrid technique to provide mechanistic information as SWV does. On the other hand, the hybrid potential

form can be commented from the perspective of SWV noting that a potential step (t_s) is inserted between potential cycles; commonly $t_s > t_p$. Obviously, the tendency is to enable longer relaxation of the system at a given potential step of the staircase potential modulation, in order to increase the ratio between the faradaic and charging current, as effectively achieved in DPV [4].

The current sampling of the hybrid technique can be done at three points, i.e., at the end of the step (I_s), as well as at the end of each potential pulse (I_f and I_r) (cf. Figure 10C). Two differential current components can be defined as $I_{dif,f} = I_f - I_s$, and $_{dif,r} = I_r - I_s$. In addition, the net component can be calculated as $I_{net} = I_{dif,f} - I_{dif,r}$. The same net component is obtained through I_f and I_r as $I_{net} = I_f - I_r$. As depicted in Figure 11 the evolution of the differential current components ($I_{dif,f}$, $I_{dif,r}$, Figure 11A) is not identical with the forward and reverse current components (I_f, I_r, Figure 11A), though the net component is identical in both cases. Interrelation between differential current components implies a quasireversible electrode process (cf. Figure 11A), whereas the forward and reverse currents are typical for the irreversible electrode reaction (cf. Figure 11B). The overall characteristics of the response are expected to depend strongly on the ratio t_p/t_s, in both mechanistic contexts, as well as in terms of the analytical performances of the technique. An in-depth theoretical analysis is in progress, which will be the subject of following communications.

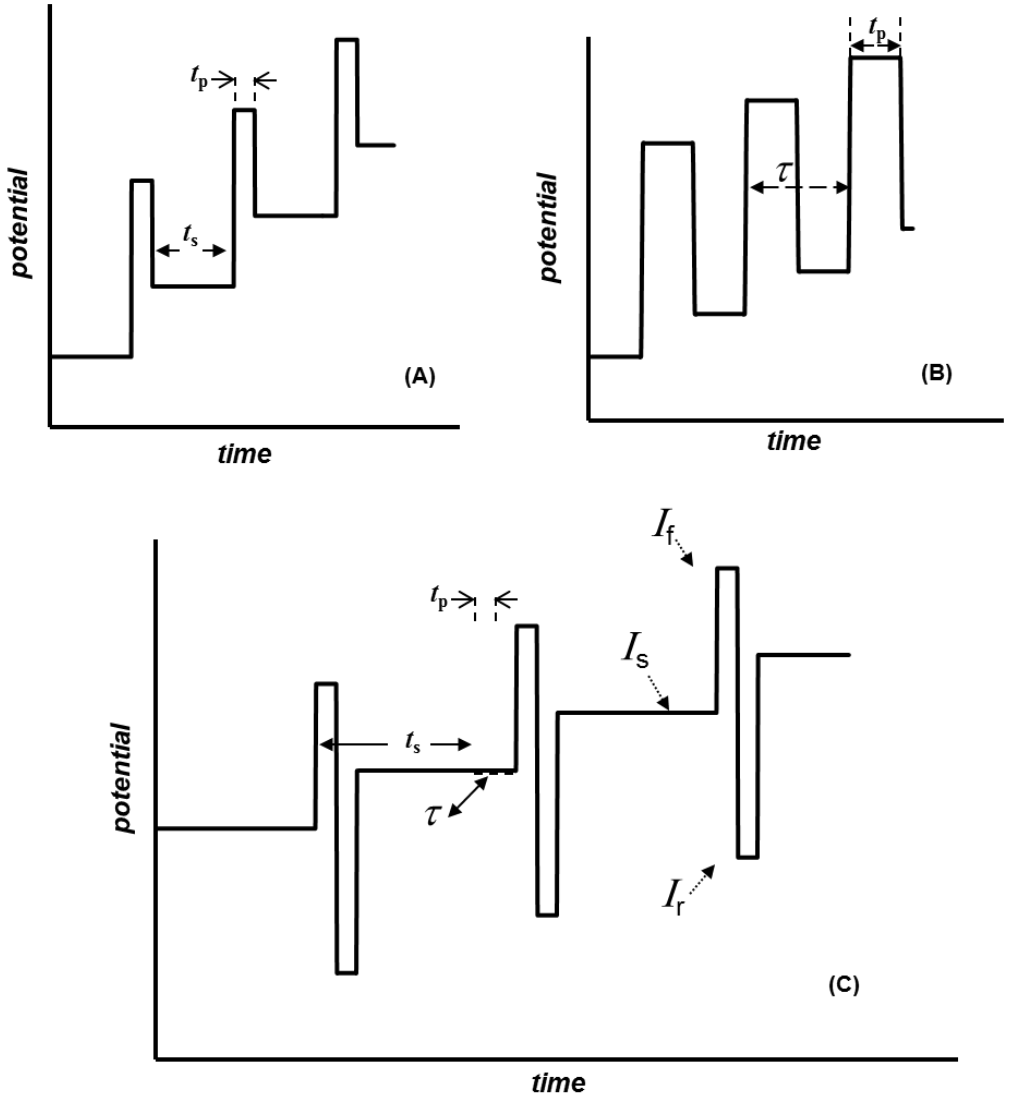

Figure 10. (A) Potential modulation in differential pulse voltammetry; **(B)** square-wave voltammetry; **(C)** hybrid differential-pulse square-wave voltammetry, showing typical time intervals and current sampling points in the new hybrid technique

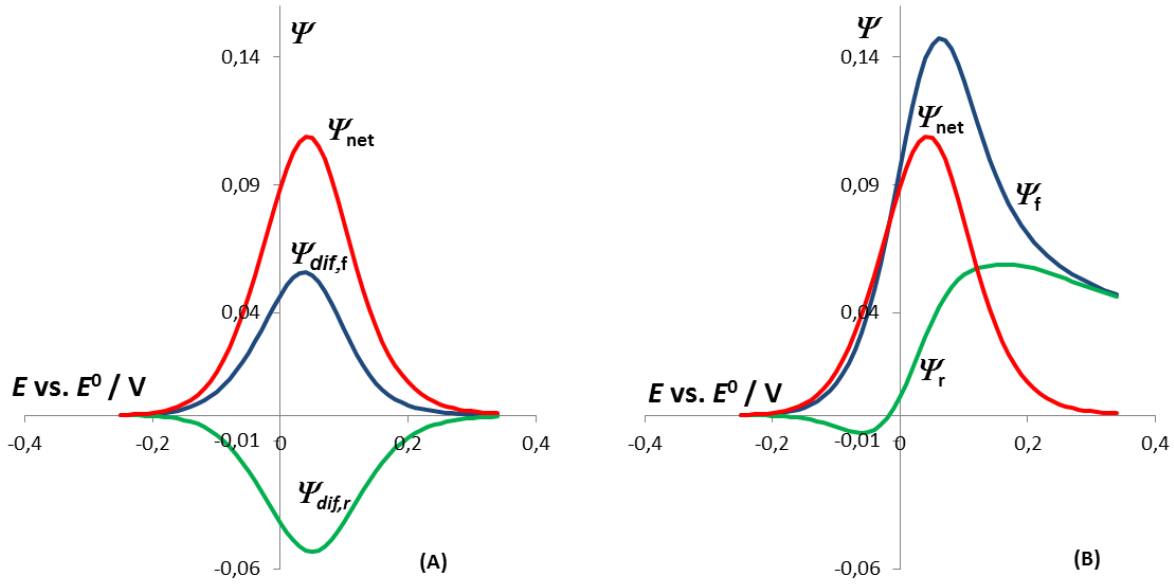

Figure 11. Quasireversible electrode reaction of a dissolved redox couple at a planar electrode. Typical theoretical response under conditions of hybrid differential pulse-square voltammetry showing: **(A)** differential ($\Psi_{dif,f}$, $\Psi_{dif,r}$) current components and **(B)** forward (Ψ_f) and reverse (Ψ_r) current components. In both cases, the net component (Ψ_{net}) is also given. The simulation conditions are: electrode kinetic parameter κ = 0.1, electron transfer coefficient α = 0.5 and stoichiometric number of electrons n = 1. The ratio between critical time parameters is t_s/t_p = 6, the amplitude of the modulation is E_{sw} = 25 mV and the scan increment is ΔE = 10 mV.

REFERENCES

[1] V. Mirčeski, Š. Komorsky-Lovrić, M. Lovrić, *Square-wave voltammetry: Theory and application*, F. Scholz (Ed.), Springer Verlag, Heidelberg, 2007.

[2] G. N. Eccles, Recent advances in pulse, cyclic and square-wave voltammetric analysis, *Crit .Rev. Anal. Chem.* **22** (1991), pp. 345–380.

[3] D. de Souza, S. A. S. Machado, L. A. Avaca, Square-wave voltammetry. Part I: Theoretical aspects, *Quim. Nova*, **26** (2003), pp. 81–89.

[4] Á. Molina, J. González, *Pulse Voltammetry in Physical Electrochemistry and Electroanalysis. Theory and Applications*, Series: Monographs in Electrochemistry, Fritz Scholz (Ed.), Springer, Berlin, 2016.

[5] M. Kalousek, Processes at the dropping electrode with a discontinuously changing potential, *Collect. Czech. Chem. Commun.*, **13** (1948), pp. 105–115.

[6] G. C. Barker, A. W. Gardner, Square-wave polarography, *Analyst*, **117** (1992), pp. 1811–1828.

[7] G. C. Barker, I. L. Jenkins, Square-wave polarography, *Analyst*, **77** (1952), pp. 685–696.

[8] G. C. Barker, Square-wave polarography and some related techniques, *Anal. Chim. Acta.,* **18** (1958), pp. 118–131.

[9] J. H. Christie, J. A. Turner, R. A. Osteryoung, Square wave voltammetry at the dropping mercury electrode: Theory, *Anal. Chem.,* **49** (1977), pp. 1899–1903.

[10] J. Osteryoung, J. J. O`Dea, Square-wave voltammetry, in: *Electroanalytical chemistry*, A. J. Bard (Ed.), Marcel Dekker, New York, 1986, **14**, pp. 209–308.

[11] M. Lovrić, Square-wave voltammetry, in: *Electroanalytical Methods*, F. Scholz (Ed.) Springer, Berlin, 2002.

[12] J. Gonzalez, A. Molina, F. Martinez Ortiz, E. Laborda, Characterization of the electrocatalytic response of monolayer-modified electrodes with square-wave voltammetry, *J. Phys. Chem. C*, **116**, 20 (2012), pp. 11206–11215.

[13] E. Laborda, A. Molina, Q. Li, C. Batchelor-McAuley, R. G. Compton, Square wave voltammetry at disc microelectrodes for characterization of two electron redox processes, *Phys. Chem. Chem. Phys.*, **14** (2012), pp. 8319–8327.

[14] A. Molina, J. Gonzalez, E. Laborda, Y. Wang, R. G. Compton, Analytical theory of the catalytic mechanism in square wave voltammetry at disc electrodes, *Phys. Chem. Chem. Phys.*, **13** (2011), 16748–16755.

[15] Y. Wang, E. Laborda, M. C. Henstridge, F. Martinez-Ortiz, A. Molina, R. G. Compton, The use of differential pulse voltammetries to discriminate between the Butler–Volmer and the simple Marcus–Hush models for heterogeneous electron transfer: The electroreduction of europium (III) in aqueous solution, *J. Electroanal. Chem.*, **668** (2012), pp. 7–12.

[16] M. C. Henstridge, E. Laborda, R. G. Compton, Asymmetric Marcus–Hush model of electron trans-

fer kinetics: Application to the voltammetry of surface-bound redox systems, *J. Electroanal. Chem.*, **674** (2012), pp. 90–96.

[17] R. Gulaboski, L. Mihajlov, Catalytic mechanism in successive two-step protein-film voltammetry—Theoretical study in square-wave voltammetry, *Biophys. Chem.*, **155** (2011), pp. 1–9.

[18] R. Gulaboski, M. Lovrić, V. Mirčeski, I. Bogeski, M. Hoth, A new rapid and simple method to determine the kinetics of electrode reactions of biologically relevant compounds from the half-peak width of the square-wave voltammograms, *Biophys. Chem.*, **138** (2008), pp. 130–137.

[19] M. Zhou, S. Gan, L. Zhong, B. Su, L. Niu, Ion transfer voltammetry by a simple two polarized interfaces setup, *Anal. Chem.*, **82** (2010), pp. 7857–7860.

[20] D. Krulic, N. Fatouros, Peak heights and peak widths at half-height in square wave voltammetry without and with ohmic potential drop for reversible and irreversible systems, *J. Electroanal. Chem.,* **652** (2011), pp. 26–31.

[21] D. Krulic, N. Fatouros, Square wave voltammetry of concentrated analytes in fully supported solutions – Cd(II)/Cd(Hg) couple in $NaNO_3$ medium. *J. Electroanal. Chem.*, 655 (2011), pp. 116–119.

[22] J. Zhang, S. X. Guo, A. M. Bond, J. M. Honeychurch, K. B. Oldham, Novel kinetic and background current selectivity in the even harmonic components of Fourier transformed square-wave voltammograms of surface-confined azurin, *J. Phys. Chem. B,* **109** (2005), pp. 8935–8947.

[23] B. D. Fleming, N. L. Barlow, J. Zhang, A. M. Bond, F. A. Armstrong, Application of power spectra patterns in Fourier transform square wave voltammetry to evaluate electrode kinetics of surface-confined proteins, *Anal. Chem*., **78** (2006), pp. 2948–2956.

[24] X. Huang, L. Wang, S. Liao, Method of evaluation of electron transfer kinetics of a surface-confined redox system by means of Fourier transformed square wave voltammetry, *Anal. Chem.*, **80** (2008), pp. 5666–5670.

[25] G. W. C. Milner, L. J. Slee, Analytical applications of the Barker square-wave polarograph. Part III. Orthophosphoric acid as a solvent and base electrolyte in direct inorganic polarographic analysis, *Analyst*, **82** (1957), pp. 139–151.

[26] W. F. Kinard, R. H. Philip, R. C. Propst, Analytical applications of Kalousek polarography, *Anal. Chem.*, **39**, 13 (1967), pp. 1556–1562.

[27] G. Geerinck, H. Hilderson, C. Vanttulle, F. Verbeck, Square wave polarography, *J. Electroanal. Chem.,* **5** (1963), pp. 48–56.

[28] R. E. Hamm, Square-Wave Polarograph, *Anal. Chem.*, **30**, 3 (1958), pp. 351–354.

[29] B. Y. Kaplan, T. N. Sevastyanova, Advantages of debalance-method in substractive square-wave polarography, *Zh. Anal. Khim*., **26** (1971), pp. 1054.

[30] H. Blutstein, A. M. Bond, Fast sweep differential pulse voltammetry at a dropping mercury electrode, *Anal. Chem.*, **48**, 2 (1976), pp. 248–252.

[31] M. Kopanica, V. Stara, Fast-scan differential pulse polarography in pre-enriched solution, *J. Electroanal. Chem.* **127** (1981), pp. 255–261.

[32] P. W. Alexander, V. Akapongkul, Differential pulse voltammetry with fast pulse repetition times in a flow-injection system with a copper-amalgam electrode, *Anal. Chim. Acta*, **166** (1984), pp. 119–127.

[33] L. Ramaley, W.T. Tan, Single drop square wave polarography, *Can. J. Chem*. **59**, 24 (1981), pp. 3326–3333.

[34] J. Y Hwang, Y. Y. Wang, C.C. Wan, A Theoretical analysis of single drop square-wave polarography, *J. Chin. Chem. Soc.,* **33** (1986), pp. 302–307.

[35] V. Mirčeski, R. Gulaboski, M. Lovrić, I. Bogeski, R. Kappl, M. Hoth, Square-wave voltammetry: a review on the recent progress, *Electroanalysis*, **25**, 11 (2013), pp. 2411 – 2422.

[36] V. Mirčeski, R. Gulaboski, Recent Achievements in Square-Wave Voltammetry – A Review, *Macedonian Journal of Chemistry and Chemical Engineering*, **33** (2014), pp. 1–12.

[37] M. Geissler, C. Kuhnhardt, *Square-wave-Polarographie*, VEB Deutscher Verlagfur Grundstoffindustrie, Leipzig, 1970.

[38] L. Ramaley, M. S. Krause Jr., Theory of square wave voltammetry, *Anal. Chem*., **41**, 11 (1969), pp. 1362–1365.

[39] M. S. Krause Jr., L. Ramaley, Analytical application of square wave voltammetry, *Anal. Chem.,* **41**, 11 (1969), pp. 1365–1369.

[40] E. Laborda, J. González, Á. Molina, Recent advances on the theory of pulse techniques: A mini review, *Electrochemistry Communications,* **43** (2014), pp. 25–30.

[41] M. Lovrić, Simulation of square wave voltammetry of three electrode reactions coupled by two reversible chemical reactions, *J. Electrochem. Sci. Eng.,* **7**, 3 (2017) pp. 119–129.

[42] M. Lovrić, Š. Komorsky-Lovrić, Theory of square wave voltammetry of three step electrode reaction, *Journal of Electroanalytical Chemistry,* **735** (2014), pp. 90–94

[43] Š. Komorsky-Lovrić, D. Jadreško, M. Lovrić, Theory of square wave voltammetry of amalgam forming ions at spherical electrodes, *Electrochimica Acta*, **130** (2014), pp. 286–289.

[44] M. Lovrić, D. Jadreško, Š. Komorsky-Lovrić, Theory of square-wave voltammetry of electrode reaction followed by the dimerization of product, *Electrochimica Acta,* **90** (2013), pp. 226–231.

[45] N. Fatouros, D. Krulic, Conditions for a nearly perfect match between pulse voltammetry and linear scan voltammetry, *Journal of Electroanalytical Chemistry,* **817** (2018), pp. 167–175.

[46] J. M. Olmos, A. Molina, E. Laborda, F. Martínez-Ortiz, Effects of unequal diffusion coefficients and coupled chemical equilibria on square wave voltammetry at disc and hemispherical microelectrodes, *Electrochimica Acta*, **176** (2015), pp. 1044–1053.

[47] S. N. Vettorelo, F. Garay, Theory of square-wave catalytic adsorptive stripping voltammetry. How to obtain mechanistic information from experimental data, *Journal of Electroanalytical Chemistry*, **826** (2018), pp. 125–132.

[48] N. Meddings, J. R. Owen, N. Garcia-Araez, A simple, fast and accurate in-situ method to measure the rate of transport of redox species through membranes for lithium batteries, *Journal of Power Sources,* **364** (2017), pp. 148–155.

[49] Parveen, R. Kant, General theory for pulse voltammetric techniques at rough electrodes: multistep reversible charge transfer mechanism, *Electrochimica Acta*, **220** (2016), pp. 475–485.

[50] L. Shaw, L. Dennany, Applications of electrochemical sensors: Forensic drug analysis, *Current Opinion in Electrochemistry,* **3** (2017), pp. 23–28.

[51] V. Jovanovski, S. B. Hočevar, B. Ogorevc, Bismuth electrodes in contemporary electroanalysis, *Current Opinion in Electrochemistry*, **3** (2017), pp. 114–122.

[52] Y. Liu, Y. Liu, L. Qiao, Y. Liu, B. Liu (in press), Advances in signal amplification strategies for electrochemical biosensing, *Current Opinion in Electrochemistry*. DOI: 10.1016/j.coelec.2018.05.001

[53] J. Hoyos-Arbeláez, M. Vázquez, J. Contreras-Calderón, Electrochemical methods as a tool for determining the antioxidant capacity of food and beverages: A review, *Food Chemistry,* **221** (2017), pp. 1371–1381.

[54] S. Huang, N. Gan, T. Li, Y. Zhou, Y. Cao, Y. Dong, Electrochemical aptasensor for multi-antibiotics detection based on endonuclease and exonuclease assisted dual recycling amplification strategy, *Talanta,* **179** (2018), pp. 28–36.

[55] X. Cao, J. X. Liu , F. Zhang, Z. Wang, H. Liu, L. Lu, A new dual-signalling electrochemical aptasensor with the integration of "signal on/off" and "labeling/label-free" strategies, *Sensors and Actuators B: Chemical,* **239** (2017), pp. 166–171.

[56] K. Biała , A. S. Mix, K. Bär, P. Orsag, M. Fojta, G. Flechsig, Amplified detection of single base mismatches with the competing-strand assay reveals complex kinetic and thermodynamic behavior of strand displacement at the electrode surface, *Electrochimica Acta*, **285** (2018), pp. 272–283

[57] N. Tonello, M. B. Moressi, S. N. Robledo, F. D'Eramo, J. M. Marioli, Square wave voltammetry with multivariate calibration tools for determination of eugenol, carvacrol and thymol in honey, *Talanta,* **158** (2016), pp. 306–314

[58] A. Taleb, X. Yanpeng, P. Dubot, Self-organized gold nanoparticles modified HOPG electrodes: Electrochemical stability and its use for electrochemical nanosensing applications, *Applied Surface Science,* **420** (2017), pp. 110–117.

[59] G. D. da Silveira, L. M. de Carvalho, N. Montoya, A. Domenech-Carbó, Solid state electrochemical behavior of organosulfur compounds, *Journal of Electroanalytical Chemistry,* **806** (2017), pp. 180–190.

[60] V. Mirceski, D. Guziejewski, K. Lisichkov, Electrode kinetic measurements with square-wave voltammetry at a constant scan rate, *Electrochimica Acta*, **114** (2013), pp. 667–673.

[61] D. Guziejewski, V. Mirceski, D. Jadresko, Measuring the electrode kinetics of surface confined electrode reactions at a constant scan rate, *Electroanalysis,* **27** (2015), pp. 67–73.

[62] V. Mirčeski and M. Lovrić, Split square-wave voltammograms of surface redox reactions, *Electroanalysis,* **9** (1997), pp. 1283–1287.

[63] V. Mirčeski, S. Smarzewska, D. Guziejewski, Measuring the electrode kinetics of vitamin B2 at a constant time window of a square wave voltammetric experiment, *Electroanalysis,* **28** (2016), pp. 385–393.

[64] C. Bonazzola , G. Gordillo, Advanced analysis for electrode kinetic studies of surface reactions by applying square-wave voltammetry, *Electrochimica Acta*, **213** (2016), pp. 613–619.

[65] V. Mirčeski, E. Laborda, D. Guziejewski, R. G. Compton, A new approach to electrode kinetic measurements in square-wave voltammetry. Amplitude-based quasireversible maximum, *Anal. Chem.* **85** (2013), pp. 5586–5594.

[66] D. Jadreško, M. Zelić, M. Lovrić, A formal scan rate in staircase and square-wave voltammetry, *Journal of Electroanalytical Chemistry,* **645** (2010), pp. 103–108.

[67] V. Mirčeski, D. Guziejewski, M. Bozem, I. Bogeski, Characterizing electrode reactions by multisampling the current in square-wave voltammetry, *Electrochim. Acta,* **213** (2016), pp. 520–528.

[68] X. Cheng, G. Pu, Cyclic Square Wave Voltammetry: Theory and Experimental, *Anal. Lett.*, **20** (1987), pp. 1511–1519.

[69] M. A. Mann, L. A. Bottomley, Cyclic Square Wave Voltammetry of Surface-Confined Quasireversible Electron Transfer Reactions, *Langmuir*, **31** (2015) pp. 9511–9520.

[70] C. J. Helfrick Jr, L. A. Bottomley, Cyclic square wave voltammetry of single and consecutive reversible electron transfer reactions, *Anal. Chem*., **81**, 21 (2009), pp. 9041–9047.

[71] C. John, Helfrick Jr., M. A. Mann, A. Lawrence, Bottomley diagnostic criteria for the characterization of electrode reactions with chemical reactions following electron transfer by cyclic square wave voltammetry, *Electrochimica Acta*, **205** (2016), pp. 20–28.

[72] A. Molina, M. M. Moreno, C. Serna, M. Lopez-Tenes, J. Gonzalez, N. Abenza, Study of multicen-

ter redox molecules with square wave voltammetry, *J. Phys. Chem. C*. **111** (2007), pp. 12446–12453.

[73] M. Zelić, M. Lovrić, Isopotential points in reverse square-wave voltammetry, *J. Electroanal. Chem.*, **637** (2009), pp. 28–32.

[74] M. Lovrić, D. Jadreško, Theory of square-wave voltammetry of quasireversible electrode reactions using an inverse scan direction, *Electrochim. Acta*, **55** (2010), 948–951.

[75] M. Lovrić, Š. Komorsky-Lovrić, Theory of reverse scan square-wave voltammetry influenced by the kinetics of reactant adsorption, *Cent. Eur. J. Chem.* **8** (2010), pp. 513–518.

[76] M. C. Henstridge, E. Laborda, N. V. Rees, R. G. Compton, Marcus–Hush–Chidsey theory of electron transfer applied to voltammetry: A review, *Electrochim. Acta*, **84** (2012), pp. 12–20.

[77] D. Jadreško, D. Guziejewski, V. Mirčeski, Electrochemical Faradaic Spectroscopy, *Chem. Electro-Chem*, **5** (2018), pp. 187–194.

[78] W. M. Smit, M. D. Wijnen, Square wave electrolysis. I. The cyclic potential-step method, *Recueil*, **79** (1960), pp. 5–21.

[79] W. M. Smit, M. D. Wijnen, Square wave electrolysis III. Apparatus for the cyclic potential-step and cyclic current-step methods, *Recueil*, **79** (1960), pp. 203–215.

[80] W. M. Smit, M. D. Wijnen, Square wave electrolysis IV. Results and discussion, *Recueil,* **79** (1960), pp. 289–312.

КВАДРАТНО-БРАНОВА ВОЛТАММЕТРИЈА: НАЈНОВИ ДОСТИГАЊА И ПЕРСПЕКТИВИ

Валентин Мирчески[1,2], Леон Стојанов[1], Sławomira Skrzypek[2]

[1]Институт за хемија, Природно-математички факултет,
Универзитет „Св. Кирил и Методиј“,Скопје, Република Македонија
[2]Department of Inorganic and Analytical Chemistry, Faculty of Chemistry,
University of Lódż, Poland

Во овој ревијален труд е даден преглед на најновите достигања на квадратно-брановата волтаммет рија, како една од најсофистицираните пулсни волтаммет риски техники. Разгледани се најновите теориски трудови, дел од напредните студии за аналитичка примена на техниката, а особен акцент е ставен на неколку нови методолошки концепти како што се методата за мерење на електродна кинетика при константна брзина на промена на потенцијалот, циклична квадратно-бранова волтаммет рија, квадратно-брановата волтаммет рија со повеќекратно мерење на струјата и електрохемиската Фарадеева спектроскопија. За понатамошно усовршување на техниката предложени се две нови методи, досега непознати во научната литература.

Клучни зборови: квадратно-бранова волтаммет рија; електрдони механизми; електродна кинетика

ПРИЛОЗИ, Одделение за природно-математички и биотехнички науки, МАНУ, том **39**, бр. 2, стр. 123–128 (2018)
CONTRIBUTIONS, Section of Natural, Mathematical and Biotechnical Sciences, MASA, Vol. **39,** No. 2, pp. 123–128 (2018)

Received: October 9, 2018
Accepted: November 26, 2018

ISSN 1857–9027
e-ISSN 1857–9949
UDC: 582.929.4-196(497.7)
DOI: 10.20903/csnmbs.masa.2018.39.2.124

Original scientific paper

CLINOPODIUM ALBANICUM (GRISEB. ex K. MALÝ) MELNIKOV NEW SPECIES FOR THE FLORA OF THE REPUBLIC OF MACEDONIA

Vlado Matevski

Macedonian Academy of Sciences and Arts, Skopje, Republic of Macedonia
*e-mail: vlado.matevski@yahoo.com

During floristical investigation in western parts of the Republic of Macedonia one new species of vascular plants was found which was not previously reported for the country – *Clinopodium albanicum* (Griseb. ex K. Malý) Melnikov.

Key words: flora; Macedonia; distribution; *Clinopodium albanicum* (Griseb. ex K. Malý) Melnikov

INTRODUCTION

The latest revision of the genera *Satureja* L., *Clinopodium* L., *Micromeria* Bentham, *Calamintha* Mill. and *Acinos* Mill, based on modern molecular-phylogenetic studies, have led to many new taxonomic solutions, to new taxonomic and nomenclature combinations [1–9]. An attempt was made to clarify the boundaries between the different genera, as well as to determine the real taxonomic status and position of certain species and lower taxa within these genera. The taxonomic solutions based on the specific morphological characteristics at the level of the genera, sections, subsections or species, especially within the genera *Micromeria* and *Clinopodium*, in many cases were not very clear and precisely defined, followed by a very complex synonymy, as well as with the inevitable author subjectivism.

On the one hand, some species, depending on author's taxonomic concept, have often changed their taxonomic and nomenclature status within the different genera [e.g. *Calamintha grandiflora* (L.) Moench, *Satureja grandiflora* (L.) Scheele, *Clinopodium grandiflorum* (L.) Kuntze], while on the other hand, some species described from the some parts of the Balkan Peninsula were neglected, such as *Clinopodium albanicum* (Griseb. ex K. Malý) Melnikov [*Micromeria albanica* (K. Malý) Šilić, *Satureja albanica* Griseb. ex K. Malý] and they were associated with related species from the other areas (*Micromeria serpyllifolia*).

Aim of the elaboration is to establish the adequate classification of the species of the genus Clinopodium found between Kichevo and Demir Hisar. As these species was often treated within different taxa (*Clinopodium albanicum*, *Clinopodium dalmaticum* subsp. *bulgaricum*, *Clinopodium serpyllifolium*) we tried to highlight also development of classification history of this species.

EXPERIMENTAL SECTION

Floristic researches were carried out in the western parts of the territory of the Republic of Macedonia (Demir Hisar, between the villages of Velmevci and Železnec). Herbarium material is deposed in the Herbarium of the Institute of Biology, Faculty of Natural Sciences and Mathematics in Skopje (MKNH). When determining the herbarium material, appropriate literature was consulted – Prodromus Florae peninsulae Balcanicae, II [10]; Flora Europaea, III [11] and other regional floras [12], as well as some special papers [1–9] and databases – Euro+Med Plant Base [13] dealing with taxonomy, nomenclature and chorology of the taxa studied.

RESULTS AND DISCUSSION

During the our work on Lamiaceae family for the edition "The Flora of the Republic of Macedonia", special attention was paid to the species *Clinopodium albanicum*, which was discovered in the southwest parts of the territory of the Republic of Macedonia (between Kichevo and Demir Hisar) as well as his relationship with the species *Clinopodium serpyllifolium* (*Micromeria serpyllifolia*) and *Micromeria bulgarica*.

The western Balkan endemic species *Clinopodium albanicum* (*Micromeria albanica*, *Satureja albanica*) was discovered in the vicinity of Prizren, Kosovo, (sub. *Micromeria albanica* Griseb., Locus classicus: Resnathal = Rekathal bei Prizren, besonders hfg. auf Kalkfelsen bei d. Ruinen d. Schlosses Demanitze, 1839; by A. Grisebach) [14].

From the chronological overview of the data cited in the botanical literature for the taxonomy, nomenclature and distribution of this species can be found the following:

Hayek [10] considers this species (as *Satureja albanica*) a synonym of the species *Micromeria serpyllifolia* (MB) Briq, citing it only for the territory of Albania. But, it should be noted that Hayek's territorial boundaries in Prodromus Florae peninsulae Balcanicae do not correspond with today's state borders of the Balkan Peninsula countries.

Malý [15] points this species under the name *Satureja albanica* Griseb. ex K. Malý.

Chater & Guinea [11] in the Flora Europaea edition do not mention the species *Satureja albanica* Griseb. ex K. Malý [= *Micromeria albanica* (K. Malý) Šilić] *et al*. They cite the taxon *Micromeria fruticosa* (L.) Druce subsp. *serpyllifolia* (Bieb.) P. H. Davis for Crimea, Southwestern Asia and Southwestern Yugoslavia, so according to this we can lead to the conclusion that the data for Southwestern Yugoslavia actually refers to *Micromeria albanica*.

Diklić [12] in the Flora of SR Serbia edition accepts the decision that *Satureja albanica* is a synonym of *Micromeria serpyllifolia* MB, so cites it for Serbia: Kosovo – Prizrenska Bistrica.

Šilić [16] in his monograph dedicated to the genera *Satureja* L., *Clinopodium* L., *Micromeria* Bentham, *Calamintha* Mill. and *Acinos* Mill. in the flora of Yugoslavia, the status of the species *Satureja albanica* Griseb ex K. Malý was actualized and he confirm the indepenadent status of the taxon and proposes the following nomenclature commbination – *Micromeria albanica* (Griseb. ex K. Malý) Šilić stat. et comb. new. Close to the classical locality (Resnathal = Rekathal bei Prizren), this species was confirmed later of the several botanists in the canyon of the Prizren Bistrica (Malý [15], Šilić [16]). In the chapter on distribution of this species, besides Kosovo, it is also cited for Albania (In the valley Crni Drim ad pagum Suhodol pr. Peškopija, 27.VIII.1917, Dr. J. Andrásovszky – Herb., Dr Antal Pénzes, Budapest) (Šilić [16]).

Šilić [16] in the same monograh on the territory of the Republic of Macedonia cites the speciec *Micromeria bulgarica* (Velen.) Vandas, based on the data of Vandas [17, 18], for the presence of this species in the area of Demir Hisar, Usunža river and Krivska river. According to Chater et Guinea [11], *Micromeria bulgarica* as a subspecies is attached to *Micromeria dalmatica* subsp. *bulgarica* (Velen.) Guinea, while Bräuchler et al. [3] think that the real position of this species is in the synonymy of *Clinopodium dalmaticum* (Benth.) Bräuchler & Heubl. The same solution is present in Euro+Med Plantbase also (http://ww2.bgbm.org/EuroPlusMed/query.asp).

Greuter et al. [19] in the Med-Checklist accept the old nomenclature solution – *Satureja albanica* K. Malý, so this species is referring to Yugoslavia (Kosovo) and Albania. In the synonymy of this species they include the previous taxonomical and nomenclature solutions for "*Micromeria serpyllifolia*" (sensu Hayek [10], Diklić [12]) and *Micromeria albanica* (K. Malý) Šilić. Greuter et al. [19], make a distinction between the species *Satureja albanica* (*Micromeria albanica*) and *Micromeria serpyllifolia*, both in terms of their particular taxonomic status and their distribution. Thus, according to Greuter et al. [19] the area of distribution of the species *Satureja serpyllifolia* covers the territory of Crimea, the Asian part of Turkey, Lebanon, Syria, Israel and Jordan, while the area of *Satureja albanica* K. Malý [= *Micromeria albanica* (K. Malý) Šilić] is located in the western parts of the Balkan Peninsula.

In the Euro + Med Plantbase [13] the old nomenclature combination is returned – *Micromeria albanica* (K. Malý) Šilić.

Bräuchler et al. [3] in the updated monograph on the genus *Micromeria*, they disputed the taxonomic value of *Micromeria albanica* (*Satureja albanica*) and this species is listed in the synonymy of the species *Clinopodium serpyllifolium* (M. Bieb.) Kuntze.

Finally, Melnikov [7] actualize again the taxonomic status of the species *Micromeria albanica* (*Satureja albanica*) and offers the following combination - *Clinopodium albanicum* (Griseb. ex K. Malý) Melnikov, comb. new. [*Satureja albanica*

Griseb. ex K. Malý ≡ *Micromeria albanica* (K. Malý) Šilić].

Of all the above, the question is whether the taxonomic status of the *Clinopodium albanicum* (Griseb. ex K. Malý) Melnikov (*Satureja albanica*, *Micromeria albanica*) is justified, or it is a synonym of *Clinopodium serpyllifolium* (M. Bieb.) Kuntze.

In clarifying this problem, we had extensive literature on these two species as well as a rich herbarium material from the *Clinopodium albanicum*, collected from the territory of the Republic of Macedonia, in the area of Demir Hisar (between the villages of Železnec and Velmevci). In this respect, the monograph of Šilić [16], which provides an extensive diagnostic description of the species *Micromeria albanica* (based on the herbarium material from the canyon of the Bistrica river above Prizren), is particularly significant, with detailed morphological characteristics, ecology, inventory of the accompanying plant species registered on his habitat, drawings of the inflorescence, calyx, corolla, bracts, leaves, a photograph of the habitat of this species from its Locus classicus as well as its synonymy.

The analysis of the herbarium material from the area of Demir Hisar showed that the registered populations can not be linked to the species *Micromeria bulgarica* (Velen.) Vandas (according to modern concepts *Clinopodium dalmaticum* or *Clinopodium dalmaticum* subsp. *bulgaricum*), cited by Šilić [16], for the territory of the Republic of Macedonia (Demir Hisar, Usunja river and Krivska river) based on the data of Vandas [17, 18]. Namely, it should be noted that Šilić [16], in the absence of authentic herbarium material of *Micromeria bulgarica* from the territory of Macedonia, uses drawings of the most important morphological characteristics of this taxon using herbarium material from the territory of Bulgaria (Rodopi). There is a noticeable difference between these two taxa in the shape and the hairy of the leaves, as well as the size of the calyx and shape of the calyx-teeth. In the herbarium material of *Clinopodium albanicum*, originating from the territory of the Republic of Macedonia (calyx is regular, 2–2.5 mm long, the calyx-teeth are triangular, about as long as wide)(Figures 1, 3, 4) while in the *Micromeria bulgarica* (i.e. *Clinopodium dalmaticum*) originating from the territory of Bulgaria (calyx is longer than 3 mm, the calyx-teeth are elongated, lanceolate to subulate, much longer than wide, acute) (Figure 2).

As for the species *Clinopodium serpyllifolium*, with whom *Clinopodium albanicum* (= *Micromeria albanica*, *Satureja albanica*) was often linked, its range extends to the territory of Crimea, the Asian part of Turkey, Lebanon, Syria, Israel and Jordan, so the presence of this species on the territory of the Balkan Peninsula is excluded [19].

Figure 1. *Clinopodium albanicum* - calyx (MK: Demir Hisar:Železnec-Velmevci)

Figure 2. *Clinopodium dalmaticum* subsp. *bulgaricum* - calyx (BG: Rodopi)

Melnikov [7] published a very important study devoted to the new sections of the genus *Clinopodium*, so that within the boundaries of this genus he described several new sections and subsections, which at the same time represent a solid basis for the solution of taxonomic and nomenclature problems at the supraspecies and spe-

cies level. Namely, Melnikov [7] distinguishes two separate sections that include the above-mentioned closely related species, which are however clearly morphologically and horologically differentiated. In the newly published Sect. *Pseudomelissa* (Benth.) Melnikov, whose representatives are characterized by a more or less irregular calyx with elongated calyx-teeth, he includes the species *Clinopodium dalmaticum* (*Micromeria bulgarica* is usually attached to this species as a subspecies or synonyms). Melnikov [7], in the newly described Sect. Brachyodontia Melnikov, which differs from the Sect. Pseudomelissa with the almost regular calyx and equal triangular or wide-triangular calyx-teeth, about as long as wide, with short soft hairs on the stems, leaves, calyx and pedicels, separates two subsections – subsect. *Brachyodontia* and subsect. *Inkermenia* Melnikov. In subsect. *Brachyodontia*, stem hairs are retrorse (here the *Clinopodium albanicum* species is attached), while in the Subsect. *Inkermenia* stem hairs are directed upwards (includes the Crimean species *C. serpyllifolium*).

Figure 3. *Clinopodium albanicum* – habitat of the species (MK: Demir Hisar:Železnec-Velmevci)

Figure 4. *Clinopodium albanicum* – habitus of the species (MK: Demir Hisar:Železnec-Velmevci

From the above, it could be concluded that the taxonomic status of the species *Clinopodium albanicum* is not questionable. The discovered populations from the area of Demir Hisar (between the villages Velmevci and Zeleznec) (Figure 5) no doubt belong to this species. In this way, the data of Vandas [17, 18] and Šilić [16] for the presence of the *Micromeria bulgarica* (Velen.) Vandas (*Clinopodium dalmaticum* or *Clinopodium dalmaticum* subsp. *bulgaricum*) in the listed localities on the territory of the Republic of Macedonia are revised.

In addition, we provide a diagnostic description of the population of the *Clinopodium albanicum* from the following locality: Republic of Macedonia: Demir Hisar: between the villages Velmevci and Zeleznec, along the road Kičevo-Demir Hisar, on limestone, 41° 21'06.14 "N; 21° 02 '29.80 "E, 853 m; 10/22/2017 (leg. et det. V. Matevski (MKNH).

Perennial plant. Stems up to 40–50 cm, erect or ascending from the base, in the upper part branched, obtuse 4-angled, with very dense, short deflexed hairs, often with a glandular hairs. Leaves ovate to ovate-elongated, (10) 13–25 (38) mm long, (5) 7–10 (17) mm wide, obtuse, gradually cuneate at base, petiole 4–9 mm long, entire or shallow dentate with 1–4 teeth on each side, with 3–4 lateral veins, both sides with short puberulent hairs, short stalked glands and glandular-punctate. Flowers shortly pedicellate, cymes many-flowered grouped in terminal inflorescences that are initially compressed, later are fragmented and branched. Bracts linear-subulate. Calyx (2) 2.2–2.8 mm long, obconical with 13 clearly distinctive veins, along the veins of the calyx there are simple retrorse hairs, between the veins with the short stalked glands and glandular-punctate, densely villosus in throat, calyx teeth 0.3-0.7 mm long, triangular, about as long as wide. Corolla 6–6.5 mm long, whitish or whitish-violet, outside hairy, 2-lipped, the upper lip entire or shallow bifid, lower lip 3-lobed. Stamens and style excerted out corolla. Nutles obtuse, 1.1–1.2 mm long, yellowish-brown.

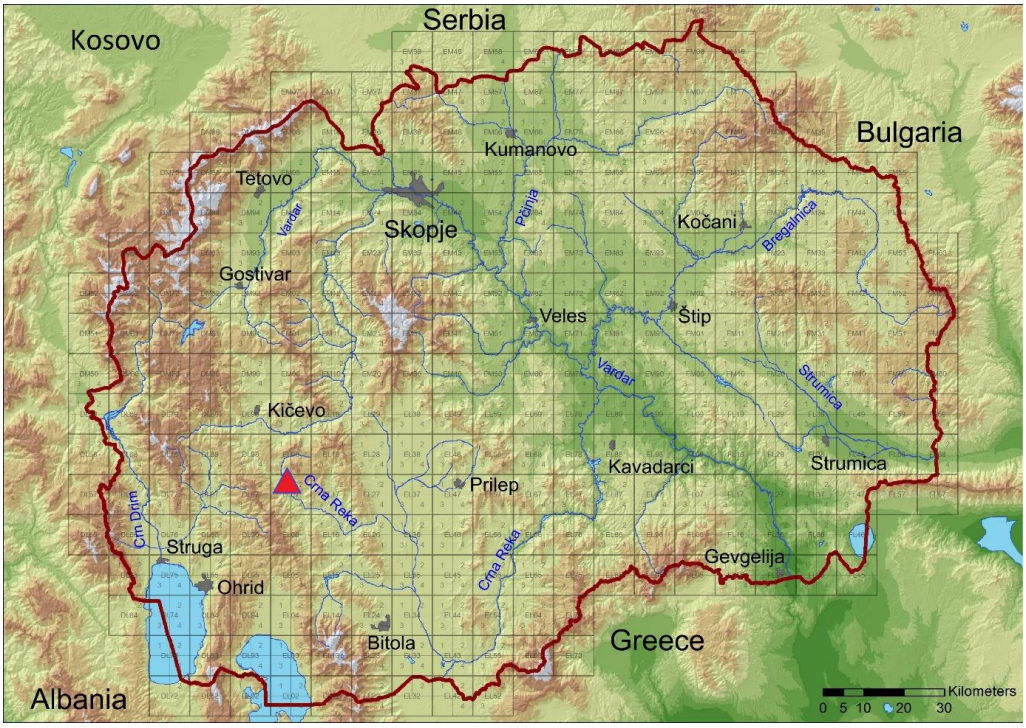

Figure 5. *Clinopodium albanicum* – Map of distribution in the Republic of Macedonia

Acknowledgement. The investigation was supported by the project fund of Macedonian Academy of Sciences and Arts. I thank to Prof. Dr. Slavčo Hristovski for assistance in the preparation of some of the photographs in the paper.

REFERENCES

[1] R. Morales, Sinopsis y distribución del género *Micromeria* Bentham, *Bot. Complutensis*, **18** (1993), pp. 157–168.

[2] C. Bräuchler, H. Meimberg, T. Abele, G. Heubl, Polyphyly of the genus *Micromeria* (Lamiaceae):

Evidence from cpDNA sequence data, *Taxon*, **54**(3) (2005), pp. 639–650. DOI: 10.2307/25065421

[3] C. Bräuchler, H. Meimberg, G. Heubl, New names in Old World *Clinopodium* – the transfer of the species of *Micromeria* sect. *Pseudomelissa* to *Clinopodium*, *Taxon*, **55**(4) (2006), pp. 977–981. DOI: 10.2307/25065692

[4] C. Bräuchler, O. Ryding, G. Heubl, The genus *Micromeria* (*Lamiaceae*), a synoptical update, *Willdenowia* **38** (2008), pp. 363–410. ISSN 0511-9618; © 2008 BGBM Berlin-Dahlem. DOI:10.3372/wi.38.38202 (available via http://dx.doi.org/)

[5] T. Arabaci, T. Dirmenci, F. Celep, Morphological character analysis in Turkish *Micromeria* Bent. (*Lamiaceae*) species with a numerical taxonomic study, *Turk. J. Bot.*, **34** (2010), pp. 379–389.

[6] E. Martin, O. Cetin, T. Dirmenci, H. Ay, Karyological studies of *Clinopodium* L. (Sect. *Pseudomelissa*) and *Micromeria* Benth. s. str. (*Lamiaceae*) from Turkey, *Caryologia*, **64**(1) (2011), pp. 398–404. DOI: 10.1080/00087114.2011.10589807

[7] D. G. Melnikov, New sections of the genus *Clinopodium* L. (*Lamiaceae*) and their synopsis, *Turczaninowia*, **18** (3) (2015), pp. 103–112.

[8] D. G. Melnikov, New taxa in the genus *Clinopodium* L. (Lamiaceae), 2. *Turczaninowia* **19** (2) (2016), pp. 86–98. DOI: 10.14258/turczaninowia.19.2.12.

[9] D. G. Melnikov, Sistematika i geografia roda *Clinopodium* L. (Lamiaceae) Evrazii. Doct. thesis 2017 p. 221. Botan. Inst. V. L. Komarov, Rus. Akad. Nauk., Sankt-Peterburg.

[10] A. Hayek, *Prodromus Florae peninsulae Balcanicae*, II. *Feddes Repert*., Beih., 30. (1928–1931), Dahlem bei Berlin.

[11] A. O. Chater et E. Guinea, *Micromeria* Bentham in T. G. Tutin et al. (eds.), *Flora Europaea* **3,** 1972, pp. 167–170, Cambridge.

[12] N. Diklić, *Micromeria* Bentham in Josifović et al., (eds.) *Flora SR Srbije*, **6,** 1974, pp. 458-462, Belgrade.

[13] Euro + Med Plantbase (http://ww2.bgbm.org/EuroPlusMed/query.asp.).

[14] A. Grisebach, *Reise durch Rumelien und nach Brussa im Jahre 1839*, II Band, 1841, p. 320. Göttingen.

[15] K. Maly, *Satureja*-Arten Südserbiens. *Bull. Inst. Jard. Botan. Univer. Belgrade*, **1**(3) (1930), pp. 229–232, Belgrade.

[16] Č. Šilić, *Monografija rodova Satureja L., Calamintha Miller, Micromeria Bentham, Acinos Miller i Clinopodium L. u flori Jugoslavije*. Zemaj. Muzej BiH, Posebno izdanje, Sarajevo, 1979, 440 p.

[17] C. Vandas, Novae Plantae Balcanicae. *Mag. Bot. Lapok*, **4** (1905) pp. 109–113.

[18] C. Vandas, Reliquiae Formánekianae, Enumeratio critica plantarum vascularium quas itineribus in haemo peninsula et Asia minore (Bithynia) factis collegit Dr Ed. Formanek, professor gymnasia Brunensis Bohemici, 1909, p. 612, Brunae.

[19] W. Greuter, H. M. Burdet, G. Long, *Med-Checklist*, Dicotyledones (*Convolvulaceae-Labiatae*), **3** (1986), p. 395, Geneve-Berlin-Dahlem.

CLINOPODIUM ALBANICUM (GRISEB. ex K. MALÝ) MELNIKOV НОВ ВИД ЗА ФЛОРАТА НА РЕПУБЛИКА МАКЕДОНИЈА

Владо Матевски

Македонска академија на науките и уметностите, Скопје, Република Македонија

Во текот на флористичките истражувања во западните делови од територијата на Република Македонија (во околината на Демир Хисар, помеѓу селата Велмевци и Железнец) е откриен еден нов вид за флората на Република Македонија – *Clinopodium albanicum* (Griseb. ex K. Malý) Melnikov [*Micromeria albanica* (K. Malý) Silic, *Satureja albanica* Griseb. ex K. Malý], досега непознат за нејзината територија. Во трудот се разгледува проблемот околу оправданоста на таксономскиот статус на овој вид и неговата поврзаност со таксоните *Clinopodium dalmaticum* (односно *Clinopodium dalmaticum* subsp. *bulgaricum* = *Micromeria bulgarica* и *Clinopodium serpyllifolium*).

Анализата на хербариумскиот материјал од околината на Демир Хисар покажа дека регистрираните популации не можат да се поврзат со видот *Micromeria bulgarica* (Velen.) Vandas (според современите концепти *Clinopodium dalmaticum* или *Clinopodium dalmaticum* subsp. *bulgaricum*), кого Šilić (1979), го наведува за територијата на Република Македонија – Демир Хисар, Усунжа Река и Кривска Река (врз основа на податоците на Vandas, 1905, 1909). Забележлива е големата разлика помеѓу овие два таксони во обликот и влакнетоста на листовите, како и во големината на чашката и обликот на запците на чашката. Кај *Clinopodium albanicum* од територијата на Република Македонија чашката е правилна, 2-2,5 мм долга, запците на чашката се триаглести, со еднаква должина и ширина додека кај *Micromeria bulgarica* (односно *Clinopodium dalmaticum*) од територијата на Бугарија чашката повеќе или помалку е двоусна, подолга од 3 мм, чашкините запци се издолжено триаглести и тие се со долг зашилен врв.

Клучни зборови: флора; Република Македонија; хорологија; *Clinopodium albanicum* (Griseb. ex K. Malý) Melnikov

ПРИЛОЗИ, Одделение за природно-математички и биотехнички науки, МАНУ, том **39**, бр. 2, стр. 129–133 (2018)
CONTRIBUTIONS, Section of Natural, Mathematical and Biotechnical Sciences, MASA, Vol. **37,** No. 2, pp. 129–133 (2018)

Received: August 30, 2018
Accepted: November 8, 2018

ISSN 1857–9027
e-ISSN 1857–9949
UDC: 597.552.51-143.6.086:546.72(497.771)
DOI: 10.20903/csnmbs.masa.2018.39.2.125

Short communication

HISTOCHEMICAL EVALUATION OF IRON CONTENT IN THE LIVER OF WILD FEMALE OHRID TROUT (*SALMO LETNICA* KAR.) ALONG THE BREEDING CYCLE

Maja Jordanova[1*], Katerina Rebok[1], Maria João Rocha[2,3], Eduardo Rocha[2,3]

[1]Laboratory of Cytology, Histology and Embryology, Institute of Biology, Faculty of Natural Sciences and Mathematics, Ss. Cyril and Methodius University, Republic of Macedonia
[2]Laboratory of Histology and Embryology, Institute of Biomedical Sciences Abel Salazar – ICBAS, University of Porto – U. Porto, Portugal
[3]Histomorphology, Physiopathology and Applied Toxicology Group, Interdisciplinary Centre of Marine and Environmental Research – CIIMAR, University of Porto – U. Porto, Portugal
[*]e-mail: majaj@pmf.ukim.mk

Iron is an essential micronutrient for the normal metabolism of all cells. Intracellular iron varies within normality ranges, and depletion or overload of brings serious consequences. As such, iron can also be deleterious when appearing as an environmental toxicant. The aim of this study was to estimate semi-quantitatively the liver iron content in female Ohrid trout, from the Lake Ohrid, during the breeding cycle. Seasonal variations in hepatocytic iron were observed. The maximum content occurred at post-spawning, which was significantly higher than loads detected at pre- and early-vitellogenesis. Positive correlations existed between iron amounts and stages of ovary maturation. By the contrary, there were no correlations between iron contents and plasma oestradiol levels. The new uncovered "iron-breeding association" strongly endorses that normal seasonal variations in hepatocytic iron content should be taken into consideration in field studies investigating and monitoring the metal burden and toxicological effects of metals on wild fish.

Key words: iron; liver; Ohrid trout; oestradiol; seasonal

INTRODUCTION

Taking into account that large number of toxic chemicals were present in the environment, eutrophication, and, potentially, global climate changes, wildlife population in aquatic ecosystems throughout the world is faced with a wide variety of stressors. In such ecosystems, among other species, fish do bioaccumulate multiple environmental contaminants, and their presence/overload may well be taken as an indicator of environmental contamination [1–4]. Besides, in the assessment of heavy metal pollution of lake ecosystems, fish have proved to be the appropriate indicator organism [5].

Information regarding either the natural background of heavy metals in Lake Ohrid – one of Europe's deepest and oldest – or the loading by human activity is rather limited. There is only one available report on heavy metal concentrations in organic samples (of liver and muscle) in fishes from Lake Ohrid [6]. Results of this study imply a possible metal contamination problem in the Lake, at least at the time. Metal pollution in aquatic ecosystems has deleterious effects on different organs. The liver is one of them and it may increase the concentration of metals in the tissue [5, 7–8]. However, the body, organs (muscle, gill and liver), tissue burden of metals seems to be influenced by the fish age, body size, condition and nutrition [5, 7]. In addition, certain authors exposed seasonal variations in the occurrence of metals in fish living in metal-contaminated lakes [8].

In view of the afore mentioned context, we aim here to investigate hystochemically iron content

in the hepatocytes of Ohrid trout (*Salmo letnica* Kar.), and to explore if eventual correlation between, on the one hand, iron load and, on the other hand, ovary maturation stages and oestradiol levels exsist. This trout is endemic of Lake Ohrid, having an invaluable biological role as the local natural predator, besides being of considerable economic value and of potential use as a bioindicator species. As there is a need to know seasonal patterns of liver iron in bioindicator, and because of the risks associated with using "metal-loaded" fish in human consumption, our study is of substantial interest.

MATERIAL AND METHODS

Ohrid trout female (n = 30, range 420–1300 g) were collected from the Lake Ohrid (41°05'N, 20°45'E) from October 2001 until September 2002. The use of archive in this 1st study is justified because there are ongoing restrictions for trout fishing in Ohrid. After the capture, the animals were rapidly sacrificed by severing the spinal cord. Blood samples were taken from the caudal vein, for measuring plasma levels of oestradiol (E_2). The liver and gonads were dissected and weighted. The gonadosomatic index (GSI), used here in correlation analysis, was calculated as: ovary mass × 100 / body mass. The liver and gonads were sliced and systematically sampled so that at least 5 slabs of each organ per animal were fixed in Bouin's fixative for 48 hours.

The fixed fragments were routinely processed to paraffin and sectioned at 5 μm. Liver sections were stained with Perls' stain, for detection of iron, and ovary sections with hematoxylin and eosin. The iron content in the cytoplasm of hepatocytes was evaluated semi-quantitatively, based on the amount of histochemical staining, using the flowing scores: 0 = absent; 1 = rare; 2 = common; and 3 = abundant. For such analysis, one section was selected from each block. Twenty fields per section were quantified, at a final magnification of 400 ×.

To characterize the maturation stage, sections from ovaries were qualitatively analysed. The gonadal maturation cycle was divided in six stages: Previtellogenesis, Early-vitellogenesis, Mid-vitellogenesis, Late-vitellogenesis, Spawning and Post-spawning stage [9].

Plasma levels of E_2 were measured with an enzyme immunoassay performed in 96-well plates, following the manufacturer's instructions (ACE™ EIA, Ref 582251, Cayman Chemical, USA). Each fish was assayed using two dilutions and running every sample in two technical replicates. Absorbance measurements (at 414 nm) were made in a microplate reader (Multiskan EX). The values for E_2 (and GSI) were used here only for making statistical correlation analyses, as detailed data for the same set of fish were previously published [9, 11].

Iron content per group is presented as median, accompanied by the respective minimum and maximum values. For statistical inferential analyses, the software Statistica 7.0 for Windows was applied. Differences between groups were first evaluated by using Kruskal-Wallis ANOVA, followed by Mann-Whitney *U*-test (with Bonferroni correction) whenever the ANOVA was statistically significant. E_2 plasma levels and GSI data were used for correlation analyses only. The Spearman correlation analysis was used to investigate the associations between the liver iron load and either the GSI or the E_2 levels. Differences were considered significant when $p < 0.05$.

RESULTS

With the Perls' staining, the iron in hepatocytes were revealed as blue granules (Figure 1). The semi-quantitative data on the iron load are presented in Figure 1, with animals grouped per gonadal maturation stage. Iron was not found in most fish in Pre vitellogenesis, Vitellogenesis and Spawning. However, its content was higher in Post spawning, particularly when compared to Pre and Early vitellogenesis (Figure 2). Both Late vitellogenesis and Spawning had "transition scores", unveiling a rising trend for the liver iron that culminates and Post spawning. Overall, the median rose from 0 at Pre/Early vitellogenesis to 3 (maximum) at Post spawning.

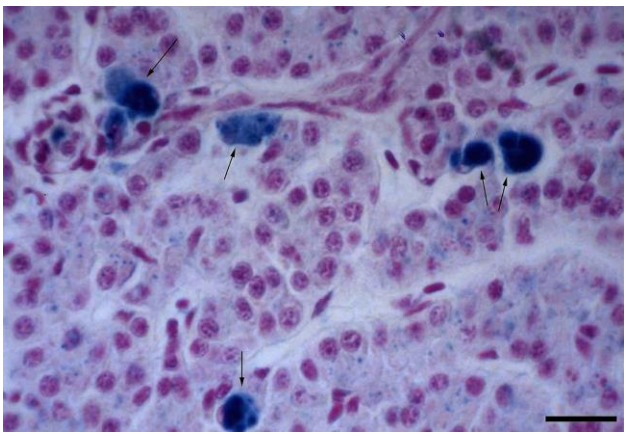

Figure 1. Micrograph of the Ohrid trout liver, displaying the iron content as blue granules within hepatocytes. Note the aggregates of pigmented macrophages laden with hemosiderin pigment. Paraffin section. Perls' stain. Bar = 20 μm.

Eventual correlations between the GSI or E_2 levels and iron content was also considered. Curiously, there was a significant positive correlation between the GSI and iron load ($r_s = 0.54$; $p < 0.001$), but no correlation at all between the latter content and E_2 levels ($r_s = – 0.07$; $p = 0.71$).

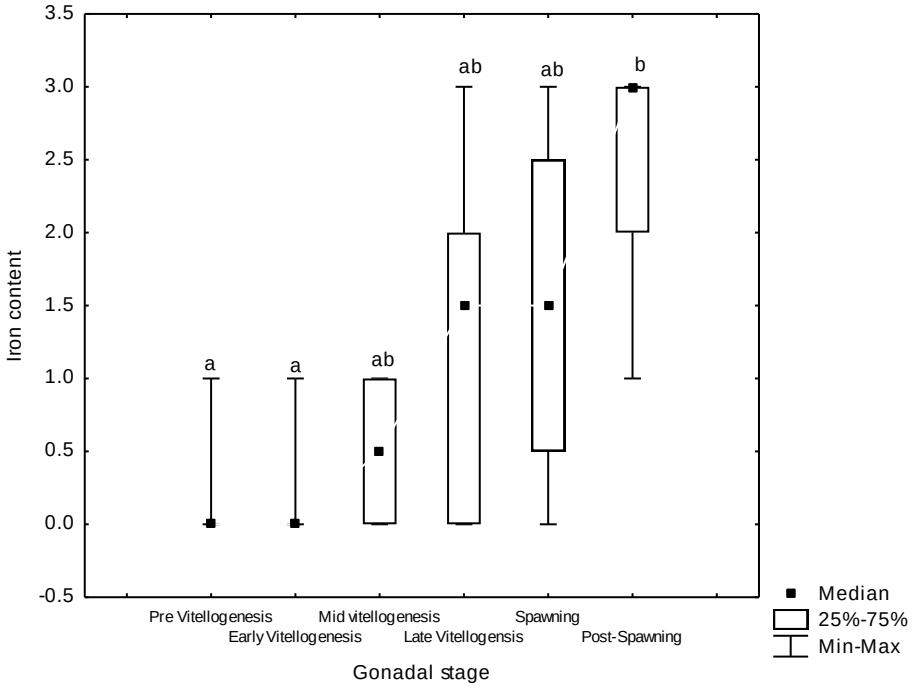

Figure 2. Iron load in the hepatocytes of Ohrid trout, during the breeding cycle, given as semi-quantitative Grades. Data sets with different superimposed letters differ significantly ($p < 0.05$).

DISCUSSION

Typically, fish are top consumers in the aquatic food chain. If living under heavy metal contamination, they often bioaccumulate many metals. In this study, histochemistry and semi-quantification at light microscopy were applied to investigate the seasonality of liver iron load in Ohrid trout, possibly in connection with the stage of ovary maturation and the E_2 plasma levels. The data showed almost an iron absence at Pre/Early vitellogenesis and a peak at Post spawning.

It is generally accepted that the concentration of heavy metals in the organs of fish is primarily determined by the level of pollution of water and food [5]. Thus, on a first analysis, at least the highest iron content in the Ohrid trout liver could be caused by metal overloading in the lake, therefore indicating a potential metal stress for the biota. This scenario is in line with earlier biochemical results for some fishes (including Ohrid trout) from Lake Ohrid [6].

However, the significant peak of iron during only one period of the reproductive cycle, preceded by a rising trend, along with a linear positive correlation with the GSI, can be related primarily to seasonal changes in physiological processes. In fact, rather than translating pollution trends only, changes in iron hepatic levels seem to be primarily governed by factors such as growth and metabolism, metal binding or changes in the feeding behaviour [5, 7], age structure, body size, and condition of the fish [5].

The differences within the Ohrid trout population – from near absence to high levels in Post spawning – could also be related, respectively, to a higher or to a lower lipid content during the breeding cycle. The higher tissue lipid content in fish samples was shown to cause a relative dilution of organ-accumulated micropollutants [5, 7]. In addition, in the liver of the platy fish, *Xiphophorus maculatus*, whose hepatocytes usually contain iron granules, those rich in lipid droplets lacked iron granules [10]. This fact perfectly agrees with our results, since Ohrid trout in the final stage of maturation in Post spawning contained a large amount of iron, but no lipid droplets in the hepatocytes [11]. Moreover, it was suggested that hepatic iron overload might be associated with hepatocytes apoptosis [12], and a cascade of death of hepatocytes by apoptosis was proposed to occur following spawning, at

least in brown trout *Salmo trutta* [13]. Finally, it was proposed that the variability of iron content and distribution in the liver of female lamprey, *Petromyzon marinus*, might be due to changes in the rate at which iron is used in vitellogenesis [14]. Accordingly, in fish ovary, as shown in swordfish, *Xiphophorus gladius*, that iron (as Fe^{3+}, detected by Perls' staining) accumulates in oocytes yolk granules and intergranular cytoplasm [15]. Here, the correlation of iron load with GSI but not with plasma E_2 levels suggests that there is no direct control of the latter on hepatocytic iron storage, but it supports an E_2 independent iron uptake of hepatocytes to support increasingly iron-dependent needs with ovary maturation.

Our results indicate the importance of making a distinction between the accumulation of exogenous iron sources and the possible normal changes in tissue iron content due to endogenous factors. Therefore, in iron/metal contamination research in fish - in addition to the information about the effect of other endogenous factors, such as age, body size, condition, and nutrition on the concentrations of metals in fish organs, information regarding the natural variations that may occur during the reproduction cycle of the species must also to be considered.

Acknowledgments: Fish collections were made with the support of the Ohrid Hydrobiological Institute, Ohrid, Macedonia. Special thanks to M. Sc. Zoran Spirkovski for his great assistance in the fieldwork.

REFERENCE

[1] D. E. Hinton, R. C. Lantz, J. A. Hampton, P. R. McCuskey, R. S. McCuskey, Normal versus abnormal structure: considerations in morphologic responses of teleosts to pollutants, *Environ. Health Perspect.* **71** (1987), pp. 139–146.

[2] D. E. Hinton, P. C. Baumann, G. R. Gardner, W. E. Hawkins, J. D. Hendricks, R. A. Murchelano, M. S. Okihiro, Histopathologic biomarkers, in: *Biomarkers – Biochemical, Physiological and Histological markers of Anthropogenic Stress*, R. Huggett, R. A. Kimerle, P. M. Meherle, H. L. Bergman (Eds), A special publication of SETAC Lewis Publishers Boca Raton, Ann. Arbor, London, Tokyo, 1992, pp. 155–212.

[3] D. E. Hinton, Toxicology-histopathology of fishes: a systematic approach and overview, in: *Pathobiology of Marine and Estuarine organisms*, J. A. Couch, J. W. Fournie (Eds), CRC Press, Boca Raton, FL, 1993, pp. 177–215.

[4] A. K. Whitfield, M. Elliott, Fishes as indicators of environmental and ecological changes within estuaries: a review of progress and some suggestions for the future, *J. Fish Biol.* **61:1** (2002), pp. 229–250.

[5] A. Farkas, J. Salánki, A. Specziár, I. Varanka, Metal pollution as health indicator of lake ecosystems, *International J. Occupat. Medicine Environmen. Health*, **14:2** (2001), pp. 163–170.

[6] Z. Spirkovski, Heavy metals and pesticides in Lake Ohrid fishes, *Lake Ohrid conservation project*; *Lake Ohrid monitoring program*; *2nd Midterm report*, Hidrobiological Inst., Ohrid (Eds), 2001.

[7] A. Farkas, J. Salánki, I. Varanka, Heavy metal concentrations in fish of Lake Balaton, *Lakes Reservoirs*, **5** (2000), pp. 71–279.

[8] S. Eastwood, P. Couture, Seasonal variations in condition and liver metal concentrations of yellow perch (*Perca flavescens*) from a metal-contaminated environment, *Aquat. Toxicol.* **58** (2002), pp. 43–56.

[9] M. Jordanova, M. J. Rocha, K. Rebok, E. Rocha, Changes in the amount of kidney pigmented macrophage aggregates throughout the breeding cycle of female Ohrid trout, *Salmo letnica* Kar. (Teleostei, Salmonidae), *Microsc. Res. Tech.,* **75:2** (2012), pp. 176–181.

[10] I. L. Leknes, The uptake of foreign ferritin by macrophages in the spleen, trunk kidney and liver of platy, *J. Fish Biol.*, **59** (2001), pp. 1412–1415.

[11] M. Jordanova, K. Rebok, F. Malhão, M. J. Rocha, E. Rocha, Seasonal changes in hepatocytic lipid droplets, glycogen deposits, and rough endoplasmic reticulum along the natural breeding cycle of female Ohrid trout (*Salmo letnica* Kar.) — A semi-quantitative ultrastructural study, *Micros. Res. Tech.*, **79:8** (2016), pp. 700–706.

[12] S. Han, Q. Tang, R. Chen, Y. Li, J. Shu, X. Zhang, Hepatic iron overload is associated with hepatocyte apoptosis during *Clonorchis sinensis* infection, *BMC Infect. Dis.*, **17**:**531 (**2017), pp. 7.

[13] E. Rocha, M. J. Rocha, M. H. Galante, M. W. Silva, R. A. F. Monteiro, The hepatocytes of the brown trout (*Salmo trutta fario*): A stereological study of the number and size along the breeding cycle, *Ichthyol. Res.*, **56** (2009), pp. 43–54.

[14] J. H. Youson, P. A. Sargent, D. Ogilvie, R. R. Shivers, Morphology of the green livers in upstream migrants of *Petromyzon marinus* L., *J. Morphol.*, **188** (1986), pp. 347–361.

[15] J. B. Ortiz-Delgado JB, Porcelloni S, Fossi C, Sarasquete C, Histochemical characterisation of oocytes of the swordfsh *Xiphias gladius*. *Scien. Marina* **72:3** (2008) 549–564.

ХИСТОХЕМИСКА ПРОЦЕНКА НА СОДРЖИНАТА НА ЖЕЛЕЗО ВО ЦРНИОТ ДРОБ НА ДИВИ ЖЕНКИ ОД ОХРИДСКАТА ПАСТРМКА (*SALMO LETNICA* KAR.) ВО ТЕКОТ НА РЕПРОДУКТИВНИОТ ЦИКЛУС

Маја Јорданова[1*], Катерина Ребок[1], Maria João Rocha[2,3], Eduardo Rocha[2,3]

[1]Лабараторија за цитологија, хистологија и ембриологија, Институт за биологија, Природно математички факултет, Универзитет Св Кирил и Методи, Република Македонија.
[2]Laboratory of Histology and Embryology, Institute of Biomedical Sciences Abel Salazar – ICBAS, University of Porto – U. Porto, Porto, Portugal.
[3]Histomorphology, Physiopathology and Applied Toxicology Group, Interdisciplinary Centre of Marine and Environmental Research – CIIMAR, University of Porto – U. Porto, Porto, Portugal.

Железото е есенцијален микронутритуент потребен за нормален метаболизам на сите клетки. Интрацелуларно содржината на железо варира во рамките на нормалните граници така што деплецијата или неговото прекумерно присуство може да доведе до сериозни последици. Со оглед на ова, железото може да биде штетно и да биде токсично во животната средина. Цел на оваа студија е да се определи семиквантитативно содржината на железо во црниот дроб кај женки од охридска пастрмка од Охридското Езеро во текот на репродуктивниот циклус. Забележани се сезонски варирања во содржината на железо во хепатоцитите. Максимални вредности се евидентирани во постмрестителниот период, значително повисоки споредено со превителогенетскиот и рановителогенетскиот период. Позитивна корелација постои помеѓу количеството железо и стадиумите на созревање на овариумите. Спротивно, корелации не се евидентирани помеѓу содржината на железо и нивото на естрадиол во плазмата. Новооткриената железо репродуктивен циклус асоцијација јасно укажува дека нормалните сезонски варирања во содржината на железото во хепатоцитите треба да бидат земени предвид во студиите во кои се испитува или се прави мониторинг на заситеност со метали и токсиколошки ефект на металите врз дивите риби.

Клучни зборови: железо; црн дроб; Охридска пастрмка; естадиол; сезони

ПРИЛОЗИ, Одделение за природно-математички и биотехнички науки, МАНУ, том **39**, бр. 2, стр. 135–141 (2018)
CONTRIBUTIONS, Section of Natural, Mathematical and Biotechnical Sciences, MASA, Vol. **39,** No. 2, pp. 135–141 (2018)

Received: September 14, 2018
Accepted: November 26, 2018

ISSN 1857–9027
e-ISSN 1857–9949
UDC: 582.282.2-12:595.78(497.7)
632.78:[635.925:582.282.2(497.7)
DOI: 10.20903/csnmbs.masa.2018.39.2.126

Original scientific paper

OCCURRENCE OF THE NEW INVASIVE INSECT *CYDALIMA PERSPECTALIS* WALKER ON BOX TREE IN THE REPUBLIC OF MACEDONIA

Sterja Načeski[1*], Irena Papazova–Anakieva[1], Blagoj Ivanov[1], Stanislava Lazarevska[2], Blagoj Šurbevski[1]

[1]Faculty of Forestry, Ss. Cyril and Methodius University, Skopje, Republic of Macedonia
[2] Faculty of Agricultural Sciences and Food, Ss. Cyril and Methodius University, Skopje, Republic of Macedonia
[*]e-mail addres: snaceski@sf.ukim.edu.mk

The box tree pyralid *Cydalima perspectalis* (Walker 1859) is a new invasive moth species in Europe. Box tree moth was recorded for the first time in the Republic of Macedonia on box seedlings in parks, gardens and other urban green spaces in the city of Skopje in 2014. The aim of this study was to investigate the distribution and spread, the biology and lifecycle, as well as the damage caused by the different generations of the box tree moth in natural box tree stands, as well as in urban areas in R. Macedonia. In natural populations of *Buxus*, it was firstly recorded on the Vodno mountain in 2015. Since then, its population has a trend of progradation. Based on the results obtained, recommendations are given with measures for gradual regulation of the box tree moth populations. Standard entomological methods (monitoring of the phenomenon, population density and percentage of defoliation) were used.

Key words: Box tree moth; *Cydalima perspectalis*; box tree (Buxus); defoliator; abundance

INTRODUCTION

The box tree moth, *Cydalima perspectalis* [1] (Lepioptera: Pyraloidea: Crambidae: Spilomelinae) is native to East Asia, India [2]; China [1, 3]; Japan [4], Taiwan, Korea [5] and Eastern Russia [6].

In Europe it was introduced most probably with box seedlings [7]. It was first registered in Europe in southwestern Germany in 2006 [8], while in 2007 it was found in Switzerland [9, 10] and Netherlands [11]. In 2008, box tree moth was found in Great Britain [12], France [13] and Austria [14]. In 2011 it appeared in Hungary [15], Romania and Turkey [16]. It was registered in Belgium [17] and Slovakia [18]. This invasive insect was found in Slovenia [19] and later in Denmark [20], while bioecological research on the development of *C. perspectalis* is provided by the authors: Maruyama [21], Maruyama & Shinaji [22–24], Székely *et al* [25], Tang *et al.* [26], Tominaga [27], Zhoo *et al.* [28].

In the Republic of Macedonia, *C. perspectalis* was recorded for the first time on box seedlings in parks, gardens and other urban green spaces in the city of Skopje, in 2014 (Novoselski Pat, 42°01'09", 21°21'11", K-265 m [29].

The highest population of *C. perspectalis* was observed in urban environments, in Skopje (2014, 2015, 2016 and 2017) [30].

Buxus sempervirens L. is mostly present in the western parts of Republic of Macedonia, mainly Polog Valley along rivers of Treska and Pchinja, as well as in the Ohrid region. The easternmost part of the *Buxus* areal in the Republic of Macedonia is in the region of Demir Kapija at the foot of the mountain Serta, at altitudes from 100 to1000 m a.s.l, and along the edges of Boropole on the massif of Jakupica on 1600 m n.v. [31, 32].

In the newly invaded regions, *C. perspectalis* larvae feed on leaves of box trees, *Buxus* spp., resulting in defoliation, which can kill the trees [3, 5]. The most significant damage, however, can be from the larvae attacking the bark of box trees causing the trees to dry out and die [3, 5]. Besides cultural and economic effects, the most serious threat from *C. perspectalis* is on the natural *Buxus* populations.

The species can be easily introduced accidentally with its host plant, which is extensively traded throughout Europe and therefore presents a serious threat [33]. Climate models predict further spread of the species in Europe, invading most areas except for Northern Fenno-Scandinavia, Northern Scotland and high mountains [33].

Recently, this species has been found in the Balkan region (Croatia, Serbia, Bosnia and Herzegovina, Republic of Macedonia, Greece) [34–37] and then in Bulgaria [38], Montenegro [36].

The significance of this research is in studying the invasiveness of the species, which from urban areas extends into the natural environment of the box populations. The aim of this study was to investigate the distribution and spread, the biology and lifecycle, as well as the damage caused by the different generations of the box tree moth in natural box tree stands, as well as in urban areas in R. Macedonia.

MATERIALS AND RESEARCH METHODS

For the realization of this research we have used standard and adapted methods for determining the abundance of *Cydalima perspectalis*, as well as the intensity of the attack and the degree of damage to leaves. These investigations were performed on stationary experimental plots, as well as at the entomological laboratory of the Faculty of Forestry in Skopje. The research was carried out from 2015 to August 2018. The methods consist of the following:

– The appearance and abundance of the box tree moth (*Cydalima perspectalis*) was monitored on experimental plots.

– Abundance is determined by the number of larvae found on 1000 leaves of box trees.

– The dynamics of emergence of butterflies and the dynamics of the number of its populations, as well as the development of the caterpillars, are observed on the experimental plots in Przino, Sredno Vodno and peak of Vodno.

– First and second-degree larvae were observed in the entomological laboratory at the Faculty of Forestry in Skopje. We followed the overall development of the box moth (*Cydalima perspectalis*): dynamics of emergence of butterflies; laying of eggs by females; larval development; the beginning of pupal stadium, i.e. the development of a whole generation [15].

– The intensity of the attack and the percentage of defoliation (damaged leaves) caused by feeding caterpillars were determined using a standard entomological method [15].

RESEARCH RESULTS AND DISCUSSION

C. perspectalis was recorded on natural *Buxus* populations for the first time on mountain Vodno in 2015. Since then, its population has a trend of progradation on Vodno. It has expanded almost everywhere, with incidents of defoliation observed in 2016 and 2017.

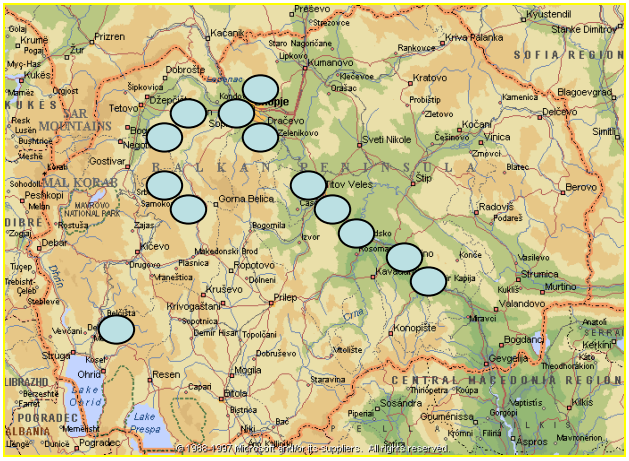

Figure 1. Natural sites of *Buxus sempervirens* in the Republic of Macedonia

Figure 2. Defoliation caused by the caterpillars of the box tree moth near Skopje (Novoselski Pat).

In the spring of 2017, we registered total defoliation on the site Sredno Vodno. The same year it was also registered in the natural *Buxus* populations on Matka. Box tree moth is not registered only on the top of Mt. Vodno, but due to its rapid spread it is expected that it will soon be present in this part of the mountain, where it appeared late in 2017.

Strong defoliations were recorded in July and August of 2018 at the base and the middle of Mt. Vodno. Particularly numerous were the second and third generation of box tree moth populations.

During its development the distinctly patterned larvae can reach several centimeters in length, and it is able to defoliate box tree shoots and totally destroy the whole bush or even hedges in public gardens, parks, cemeteries or home gardens. Due to the characteristic appearance of the pest and the damage caused (peeling and chewing of leaves, web and visible pieces of excrement on box tree shoots), the insect and the damage are not likely to be misinterpreted as other insect species or damage caused by diseases of box tree.

As the box tree moth may have several generations per year in Europe, and as the species is spreading not only by natural means but also with infested planting material via trade, its area of distribution and the levels of caused damage will probably grow rapidly in the coming years.

Table 1. Representation of *C. perspectalis* in Skopje areas

No.	Site	Year of appearance	Area under attack	Intrensity of attack	Defoliation
			per ha		%
1.	Skopje – urban area	2014	+(of all area)	Very high	75–100
2.	Skopje – urban area	2015	+(of all area)	Very high	85–100
	Skopje – Vodno-natural area of box	2015	100	Moderate high	30–85
	Skopje – Vodno -natural area of box	2016	500	Moderate	
	Skopje – Matka-natural area of box	–	–	very high	55–90
4.	Skopje – Vodno-natural area of box	2017	1000	Very high	75–100
	Skopje – Matka-natural area of box	2017	150	Moderate very high	25–80

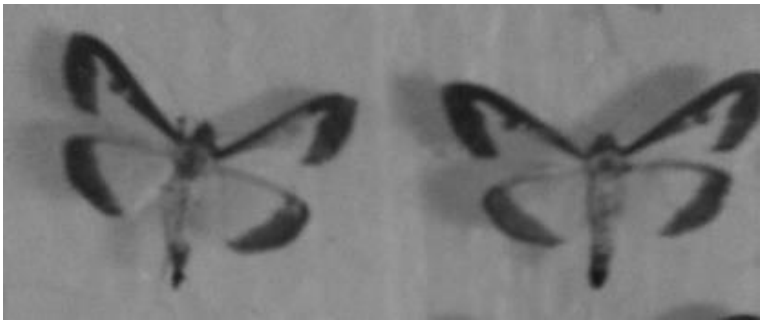

Figure 3. Adults of *Cydalima perspectalis* Walker
(collected at the site of Sredno Vodno, 15.VIII 2015)

Table 2. Abundance of the *Cydalima perspectalis* populations in Skopje region

Year	2015			2016			2017			2018	
Generation	I	II	III	I	II	III	I	II	III	I	II
Locality	Number of caterpillars per 1000 leaves										
Skopje-Przino	22.3	74	89	38.1	89.4	105.3	32.7	49.2	100.5	17.6	56.8
Sredno Vodno	0	4.8	12.8	14.3	35.4	92.3	27.6	55.3	98.3	45.4	122.5
Vrv Vodno	0	0	0	0	0	0	0	1.2	2.4	12.5	41.7

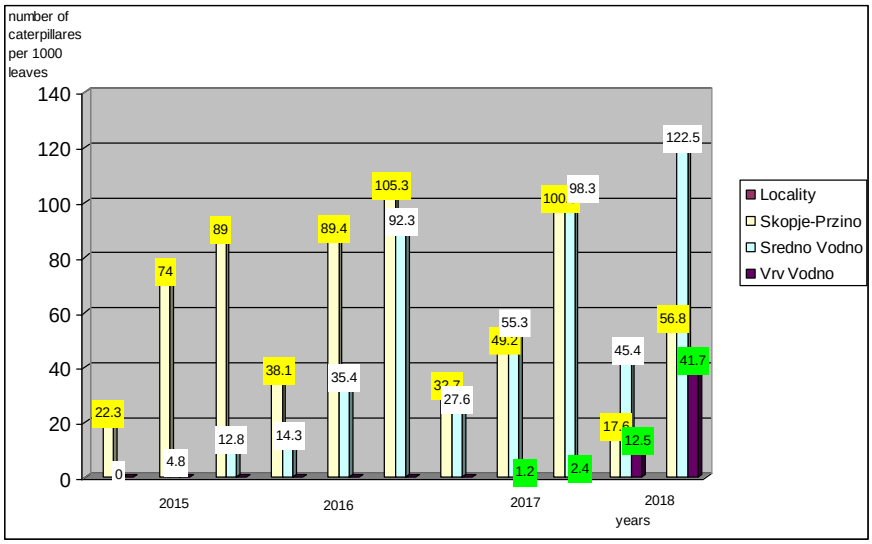

Figure 4. Abundance of *Cydalima perspectalis* populations in the Skopje region

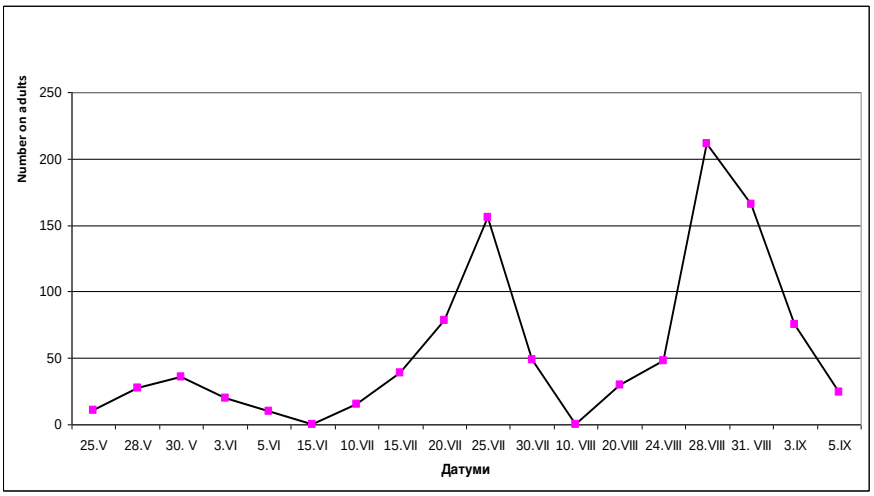

Figure 5. The dynamics of the appearance of butterflies of *C. perspectalis*, at the site of Vodno, Skopje in 2016

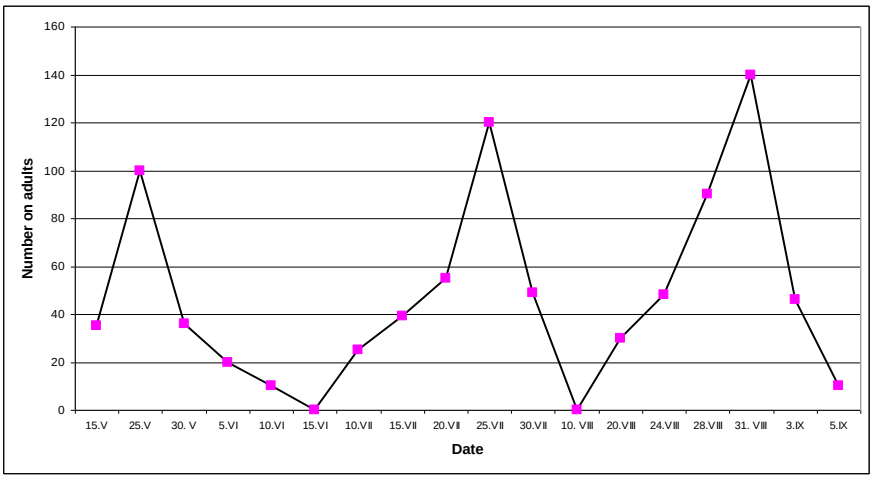

Figure 6. The dynamics of the appearance of butterflies of *C. perspectalis*, at the site of Vodno, Skopje in 2017

During this research, three generations of *Cydalima perspectalis* were identified.

We are presenting the results of the dynamics of the abundance of *C. perspectalis* in Figure 4 and Table 2. It is most abundant at the site Pržino – in 2015 we registered 89 caterpillars on 1000 leaves of box; 105.3 in 2016 and 100.5 in 2017.

For the site of Sredno Vodno we registered gradation ranging from 12.8 in 2015, 92.3 in 2016, 98.3 in 2017, to 122.5 in 2018. At the site near the peak of Vodno, its abundance is the least of all, with an average of 2,4 caterpillars on 1000 leaves in 2017.

High populations of *C. perspectalis* are registered at the site of Matka and in the urban areas of Kavadarci, Ohrid, Prilep and other cities in the Republic of Macedonia in 2018.

CONCLUSION

Based on the field analysis and laboratory research we can give the following conclusions:

– *Cydalima perspectalis*, box tree moth was recorded for the first time in the Republic of Macedonia on box seedlings in parks, gardens and other urban green spaces in the city of Skopje in 2014.

– The most numerous populations of *C. perspectalis* were observed in urban environments, in Skopje (2014, 2015, 2016 and 2017), Kavadarci (2015, 2016, 2017) and Ohrid (2017).

– In the natural *Buxus* populations it was recorded for the first time on mountain Vodno in 2015. Since then, this population started to have a trend of progradation on Vodno. It has expanded almost everywhere, with evident defoliations in 2016 and in 2017. In the spring of 2017, total defoliation was detected on box trees at site Sredno Vodno.

– Box tree moth was registered at the peak of mountain Vodno at the end of 2017.

– It was also registered in the natural *Buxus* populations on Matka in 2017.

– It's most abundant at the site Przino - 89 caterpillars per 1000 leaves of box in 2015, 105,3 in 2016 and 100,5 in 2017; SrednoVodno- 12,8 in 2015, 92,3 in 2016, 98,3 in 2017 and 122,5 in 2018;

– At the site on the peak of Vodno, its abundance is the lowest of all, and is 2,4 caterpillars in 1000 leaves in 2017.

– The number of the first generation is the lowest in contrast to the second and third, when the number is multiplied.

– Strong defoliations were recorded at the base and the middle of the mountain Vodno, in July and August. Particularly numerous were the second and third generation of box tree moth populations.

– Accordingly, the population of the box tree moth varies from generation to generation over the years when the research was carried out.

– The number of the first generation is the lowest in contrast to the second and third, when the number is multiplied. The most numerous generation is the one that appears in the middle of the summer, i.e. August - September.

– Based on the results obtained, and especially due to the high population of *C. perspectalis*, recommendations should be given for the control of its populations for the regions of Vodno and Matka

REFERENCES

[1] F. Walker, *List of the Specimens of Lepidopterous Insects in the Collection of the British Museum. Part XVIII. Pyralidae*, British Museum (Nat. Hist.) London, 1859, pp. 509–798.

[2] G. F. Hampson, *The Fauna of British India, including Ceylon and Burma*, Taylor & Francis, London, XXVIII, 1896, pp. 594.

[3] Y. Choo, H. T. Kaya, S. M. Lee, T. O. Kim, J. B. Kim, Laboratory evalution of entomophathogenic nematodes, Steinernema carpocapse an Heterorhabditis bacteriophora against some forest insects pests, *Kor., J. Appl. Entomol*., **30** (1991), pp. 227–232, (in Korean, English abstr.).

[4] H. Inoue, *Pyralidae, Moths of Japan 1, 2*, H. Inoue, S. Sugi, H. Kuroko, S. Moriuti, A. Kawabe (Eds), Kodansha, Tokyo, Japan, 1982, pp. 223–254, 307–404 (vol. 1), pp. 36–48, 228, 296–314 (vol. 2).

[5] I. K. Park, Ecological characteristic of *Glyphodes perspectalis*, *Kor. J. Appl. Entomol*., **47** (2008) pp. 299–301.

[6] V. A. Krpichnikova, Pyralidae, *Key to the Insects of Russian Far East*, **5 (2)** 2005, pp. 526–539, (in Russian).

[7] R. Mally, M. Nuss, Phylogeny and nomenclature of the box tree moth, *Cydalima perspectalis* (Walker, 1859) comb. n., which was recently introduced into Europe (Lepidoptera: Pyraloidea: Crambidae: Spilomelinae). *European journal of Entomology* **107 (3)** (2010), pp. 393–400.

[8] E. O. Krüger, *Glyphodes perspeclis* (Walker, 1859)– neu für ie Fauna Europas (Lepidoptra: Crambidae), *Entomol. Z*. **118** (2008), pp. 81–83.

[9] F. Käppeli, Der Buchsbaumzünler, Elitempo durh basler Gärten, *G'pluse-die Gärtner-Fachzeitschrift*, **(20)** (2008), pp. 33.

[10] C. R. Sigg, (Auch das noch: Ein neuer Buchs-Schadling schlagt zu. Massive Schaden durch den Buchsbaumzunsler.), *Der Gartenbau* , **4** (2009), pp. 2–4.

[11] M. Muus. T. S. T., E. van Haaften, J. van Deventer, L. J. van Deventer, De buxusmot *Palpita per-*

spectalis (Walker) in Nederland (Lepidoptera: Crambidae), *Entomol. Ber*., **69** (2009), pp. 66–67.

[12] A. Mitchell, Box tree moth *Diaphania perspectalis* (Walk.) –a new pyralid moth to Britain and Ireland, *Atropos*, **36** (2009), pp. 17–18.

[13] J. F. Feldtrauer, J. J. Feldtrauer, C. Brua, Premiers signalements en France ela Pyrale u Buis iaphania perspectalis (Walker, 1859), espèce exotique envahissante s'ataquant aux (Lepidoptera, Crambidae), *Bull. SocEntomol*., **65** (2009) pp. 55–58.

[14] J. Rodeland. (ed.), Lepiforum, (2009) URL.; www. Lepiforum de.

[15] Sz. Sáfián, B. Horváth, Box Tree Moth – *Cydalima perspectalis* (Walker, 1859), new member in the Lepidoptera fauna of Hungary (Lepidoptera: Crambidae), *Natura Somogyiensis*, **19** (2011) pp. 245–246.

[16] E. Hizal, M. Kose, C. Yesiland, D. Kaynar, The New Pest *Cydalima perspectalis* (Walker, 1859) (Lepidoptera: Crambidae) in Turkey, *Journal of Animal and Veterinary Advances*, **11** (3) (2012), pp. 400–403.

[17] H. Casteels, J. Witters, S. Vandierendonck, L. van Remoortere, First report of Cydalima perspectalis (Lepidoptera: Crambidae) in Belgium, *63rd International Symposium on Crop Protection*, Gent, Belgium, 2011, poster presentation.

[18] G. Pastorális, G. Elsner, F. Kopecek, F. Kosorin, A. Laštůvka, A. Lendela, J. Liška, J. Nimy, I. Richter, R. Stefanovie *et al*., *Štrnást novÝch* (2013).

[19] G. Seljak, Six new alien phytophagous insect species recorded in Slovenia in 2011, *Acta Entomologica Slovenica*, **20(1)** (2012), pp. 31–44.

[20] D. Hobern– *Cydalima perspectalis* (Walker, 1859). https://www.flickr.com/photos/dhobern/941897008 3/ (2013). (accesed 8.08.2016)

[21] T. Maruyama, Life cycle of the box tree pyralid, *Glyphodes perspectalis* (Walker) (Lepidoptera: Pyralidae). IV. Effect of various host plants on larval growth and food utilization, *Jap. J. Appl. Entomol. Zool.*, **37** (1993), pp. 117–122.

[22] T. Maruyama, N. Shinaji, Studies on the life cyle of the box tree pyralid, *Glyphodes perspectalis* (Walker) (Lepidoptera: Pyralidae). I. Seasonal adult emergence and developmental velocity, *Jap. J. Appl. Entomol. Zool.*, **31** (1987), pp. 226–232.

[23] T. Maruyama, N. Shinaji, The life cyle of the box tree pyralid, *Glyphodes perspectalis* (Walker) (Lepidoptera: Pyralidae), II. Developmental characteristics of larvae diapause, *Jap. J. Appl. Entomol. Zool.*, **35** (1991), pp. 221–230.

[24] T. Maruyama, N. Shinaji. The life cyle of the box tree pyralid, *Glyphodes perspectalis* (Walker) (Lepidoptera: Pyralidae). III. Potoperiodic induction of larval diapause, *Jap. J. Appl. Entomol. Zool*., **37** (1993), pp. 45–51.

[25] L. Székely, V. Dinca, C. Mihai, *Cydalima perspectalis* (Walker, 1859), a new species for the Romanian fauna (Lepidoptera: Crambidae: Spilomelinae), *Buletin de Informare Entomologica*, **22 (3–4)** (2011), pp. 73–77.

[26] S. J. Tang, H. Z. Qin, W. Sun, Studies on bionomics of *Diaphania perspectalis*, *J.Shanghai Agric. Collection*, **8** (1990), pp. 307–312.

[27] S. Tominaga, Biological notes on *Glyphodes perspectalis* (Walker) an Herpetogramma basalis (Walker) (Pyraliae) in Okinawa, *Yugato* **154** (1998), pp. 119–120.

[28] W. Zhoo, C. Y. Xia, X. Q. Sun, B. Zhu, Z. P. Liu, Z. C. Liu, Y. Wang, Studies on the biological characteristics and control of *Diaphania perspectalis* Walker, *J. Spanghai Jiotong Univ. Agric. Sci.*, **23** (2005), pp. 52–56.

[29] S. Nacheski, S. Lazarevska, I. Papazova-Anakieva, *Cydalima perspectalis* Walker (*Lepidoptera, Crambidae*) a new insect of *Buxus sempervirens* in the Republic of Macedonia, *Plant protection journal*, **XXVII**, (2015).

[30] S. Nacheski, I. Papazova-Anakieva, S. Lazarevska, Cydalima perspectalis new defoliator threat to natural population of boxwood in the Skopje region, *Book of abstracts 70 years Faculty of Forestry-Skopje*, (2017) pp. 27.

[31] H. Em, *Review of the enroflorate of Macedonia*, (spontaneous and suppositional VII), Union of Engineers and Forestry Technicians and Wood Processing Industry of the Republic of Macedonia, Skopje, 1967.

[32] S. Džekov, *Dendrology*, University Ss. Cyril and Methodius-Skopje, Skopje, 1988.

[33] S. Nacambo, F. L. G. Leuthardt, H. Wan, H. Li, T. Haye, B. Baur, R. M. Weiss, M. Kenis, Development characteristics of the box‐tree moth *Cydalima perspectalis* and its potential distribution in Europe, *J. App. Entomol*, **Volume 138**, **Issue 1-2** (2013), pp. 14–26.

[34] T. Koren, M. Crne, The first record of the box tree moth, Cydalima perspectalis (Walker, 1859) (Lepidoptera, Crambidae) in Croatia. *Natura Croatica*, **21(2)** (2012), pp. 507–510.

[35] D, Matosevic, Box tree moth (Cydalima perspectalis, Lepidoptera; Crambidae), new invasive insect pest in Croatia, *SEEFOR*, **4(2)** (2013), pp. 89–94. http://www.seefor.eu/36-vol4-no2-matosevic.html

[36] I. Ostojic, M. Zovko, D. Petrovic, D. Elez, New records of box tree moth Cydalima perspectalis (Walker, 1859) in Bosnia and Herzegovina. (Novi nalazi simsirova moljca Cydalima perspectalis (Walker, 1859) u Bosni i Hercegovini.), *Radovi Poljoprivrednog Fakulteta Univerziteta u Sarajevu (Works of the Faculty of Agriculture University of Sarajevo)*, **60(65(1))** (2015), pp. 139–143.

[37] I. Strachinis, C. Kazilas, F. Karamaouna, N. Papanikolaou, G. Partsinevelos, P. Milonas, First record of Cydalima perspectalis (Walker, 1859) (Lepidoptera: Crambidae) in Greece, *Hellenic Plant Protection Journal*, **8(2)** (2015), pp. 66–72.

[38] S. Beshkov, S. Abadjiev, D. Dimitrov, Cydalima perspectalis (Walker, 1859) (Lepidoptera: Pyraloidea: Crambidae: Spilomelinae). New invasive pest moth in Bulgaria. *Entomologist's Record and Journal of Variation*, **127** (2015), pp. 18–22.

[39] G. Pastorális, G. Elsner, F. Kopecek, F. Kosorin., A. Laštůvka., A. Lendela, J. Liška, J. Nimy, I. Richter, R. Stefanovie *et al*. Štrnást novÝch druhov motÝlov (Lepidoptera) pre faunu Slovenska, *Folia Faunistica Slovaca*, **18** (2013), pp. 1–12.

ПОЈАВА НА НОВ ИНВАЗИВЕН ИНСЕКТ *CYDALIMA PERSPECTALIS* WALKER НА ШИМШИРОТ ВО РЕПУБЛИКА МАКЕДОНИЈА

Стерја Начески[1*], Ирена Папазова–Анакиева[1], Благој Иванов[1], Станислава Лазаревска[2], Благој Шурбевски[1]

[1] Шумарски факултет, Универзитет „Св. Кирил и Методиј“, Скопје, Република Македонија
[2] Факултет за земјоделски науки и храна, Универзитет „Св. Кирил и Методиј“, Скопје, Република Македонија

Шимшировиот молец *Cydalima perspectalis* (Walker 1859) е нов инвазивен вид молец во Европа. *C. perspectalis*, беше за прв пат забележан во Р. Македонија на садници од шимшир во паркови, градини и други урбани зелени површини во градот Скопје во 2014 година. Целта на ова истражување беше да се определи распространувањето, биологијата и животниот циклус, како и оштетувањата предизвикани од различните генерации на шимшировиот молец во природните насади од шимшир, како и во урбаните подрачја во Република Македонија. Во природните насади од *Buxus*, за прв пат овој молец беше забележан на планината Водно во 2015 година. Од тогаш па наваму неговата популација таму има тренд на проградација. Врз основа на добиените резултати, и особено поради бројната популација на *Cydalima perspectalis*, се дадени препораки со мерки за постепено намалување на неговата популација на Водно. За ова истражување беа користени стандардни ентомолошки методи (набљудување на појавата, густината на популацијата и процентот на дефолијација).

Клучни зборови: Шимширов молец; *Cydalima perspectalis*; Шимшир (*Buxus*); дефолијатор; абунданца

INSTRUCTIONS FOR AUTHORS

The journal *Contributions, Section of Natural, Mathematical and Biotechnical Sciences* is an official publication of the Macedonian Academy of Sciences and Arts. It is published twice a year. The journal publishes **original scientific papers, short communications, reviews, professional papers** and **educational papers** from all fields of:

natural sciences – physics, chemistry, biology, geography, geology;

mathematical sciences – mathematics, informatics;

biotechnical sciences – agriculture and food, forestry.

This journal also publishes, continuously or occasionally, the bibliographies of the members of the Macedonian Academy of Sciences and Arts, book reviews, reports on meetings, information on future meetings, important events and dates, and various headings which contribute to the development of the corresponding scientific field.

The **original scientific papers** report unpublished results of completed original scientific research. Experimental data should be presented in a way that enables reproduction and verification of analyses and deductions on which the conclusions are based. The manuscripts should normally not exceed 6000 words.

The **short communications** should contain completed (but briefly presented) results of original scientific research. The manuscripts should normally not exceed 2000 words.

The **reviews** are submitted at the invitation of the Editorial Board. They should be critical surveys of an area in which preferably the author himself is active. The reviews can be longer than typical research articles but should generally be limited to 10000 words including references, tables and figures.

The **professional papers** report on useful practical results that are not original but help the results of the original scientific research to be adopted into scientific and production use. Manuscripts should normally not exceed 4000 words.

The **educational papers** report on the activities in the laboratory and classroom and the needs of the community of educators in all mentioned fields. Manuscripts should normally not exceed 4000 words.

Submission of manuscripts

The authors bear the sole responsibility for the content of the contributions. It is assumed that by submitting their paper the authors have not violated any internal rules or regulations of their institutions related to the content of the contributions. Submission of a paper implies that it has not been published previously, that it is not under consideration for publication elsewhere, and that, if accepted, will not be published elsewhere in the same form, in English or in any other language, without the written consent of the Publisher.

A cover letter must accompany the manuscript submission. It should contain full names of all authors and their affiliation, the manuscript title and the name and contact information for the corresponding author. Please provide e-mail address and phone number. For submission, please send an electronic version of the manuscript (in MS Word) at: smalinovska@manu.edu.mk

Preparation of manuscripts

Prepare the entire manuscript in double-space typing, on numbered pages of A4 format with margins of 2.5 cm on each side. Do not use footnotes.

The papers should be written in the shortest possible way and without unnecessary repetition. The original scientific papers, short communications, professional papers and reviews should be written in English. An Abstract and list of key words in Macedonian must accompany each manuscript. For contributions by authors who are not speakers of Macedonian, the above data will be provided by the Editorial Board.

The manuscript should contain: title, authors names and addresses, abstract, key words, introduction, experimental or theoretical background, results and discussion, acknowledgement (if desired) and references.

Title. It should be brief and informative but should define the subject of the manuscript. It should include most of the key words.

Authorship. List the first and last name of each author. Omit professional and official titles. Give the complete mailing address of each author. For the corresponding author include an e-mail address and a phone number. The name of the corresponding author should carry an asterisk.

Abstract. Each manuscript should be provided with an abstract of about 100–150 words. It should give the aim of the research, methods or procedures, significant results and conclusions. Define any abbreviations used in the abstract. The text of the abstract should contain as many key words as possible.

Key words. Up to 5 key words or phrases should be given separately to facilitate indexing and on-line searching.

Introduction. The most important previous results related to the problem in hand should be reviewed avoiding a detailed literature survey but clearly pointing to the place of the research in hand within the general area of scientific knowledge. The aim and importance of the research should be clearly stated.

Experimental section. This section should contain a description of the materials used and methods employed in form which makes the results reproducible, but without detailed description of already known methods.

Manuscripts that are related to theoretical studies, instead of experimental section should contain a sub-heading *theoretical background* where the necessary details for verifying the results obtained should be stated.

Results and discussion. The authors should discuss their findings, postulate explanations for the data, elucidate models and compare their results with those of other works. Irrelevant comparisons and speculations unsupported by the new information presented in the manuscript should be avoided. The conclusions should be not given separately but included in this section. In special cases a separate section containing conclusions could be included.

Tables. They should be given with a suitable caption and should be numbered consecutively with Arabic numerals. Footnotes to tables should be typed below the table and should be referred to by superscript lowercase letter. Each table should be typed on a separate sheet. The correct position of the tables should be marked on the manuscript.

Figures. Figures (photographs, diagrams and schemes) should be numbered consecutively with Arabic numerals in order to which they mentioned in the text. They should accompany the manuscript but should not be imbedded in the text. Each figure should be clearly marked with the figure number and the first author's name. All figures should have captions that should be supplied on a separate sheet. Correct position of the figures should be marked on the manuscript. The size of the symbols for the physical quantities and units as well as the size of the numbers and letters used in the reduced figures should be comparable with the size of the letters in the main text of the paper. Each figure or group of figures should be planned to fit, after appropriate reduction, into the area of either one or two columns of text. The maximum finished size of a one-column illustration is 8.0 cm and that of a two-column illustration is 17.0 cm width. Make sure you use uniform lettering and sizing of your original artwork. All figures should be printed on a high quality printer or graphics plotter. Figures should be also sent in electronic form as TIFF or JPG files with minimum 300 dpi or higher resolution.

Color illustrations in print can be included only at the author's expense.

Units. The SI (Systeme Internationale d'Unites) for quantities and units should be used throughout the whole text. In marking the axes, the symbol, of the corresponding quantity (in italics) should be **divided** by the unit of this quantity. If nomenclature is specialized, nomenclature section should be included at the end of the manuscript, giving definitions and dimensions for all terms.

The **names of chemical substances** should be in accordance with the IUPAC recommendations and rules or *Chemical Abstract* practice.

The results of elemental analyses of organic compounds should be given in the following form:

Anal. $C_{12}H_{l6}O$ (176.26).

Calc'd: C 81.77; H 9.15; O 9.08 %.

Found: C 81.63; H 9.36; O 9.01 %.

When a large number of compounds have been analyzed, the results should be given in tabular form.

Formulas and equations. Chemical equations should be balanced and numbered consecutively along with mathematical equations or other mathematical expressions. All of them should be marked with Arabic numerals in parenthesis in the right hand margin. The use of equation editor (Word) for typesetting the equations is recommended. Strokes (/) should not be used instead of parentheses.

Acknowledgement. Financial support, advice or other kinds of assistance can be included in this section.

References. Literature references should be numbered and listed in order of citation in the text. They should be selective rather than extensive with the exemption to review articles. Avoid references to works that have not been peered-reviewed. Citation of a reference as "in press" implies that it has been accepted for publication. Abbreviations of the titles must follow the internationally accepted practice.

The surname (not first name and/or initials) of one or two authors may be given in the text, whereas in case of more than two authors they should be quoted as, for example, Julg *et al.* [1]. In the list of references the citation should be as follows:

Journals:

[1] J. Zhang, X. Wang, H. Xie, Phonon energy inversion in graphene during transient thermal transport, *Phys. Lett*. A, **377** (2013), pp. 721–726.

[2] G. Jovanovski, P. Makreski, B. Šoptrajanov, B. Kaitner, B. Boev, Minerals from Macedonia, *Contributions, Sec. Math. Tech. Sci*., MANU, **XXVI**, 1 (2005), pp. 7–84.

[3] A. Čarni, M. Kostadinovski, V. Matevski**,** Species composition and syntaxonomic consideration of two communities of the Drabo-Cardaminion hirsutae in the southern part of the Republic of Macedonia, *Acta Bot. Croat*., **62** (2003), pp. 47–56.

[4] D. Dimovski, A geometric proof that boundary links are homotopically trivial**,** *Topology Appl.*, **29** (1988), pp. 237–244.

[5] F. C. Oliveira, Á. C. Collado, L. F. C. Leite, Autonomy and sustainability: An integrated analysis of the development of new approaches to agrosystem management in family-based farming in Carnaubais Territory, Piauí, Brazil, *Agr. Syst.*, **115** (2013), pp. 1–9.

Books:

[1] J. A. Roels, *Energetics and Kinetics in Biotechnology*, Elsevier Biomedical Press, Amsterdam, New York, Oxford, 1983.

[2] H. Chum, M. Baizer, *The Electrochemistry of Biomass and Derived Materials*, ACS Monograph 183, American Chemical Society, Washington, DC, 1985, pp. 134–157.

[3] J. W. Finley, G. A. Leveille, Macronutrient substitutes, in: *Present Knowledge in Nutrition*, E. K. Ziegler, L. J. Filer Jr. (Eds), ILSI Press, Washington DC, 1996, pp. 581–595.

[4] Gj. Filipovski: *Characteristic of the Climatic and Vegetational Soil Zones in the Republic of Macedonia*, Macedonian Academy of Sciences and Arts, Skopje, 1996.

Scientific meetings:

[1] M. S. Steel, Creating woodlands for wildlife and people in Scotland, *18th Commonwealth Forestry Conference; Restoring the Commonwealth's Forests: Tackling Climate Change*, Edinburgh, Scotland, 2010, Book of Abstracts, p. 3.

Note that the *full titles* of the cited papers should be included.

For the web references, as a minimum the full URL should be given. Any further information, if available (author names, dates, reference to a source publication, etc.) should also be given.

Editorial process

Receipt of manuscripts. The received manuscript is read and examined for conformity to these Instructions to Authors. Failure to meet the criteria outlined will result in return of the manuscript for correction before evaluation.

Peer review/evaluation. Papers received by the Editorial Board are sent to two referees (one in the case of professional and educational papers). Identities of the reviewers will not be released to the authors. The review process is expected to be complete within 3 months, but conflicting recommendations and other unpredictable events may cause some delay.

The comments and recommendations of the referees and the Editorial Board are sent to the authors for further action. The authors are allowed 30 days to undertake revisions and return the corrected text to the Editorial Board. The final decision on acceptance or rejection is made by the Editorial Board. This decision, together with any relevant reasons, will be send to the corresponding author.

Publication process. The accepted manuscript is again checked for conformation to the Instructions to Authors and to ensure that all necessary paperwork is present. Any areas that are identified as problematic will be addressed by the Editorial Board in consultation with the corresponding author. The papers will be prepared for publication by a professional copy editor responsible for ensuring that the final printed work is consistent in form and style.

Galley proofs. A galley proof is sent to the corresponding author. It should be checked very carefully and must be returned within 2 days of receipt. The proof stage is not the time to make extensive corrections, additions, or deletions.

Reprints. The corresponding author will receive, free of charge, 20 reprints of the paper published in the *Contributions*. Additionally he will receive a complementary copy of the journal.